

**Nonlinear Spectroscopy
of Closed Degenerate Two-level Systems**

Von der Fakultät für Mathematik und Physik
der Gottfried Wilhelm Leibniz Universität Hannover
zur Erlangung des Grades

Doktor der Naturwissenschaften
– Dr. rer. nat. –

genehmigte Dissertation von

Dottore in Fisica
Luca Spani Molella

geboren am 4. April 1974 in Piacenza, Italien.

(2006)

Referent: Prof. K. Danzmann
Korreferent: Prof. M. Kock
Tag der Promotion: 21. Juli 2006

Zusammenfassung

Die Physik der Zwei-Niveau-Systeme ist seit der Entwicklung der Quantenmechanik gut verstanden. Bei der Interpretation der atomaren Spektren zeigte die neue Theorie große Erfolge. Mit dem Einsatz von Lasern in der Spektroskopie begann dann eine verstärkte systematische und ausführliche Untersuchung der Viel-Niveau-Systeme. Durch die Laserspektroskopie wurde es möglich, tiefer in die Kenntnisse der kohärenten Dunkelzustände vorzustoßen. Die darauf folgende erfolgreiche Entdeckung der elektromagnetisch induzierten Transparenz und der kohärenten Dunkelzustände begründete den Beginn der Untersuchungen an stark dispersiven und kohärenten Medien, die besondere Absorptionseigenschaften aufweisen. Das Interesse an diesen Medien wuchs in den vergangenen Jahren, denn sie eröffnen die Möglichkeit, Licht mit vernachlässigbarem Verlust zu speichern, was für die Entwicklung zukünftiger Rechenanlagen nützlich sein kann.

In dieser Arbeit habe ich einige Übergänge im gasförmigen Cäsium als nicht lineare kohärente Medien unter dem Einfluss von extern einwirkenden elektromagnetischen Feldern untersucht.

Die Untersuchungen begannen an Λ -Systemen, in denen elektromagnetisch induzierte Transparenz gemessen wurde. In diesen Experimenten wurde die induzierte Transparenz des Probe- oder des Koppellasers verbessert bis zu Werten, die vergleichbar sind mit denen bei nicht resonanten elektromagnetischen Feldern. Die Studie wechselte dann zum entarteten Zwei-Niveau-System, in dem in den letzten Jahren elektromagnetisch induzierte Absorption entdeckt wurde. Die Phänomenologie der entarteten Zwei-Niveau-Systeme ist immer noch teilweise unbekannt und es wird erwartet, dass die kohärente Wechselwirkung ungewöhnliche Spektren erzeugt. Durch die Ausnutzung der Fähigkeit des experimentellen Aufbaus zur simultanen Messung der Absorption und der Dispersion des Koppel- oder des Probelasers wurden theoretische Vorhersagen, die sich teilweise noch im Entwicklungsstadium befinden, über das Verhalten der entarteten Zwei-Niveau-Systeme bestätigt. Diese Vorhersagen beschreiben klar die Erzeugung der elektromagnetisch induzierten Absorption und Transparenz im entarteten Zwei-Niveau-System; sie basieren auf numerischen Simulationen, die sich auf dem theoretischen Konzept des spontanen Transfers der Kohärenz zwischen Gruppen von unterschiedlichen entarteten Unterniveaus eines gegebenen Systems gründen. Die erhaltenen experimentellen Resultate bestätigen die Wichtigkeit, den spontanen Transfer der Kohärenz als grundlegenden Prozess der Physik der kohärenten Systeme zu betrachten. Dieser Prozess ist in seiner Bedeutung vergleichbar mit der spontanen Emission bei Zwei-Niveau-Systemen.

Zum Schluss dieser Arbeit wurde ich motiviert durch die derzeitigen Vorschläge aus der Gravitationswellenforschung zur Entwicklung von Kerr-Interferometern, um das Signal-zu-Rausch-Verhältnis zukünftiger Gravitationswellendetektoren zu verbessern. Da die in dieser Arbeit untersuchten nichtlinearen Systeme extrem steile Profile (bei erhöhter Absorption oder Transparenz) zeigten, waren sie perfekte Kandidaten für die Erzeugung großer Kerr-Nichtlinearitäten des Brechungsindex. In diesem Zusammenhang wurde experimentell gezeigt, dass die als kohärente Dunkelzustände beschreibbaren transparenten Medien Kerr-Koeffizienten besitzen, die um Größenordnungen größer sind als die Koeffizienten typischer Kerr-Medien aber bei fast vollständiger Transparenz erzeugt werden können. Diese Eigenschaft macht sie sehr attraktiv für zukünftige Anwendungen.

Stichworte: Kohärente Dunkelzustände, elektromagnetisch induzierte Transparenz, elektromagnetisch induzierte Absorption, Kerr-Effekt, licht-induzierte Doppelbrechung.

Summary

The physics of atomic two-level systems has been well understood since the foundations of quantum mechanics, when the interpretation of the atomic spectra was a major success of the new theory. However, it was only after the invention of the laser that multilevel systems could be easily and systematically explored. With this powerful new instrument of analysis it was possible to deepen the knowledge of coherence-dominated phenomena. The later discovery of electromagnetically induced transparency and coherent population trapping constituted the beginning of research into highly dispersive coherent media which show peculiar absorption properties. Such media have gained more and more interest in recent years because they open the possibility to store light with negligible loss, a characteristic which may be useful for the future development of computation.

In this work I studied several atomic-level schemes in which gaseous atomic caesium behaves as a nonlinear coherent medium under the action of externally applied electromagnetic fields.

The research began with Λ -systems, where electromagnetically induced transparency was analysed. In this context it was possible to improve the induced transparency for either the probe or the coupling laser to values comparable with those experienced by off-resonant electromagnetic fields. This study then moved to degenerate two-level systems, where in recent years electromagnetically induced absorption has been discovered. The phenomenology of degenerate two-level systems is still partially unknown and the coherent interactions taking place are expected to generate unusual spectra. Exploiting the capability of the adopted experimental setup to simultaneously measure the absorption and dispersion of either the coupling or the probe laser I verified theoretical predictions (partly still in development) concerning the behaviour of degenerate two-level systems. These predictions clearly describe the appearance of electromagnetically induced absorption or electromagnetically induced transparency in degenerate two-level systems; they are based on numerical simulations which are grounded on the theoretical concept of spontaneous transfer of coherence between groups of different degenerate sublevels of a given system. The obtained experimental results stressed the importance of considering spontaneous transfer of coherence as a fundamental process of the physics of coherent systems: a process with an importance comparable to that of spontaneous emission in the physics of two-level systems.

In the final stages of this work I was motivated by current proposals in the gravitational wave community to develop Kerr interferometers and thus enhance the signal-to-noise ratio of future gravitational wave detectors. Since the nonlinear systems analysed here were all characterised by unusually steep dispersion patterns (either in the presence of enhanced absorption or transparency) they presented themselves as perfect candidates in generating giant Kerr nonlinearities of the refractive index. In this context I experimentally showed that the transparent media obtainable through coherent population trapping are characterised by Kerr coefficients which are orders of magnitudes greater than those typical of other Kerr-media and are obtainable under transparency conditions, a property which makes them very attractive for future applications.

Keywords: Coherent population trapping, electromagnetically induced transparency, electromagnetically induced absorption, Kerr effect, light-induced birefringence.

Contents

Zusammenfassung	i
Summary	iii
Contents	v
Glossary	vii
Introduction	1
1 Theoretical Background	5
1.1 Atomic system	6
1.2 Lambda systems	6
1.3 Classical analog of electromagnetically induced transparency	8
1.4 Semiclassical models	15
1.4.1 Density matrix formalism	15
1.4.2 Spontaneous processes within the density matrix formalism	17
1.4.3 Electromagnetically induced transparency	20
1.4.4 Electromagnetically induced absorption	23
1.4.5 Stationary solutions of the optical Bloch equations for a Λ -system	29
1.4.6 Stationary solutions of the optical Bloch equations for an N-system	31
1.5 Calculation of experimentally relevant quantities	36
1.5.1 Calculation of the Rabi frequencies	38
1.5.2 Calculation of the Rabi frequency for the transition $4 \rightarrow 5$	39
1.5.3 Calculation of the dispersion profile	42
2 Experimental Setup	47
2.1 Laser	47
2.1.1 Laser diodes	48
2.1.2 External cavity diode laser	49
2.2 Heterodyne interferometer	50
2.3 Frequency lock	52
2.3.1 Doppler-free saturation spectroscopy	53
2.3.2 Frequency modulation spectroscopy	55
2.4 Phase lock	57
2.4.1 Phase coherence adjustment	59
2.4.2 Phase lock for a three-level configuration	60
2.4.3 Phase lock for a degenerate two-level configuration	61

2.5	Dispersion measurements with the heterodyne interferometer	62
2.6	Atomic source	64
2.6.1	Doppler broadening	64
2.6.2	Reflux oven	65
2.7	Interaction volume	66
3	Experimental Results	69
3.1	Optimisation of the detected signal in a Λ -system	69
3.2	Measurements in a Λ -system	72
3.3	Broad spectral measurements within the caesium D_2 line	73
3.4	Degenerate two-level systems	77
3.5	Kerr coefficients	86
	Outlook	91
	Bibliography	93
	Acknowledgements	96
	Curriculum vitae	97
	Publications	99

Glossary

$\alpha(\delta)$	absorption coefficient as a function of the probe detuning
δ	probe laser detuning from the two-photon resonance
Δ_{ab}	probe laser detuning from the one-photon resonance
Δ_{ac}	coupling laser detuning from the one-photon resonance
γ_{ij}	spontaneous decay rate from level $ i\rangle$ into level $ j\rangle$
Γ_{ij}	total decay rate from level $ i\rangle$ into level $ j\rangle$
γ	sum of the optical decay rates
γ_0	coherence decay (in the present case transient loss)
F	quantum numbers of the total angular momentum (ground state)
F'	quantum numbers of the total angular momentum (excited state)
l	interaction length
L_{probe}	length of the interferometer probe arm
L_{ref}	length of the interferometer reference arm
μ_{ij}	electric dipole moment for the transition $ i\rangle \rightarrow j\rangle$
n	refractive index
n'	$n - 1$
N	atomic density
ρ	density matrix
σ	reduced density matrix
φ'	phase shift induced by n'
Ω_{ij}	reduced Rabi frequency relative to the states $ i\rangle$ and $ j\rangle$
$\tilde{\Omega}^2$	$\Omega_{ab}^2 + \Omega_{ac}^2$
ω_{ij}	transition frequency between the states $ i\rangle$ and $ j\rangle$
ω_{probe}	probe laser (angular) frequency
ω_{coupl}	coupling laser (angular) frequency
ω_{ref}	reference laser (angular) frequency

Introduction

Since the discovery of the laser physicists have had the possibility to manipulate the properties of optical media in a way which can no longer be understood in terms of classical concepts. With laser-generated coherent optical fields it is easy to arrange atoms so that they are in a superposition of different atomic levels, i.e. it is possible to induce coherence in an atomic medium. These coherent atomic media are characterised by special optical properties which are unusual for the classical world. The induction of coherence into an atomic system can produce interference between the different paths which the atoms can follow to perform an atomic transition. In the case of destructive interference this coherence can be responsible for transparency even when the impinging radiation is resonant: electromagnetically induced transparency (EIT) [6, 10]. Similarly, in the case of a constructive interference the absorption of the radiation can be strongly enhanced: electromagnetically induced absorption (EIA) [1, 2].

Coherent atomic media possess not only unusual absorptive properties. They also display extremely strong dispersive characteristics, which are even more impressive when they appear in combination with transparency, because in the classical world a high dispersion is always in combination with high absorption.

Strongly dispersive media have been studied for various experimental applications. Electromagnetically induced transparency has been exploited to decelerate light to walking speed [20]. Recent experiments have demonstrated that it is even possible to stop and restart the electromagnetic radiation mapping the information carried by the light onto a nonlinear EIT-medium while reducing the group velocity of the radiation to zero and then re-extracting the information while reaccelerating the radiation [33]. Since photons are very robust and are rapid carriers of information the possibility to trap them even for short times (at present, storage times up to 0.5 ms have been obtained [25]) sounds very promising for all quantum information applications. The hope is to be able to exploit the laws of quantum mechanics to improve the capabilities of future computational devices, either enhancing their speed or improving the security of the communication channels between different parties. All these experiments have been characterised by a strong positive dispersion associated with transparency of the medium.

Even media with negative dispersion (sometimes called anomalous dispersion) are of particular interest. They have been used to realise negative group velocities of light, an effect which is often referred to as superluminal propagation [40], and they have been suggested for the realisation of broadband high-finesse optical resonators (also called white-light cavities) [41, 43, 35]. Within these cavities the anomalous dispersion is supposed to cancel the variation of the optical length as a function of the radiation frequency. While

white-light cavities require a transparent medium, superluminal propagation has been realised in the presence of either enhanced transparency [40] or enhanced absorption [3]. All experiments on superluminal propagation used media characterised by a very steep dispersive profile. On the contrary the intracavity applications—which have been studied but not yet experimentally realised—should not require such extreme dispersion values but a fine tuning of the transparency properties of the medium, so that the transmission losses can be suppressed to a level which no longer degrades the finesse of the cavity.

Because the realisation of white-light cavities is of particular interest for the future generations of gravitational wave detectors and its feasibility is related to the degree of extinction of the absorption induced by the medium, we have propaedeutically tried in this experiment to improve the transparency of *positive* dispersive media to the level typical for a non-resonant interaction between the light and the medium. The experience gained in this sense and the results obtained make us quite optimistic of the possibility to extend them to *negative* dispersive media with transparency. The absorption extinction achieved at the EIT resonance either in Λ -systems or in degenerate two-level systems was about 98% of the value obtainable with an off-resonant field.

Such a performance could only be obtained with a careful extinction of the residual environmental magnetic field at the interaction zone. The extreme sensitivity of the enhanced transparency on the magnetic fields has also inspired researches on the possibility to use EIT-media for magnetometry applications; these studies have obtained promising results.

Absorptive media with anomalous dispersion were discovered only in the last decade [1]. They were found in an N-like atomic system within the D_2 line of alkali atoms. Even if such media are very absorptive with respect to EIT-media they retain a relatively small absorption coefficient when compared with crystals (the absorption coefficient which we were able to measure is of the order of 0.1 cm^{-1}). For this reason it was possible to demonstrate superluminal propagation even in the presence of enhanced absorption. Moreover, the dispersion is characterised by a very steep profile. This makes the group velocities of light reported in the presence of EIA about one orders of magnitude greater than those reported for transparent systems (values of $-c_0/310$ [40] have been measured for transparent media and values of $-c_0/4100$ have been reported by EIA [3]).

In this research we have concentrated much of our attention on such EIA-media. Through the use of a three-beam heterodyne interferometer we were able to investigate the optical properties of either the coupling or the probe laser. The research experimentally demonstrated for the first time that while the probe laser is subject to enhanced absorption, the coupling laser experiences a bright enhanced transmission with an extra absorption peak in correspondence with the two-photon resonance. At the same time it was also possible to take the first measurement of parametric dispersion of the coupling laser in an EIA system. The measured dispersion was, in contradistinction to what was measured for Λ -systems, positive. These results are presented in the third chapter of this work.

The obtained results confirmed the interpretation of EIA as an effect generated through spontaneous transfer of coherence. This effect has often been neglected in the analysis of atomic systems. However, its introduction gave the research on EIA media a solid

theoretical background which, at present, seems to be confirmed by all experimental results. In particular, we were able to verify the results of several simulations made for the coupling and the probe laser in an N-system showing EIA. These simulations were partly stimulated by the results obtained in this research. Therefore we present them in some detail in the first chapter, together with a more general background on the concept of spontaneous transfer of coherence and the semiclassical approach used for the description of the physics of coherent systems.

All measurements were performed in an atomic caesium beam. The peculiarity of using an atomic beam opened us to the possibility to circumvent undesired Doppler shift of the lines thus obtaining spectra which were characterised by subnatural linewidths starting from about 10 kHz. This and other aspects of the experimental apparatus are described in the second chapter of the thesis.

The choice of caesium among the various alkali atoms was determined by its very rich hyperfine sublevel structure. Within the D_2 line it was possible to choose between two different Λ -systems, two closed two-level systems (one satisfying EIA-conditions and the other not), and many other level configurations which were also, at least partially, explored. In one of these other configurations it was possible to detect light-induced birefringence, an effect concerning a rotation of the polarisation of the probe beam caused by the alignment induced in the medium through the coupling beam. This effect is described in the third chapter together with results concerning the Kerr coefficients which can be measured for EIT-media and EIA-media. These last results show how the giant Kerr coefficients obtainable in the presence of EIA or EIT are orders of magnitudes greater than those in usual Kerr-media, thus making these nonlinear coherent media extremely attractive for all applications involving giant Kerr effects.

The rich caesium hyperfine structure is the natural environment in which the measurements performed in this experiment can be extended to multi-level systems. Some of these multilevel systems (for example the bichromatic off-resonant driven two-level system or the N-like four-level system [44]) will have to be experimentally studied to foresee applications for future generations of gravitational wave detectors. A brief outlook concerning the possibility to extend this research into such new direction closes the thesis.

Chapter 1

Theoretical Background

Introduction

In this section I will introduce much of the formalism which is needed for the description and the analysis of the experiments performed in the continuation of this work. For reasons of space and opportunity I have chosen to limit the mathematical details everywhere I had the impression that they were overwhelming and too general for the purposes described here. For the same reason I have also kept the discussion to the level of the first quantisation. However, some effects due to the interaction between the vacuum and the system were not avoidable, since they played a crucial role in some of the experiment performed. The interaction with the vacuum was then introduced with the help of a semiclassical model and an analogy with Brownian motion. For much of this picture I relied on the works of Claude Cohen-Tannoudji, Jaques Dupont-Roc, and Gilbert Grynberg [11, 12], which were an invaluable source of information and inspiration. The interested reader should refer to these books for all the mathematical details. Of course, the purpose to stress the physics rather than the mathematics may have brought to some oversimplifications: they, hopefully, do not compromise too much the understandability of the following paragraphs.

The chapter begins with a short review of the atomic system which constituted the environment in which all measurements were performed. After the presentation of the phenomenology of electromagnetically induced transparency with the aid of classical model we introduce the density matrix formalism. Some considerations on the opportunity to introduce supplementary terms in the evolution equation for the density matrix bring the reader to the concept of spontaneous trapping of coherence, which reveals to be crucial for the explanation of electromagnetically induced absorption, a kind of counterpart of electromagnetically induced transparency which is the object of many measurement in this work. Finally, I show the results of some numerical calculations simulating the appearance of electromagnetically induced absorption in N-systems. These results were obtained by another research but were partly stimulated from the discussion on the spectra measured within this project and presented in chapter 3 which they contribute to explain.

1.1 Atomic system

An atomic system which is particularly suitable for the study of electromagnetically induced transparency and absorption (in the following called EIT and EIA) is the D_2 line of the alkali atoms. In this line several different level configurations can be excited to give rise to either electromagnetically induced transparency or absorption. The line is easily accessible through diode lasers which can be tuned to the desired frequency and is, therefore, very suitable for experimental investigation.

The objects of analysis in this work were various transitions within the ^{133}Cs D_2 line (852 nm), which were coupled and probed with two linearly polarised lasers orthogonally polarised to each other. The use of two lasers was crucial to induce coherence in the system. The choice of orthogonal polarisations was caused by reasons of distinguishability. The possibility to discriminate between the two lasers by means of their polarisation was particularly important in case of degenerate systems, where the probe and the coupling lasers acted on the same atomic transition, thus becoming indistinguishable in any other way in case of collinear propagation. Furthermore, the laser distinguishability was used, in the special kind of heterodyne interferometer adopted here [28, 30, 31, 37], to perform dispersion measurements, a characteristic of this experimental setup which opened the possibility to fill several gaps in the experimental knowledge of the analysed systems.

In the caesium D_2 line the hyperfine splitting between the two F hyperfine sublevels amounts to roughly 9.2 GHz while the hyperfine splitting of the F' sublevels is of the order of 150 MHz to 250 MHz depending on the sublevels considered (here and in the following of this work we call F the quantum numbers of the total angular momentum associated with the ground state of the line and F' those associated with the excited state). A schematic of the system, which does not represent the frequency differences between the atomic transitions as a scale drawing would do, but is intended only as a pictorial reference, is given in Fig. 1.1. In Fig. 1.1 the representation of the Zeeman sublevels is omitted. Those levels could be considered degenerate all through the work thanks to an accurate tuning of the magnetic field to a negligible level around the interaction zone. Nevertheless, we will see that even degenerate sublevels may introduce important effects in the spectroscopy of the lines. This is especially true for degenerate two-level transitions, where the degeneracy is a necessary condition for the appearance of electromagnetically induced absorption.

1.2 Lambda systems

In this section we will concentrate our attention on electromagnetically induced transparency. In this particular case we will analyse the emergence of EIT in Λ -systems.

A Λ -system consists of a group of three atomic levels, the scheme of which resembles, once graphically representing also the electromagnetic fields involved in the process (i.e. a field coupling one transition from one of the two ground levels to an excited level and a

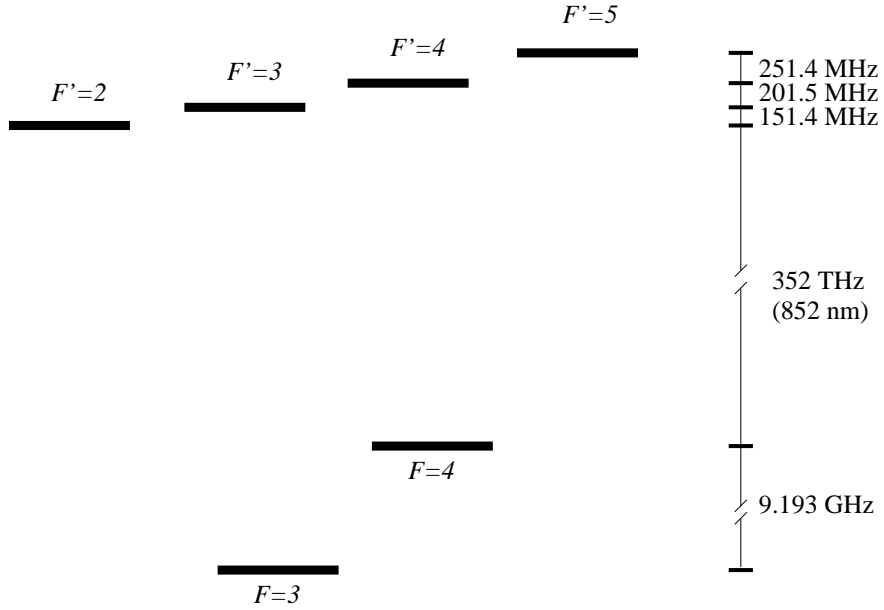


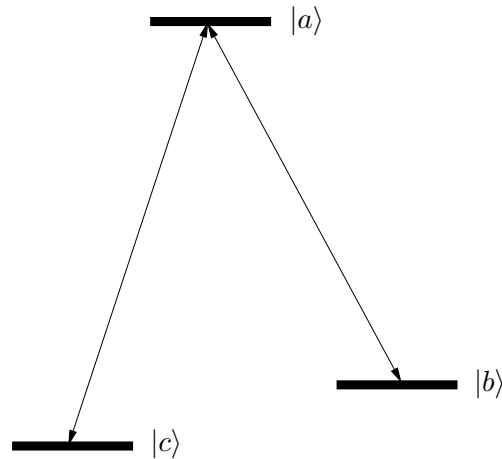
Figure 1.1: Level schematic of the D_2 line of atomic Caesium. The F levels are the hyperfine levels of the ground level $6s\ ^2S_{1/2}$. The F' are the hyperfine levels of the excited level $6p\ ^2P_{3/2}$.

second field probing the transition from the other ground level to the excited level), the form of a Greek letter Λ . A pictorial representation of a Λ -system is given in Fig. 1.2. Depending on whether the two ground levels share the same energy or not we will speak in the following of a degenerate or a non-degenerate Λ -system.

It is well known that, if an atomic transition is probed with a probe laser only, the amount of laser light absorbed by the atom can be described through a lorentzian absorption profile centred at the frequency of the transition itself. This behaviour can be radically changed in the presence of a second laser coupling one of the levels (or both) involved in the probed transition.

Let us consider the case of a Λ -system (Fig. 1.2). In this case a second laser, called the coupling laser, couples the upper level of the probed transition with a second level, whose energy is lower than that of the upper one and comparable with that of the lower level of the probed transition (i.e. the condition $\omega_{bc} \ll \omega_{ab}, \omega_{ac}$ is satisfied). If the probe frequency is varied and the probe frequency matches the condition for a two-photon transition between $|b\rangle$ and $|c\rangle$, the probe laser light is not absorbed any more by the atom. Due to the combined coherent effect of the two lasers the system has entered in a so-called *dark state* which is non-absorbing for the probe radiation. The system has developed a destructive interference between different evolution paths which the probe laser light can follow in its interaction with the atom. This transparency effect induced by the radiation is called *electromagnetically induced transparency* or shortly *EIT*.

The emergence of EIT is not limited to Λ -systems. One can encounter it in V-systems

Figure 1.2: Energy diagram of a Λ -system.

and in degenerate two-level systems. In the last ones one can also detect the experimental counterpart of electromagnetically induced transparency, namely *electromagnetically induced absorption* (abbreviated in *EIA*), which corresponds to an enhancement of absorption by the system induced by coherence effects between the levels involved. Similarly to the case of EIT, one can say that the system has entered into a *bright state* which is related to a constructive interference between different quantum paths for the probe laser light interacting with the atom.

1.3 Classical analog of electromagnetically induced transparency

Before starting with a quantum mechanical model of the system, I would like to present a classical analog of electromagnetically induced transparency. This analog helps to understand some elementary aspects of the underlying physics. Furthermore, such a model can be used as an introductory one when introducing coherent systems to beginners and laymen.

Let us consider again the system depicted in Fig. 1.2. If one considers the system from a purely quantum mechanical point of view one would have to quantise not only the atom but also the electromagnetic fields. In building a classical analog, the atomic levels and the fields could be then represented as a system of four coupled oscillator: two for the two atomic two-level systems and the two for the fields coupling them. However, when one performs an experiment on a Λ -system, one usually probes one atomic transition with a probe laser *after* having prepared the atoms by coupling the other transition (this condition is in reality not essential, since the system shows an ability to prepare itself in the right way in any case, as pointed out in ref. [19], but we will assume that this is true here because this is the more usual configuration and the configuration experimentally tested in the rest of this work). In this case the oscillator associated with the coupling

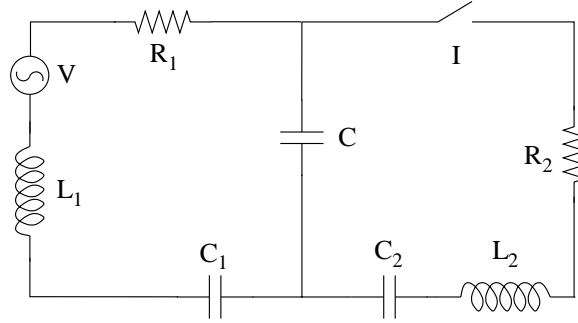


Figure 1.3: Electromagnetic classical analog of electromagnetically induced transparency

laser plays a double role: firstly, it enables the participation of the second two level system (here between $|a\rangle$ and $|c\rangle$), which would remain otherwise isolated from the action of the probe laser, coupling it to the first one (between $|a\rangle$ and $|b\rangle$); secondly, it determines the intensity of the coupling between the various oscillators, thus strongly determining the response of the system. Keeping these roles in mind and assuming that the system has reached stationarity and that the losses are negligible, it is a useful simplification to schematise not only the two two-level systems but also the coupling laser as a classical *passive* oscillator which is coupled with two other passive oscillators (schematising the atomic transitions). This system can be probed by an *active* external probe oscillator which needs to be tuneable in frequency (as is usually the case for the probe laser) and plays the role of the probe laser. With this setup it is possible to easily study the system response as a function of the probe detuning.

Such a model has been proposed in recent years [5]. It is possible to construct either a mechanic model or an electromagnetic one. The practical realisation of the latter is, however, much easier since it offers the possibility to quickly interchange components to test various experimental configurations. Let us explain such a model briefly.

Consider the circuit represented in Fig. 1.3. It shows a system of two RLC meshes coupled through a capacitor of capacity C and driven by an external oscillator. Depending on the position of the switch, the second mesh can be switched on and off. The following parallels may be built:

- The first mesh represents the probed atomic transition between $|a\rangle$ and $|b\rangle$. It includes a resistor R_1 , an inductor L_1 and two capacitors: C and C_1 . The capacitors are in series and compose to an effective capacity C_{e1} .
- The second mesh represents the atomic transition coupled by the coupling laser. It contains an RLC circuit analogous to that used for the probed transition but a switch is present. The switch gives the opportunity to simulate the presence or absence of the coupling laser and, as a consequence, the involvement of the coupled two-level system in the experiment.
- The capacitor C represents the coupling between the two meshes operated by the coupling laser. The value of the capacitance C is directly related with the intensity of the coupling laser and through it one can study how the system behaves for

various coupling laser intensities.

The analog has one major imperfection: a change in the capacitance C causes a change in the absolute resonance frequencies of the two RLC meshes (corresponding to those of the two atomic transitions). However, since the width of the lorentzian resonance curve is only determined by the resistive components of the corresponding RLC mesh, the change in C will not affect the shape of the resonance curve. A simple substitution of the variable used in plotting the taken data from the absolute frequency of the probe oscillator to its detuning from the resonance frequency will then circumvent the problem.

It is obvious that, when the switch is opened, the system behaves like a driven two-level system, showing a lorentzian pattern for the absorbed power during one cycle of oscillation. When, however, the switch is closed, the response of the system changes and shows a series of various phenomena, going from the analog of EIT to that of the Autler-Townes effect.

Component	Value
R_1	1Ω
R_2	51Ω
L_1	$1 \mu\text{H}$
L_2	$1 \mu\text{H}$
C_1	100 nF
C_2	100 nF
C	47 nF
	100 nF
	150 nF
	220 nF
	300 nF
	400 nF
	500 nF
	$1 \mu\text{F}$
	$2 \mu\text{F}$
	$5 \mu\text{F}$
$10 \mu\text{F}$	

Table 1.1: Simulation parameters tested for the classical analog of electromagnetically induced transparency.

In the real system a current measurement would alter the performance of the circuit. For this reason it is convenient to decouple the voltage drop at the poles of the inductor output with a buffer and subsequently to integrate it in order to obtain a signal proportional to the current flowing through it. Such a signal will then simulate the absorptive characteristics of the atoms. Also for the measurement of the dispersive spectra the experimental

The various spectra can be obtained changing the capacity of the coupling capacitor C . This stands for the intensity of the coupling laser in the physical system. For low coupling a dip in the middle of the resonance curve emerges, similarly to what happens for EIT. At higher coupling the dip evolves in a structure with two peaks which move apart from each other once the coupling increases. When the coupling is large enough the separation between the peaks is well-defined and the system behaves like an atom in the presence of the Autler-Townes effect. In addition to such absorption measurements, it is possible to measure the phase shift between the input power and the absorbed power. The derivative of such a phase shift constitutes the dispersion curve for our probe and properly simulates the dispersive behaviour of a probe laser probing the atomic system.

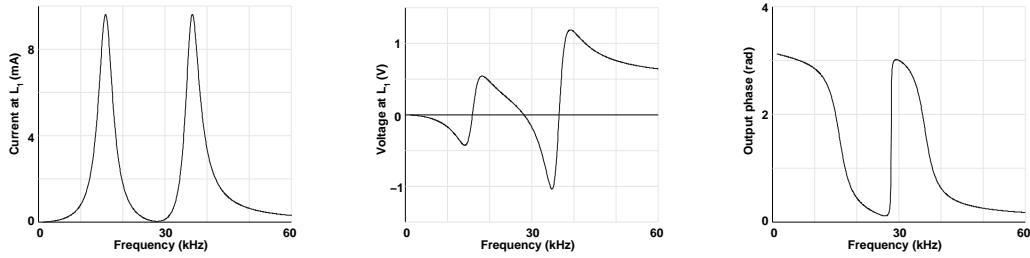
One can easily simulate the features described above with a simulation program for electrical nets. The parameter chosen for the simulations can be read in table 1.1.

The current flowing through the inductor L_1 has the same frequency dependence of the power dissipated in the circuit. Since the aim of the simulation is to qualitatively reproduce the behaviour of the real system, it suffices to measure the frequency dependence of such a current. This is easily performed by one of the simulation program routines. In the real

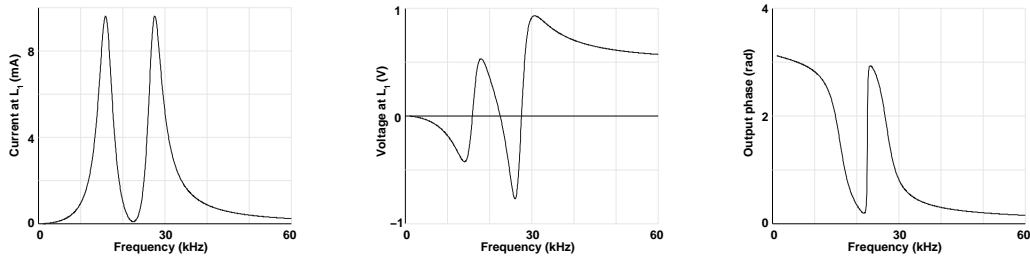
procedure is different than that used in the simulation. The relative phase between the current flowing through the inductor and the applied voltage represents the phase shift of our system. However, the performance of a measurement with a lock-in amplifier requires the comparison between the frequencies of two alternate voltages. Therefore, one should follow the same procedure suggested for the absorption measurement, integrating the current through L_1 to get a voltage proportional to the current and then comparing the two values. In reality, it is easier to directly measure the phase of the voltage at the input of L_1 . In fact the derivative of the phase shift with respect to the detuning is again the dispersion. One can then avoid the integration and still find a signal which is directly proportional to the dispersion.

In Fig. 1.4 we plot the results of several simulation for various values of the coupling capacity. The left column shows the current flowing through the inductor L_1 ; in the central column one can read the voltage drop at the poles of L_1 ; the right column presents the phase shift between the voltage at the input of L_1 and the output of the signal generator.

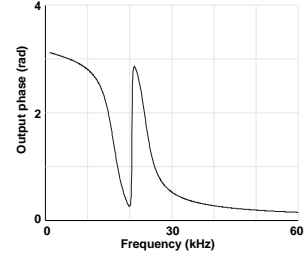
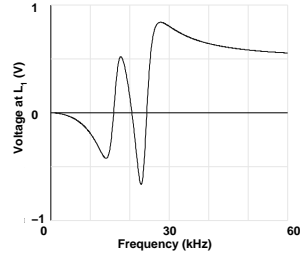
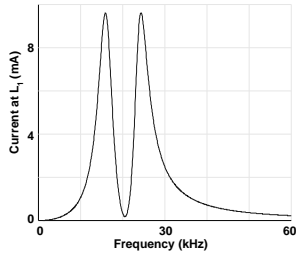
According to what we have explained, the left column simulates the absorptive behaviour of the probe laser within the Λ -system and the right column its dispersive characteristics. From this classical analog one understands that EIT arises because of the destructive interference between two oscillators.



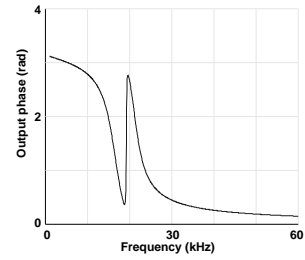
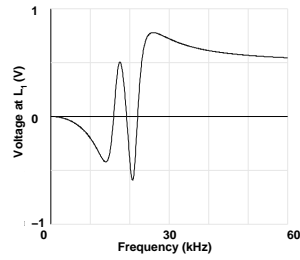
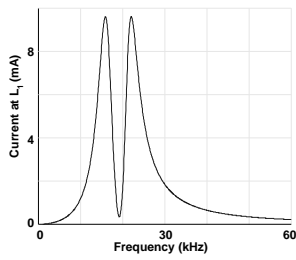
$C=47$ nF, closed circuit.



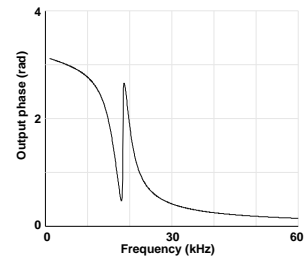
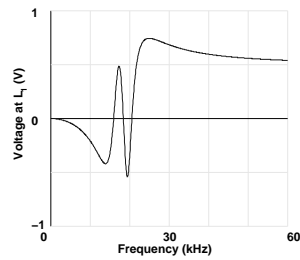
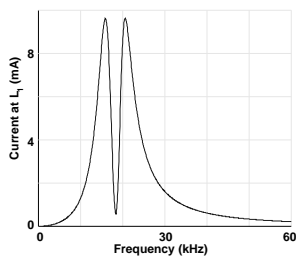
$C=100$ nF, closed circuit.



$C=150$ nF, closed circuit.

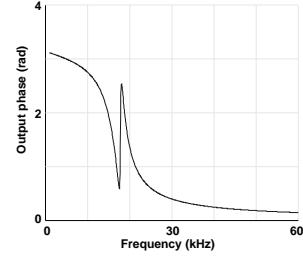
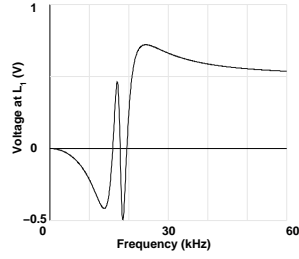
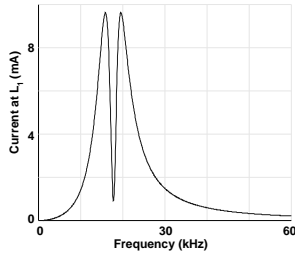


$C=220$ nF, closed circuit.

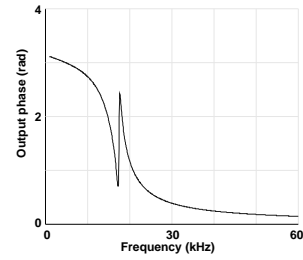
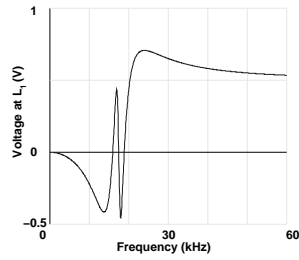
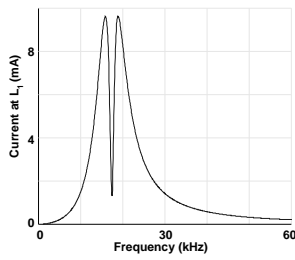


$C=300$ nF, closed circuit.

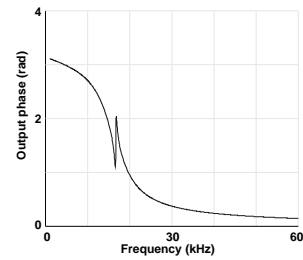
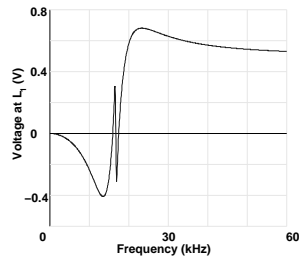
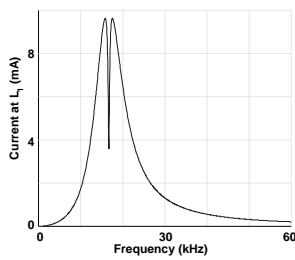
1.3 Classical analog of electromagnetically induced transparency



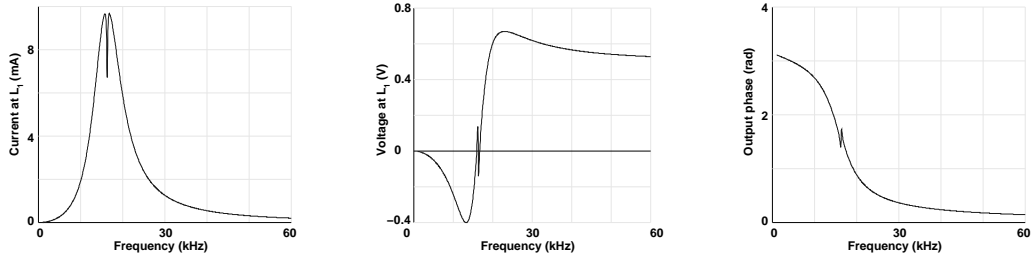
$C=400$ nF, closed circuit.



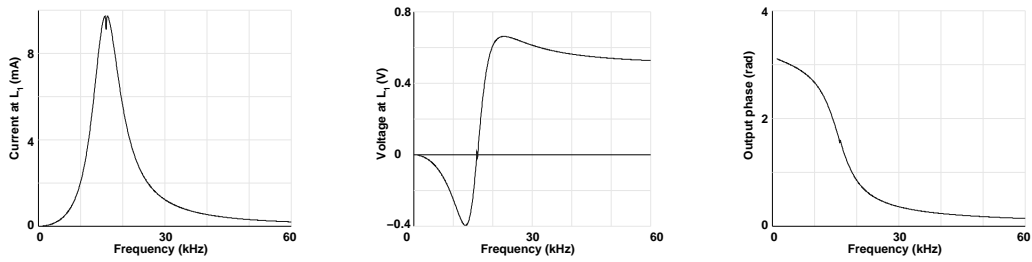
$C=500$ nF, closed circuit.



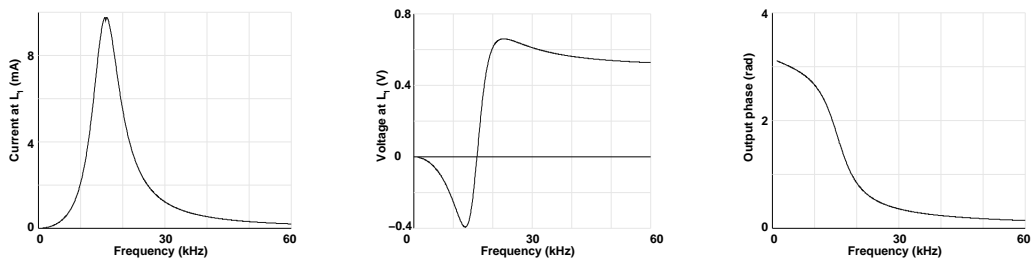
$C=1$ μ F, closed circuit.



$C=2\ \mu\text{F}$, closed circuit.



$C=5\ \mu\text{F}$, closed circuit.



$C=10\ \mu\text{F}$, closed circuit.

Figure 1.4: Simulation results for the circuit depicted in Fig. 1.3

1.4 Semiclassical models

To further describe the spectroscopic results of the measurements performed in this work we need to introduce an appropriate formalism. Among the various possibilities it is often convenient to introduce a semiclassical treatment in which the atoms are quantised but the electromagnetic fields are still treated as classical ones. Within this formalism it is simple to introduce a description which can be easily related to what happens in the experiment. Since a large quantity of atoms is involved, the best suited formalism is the one involving the so-called density matrix.

1.4.1 Density matrix formalism

For a system consisting of large amount of replica identical particles, it is practically impossible to have a complete information on the prepared system, thus being able to describe it in terms of a pure state. Therefore, one cannot follow the pure Schrödinger formalism. The statistical knowledge one has on the various replicas of the system may be used if one works with the so-called density matrix formalism, in which to each state $|\psi\rangle$ is associated the classical probability P_ψ . In this context the density matrix operator is defined as

$$\rho = \sum_{\psi} P_{\psi} |\psi\rangle \langle \psi|.$$

Similarly to the Schrödinger equation for pure states, the evolution of the system is described by the Liouville-von Neumann equation

$$\dot{\rho} = -\frac{i}{\hbar} [H, \rho].$$

In treating with atomic transitions it is convenient to separate the Hamilton operator into a time independent part H_0 , which gives rise to what we describe as the unperturbed atomic states, and a perturbative time-dependent part $H_{\text{int}}(t)$ which represents the interaction of the atom with the electromagnetic field. Such an approximation is valid as long as the wavelength of the electromagnetic field is small in comparison with the spatial dimensions of the atom. This approximation is known as long-wavelength dipole approximation. In this scheme one can decompose the Hamiltonian as

$$H = H_0 + H_{\text{int}}(t).$$

It is easy to understand several details of the formalism used if one concentrates for a moment on an ideal two-level system. In this case one could rewrite the unperturbed Hamiltonian in the form

$$H_0 = \hbar\omega_a |a\rangle \langle a| + \hbar\omega_b |b\rangle \langle b|,$$

where ω_a and ω_b are the eigenfrequencies of the atom with respect to an arbitrary chosen fixed energy offset. The interaction with the external electromagnetic field is described through the Hamiltonian (in the dipole approximation)

$$H_{\text{int}} = -(\mu_{ab}|a\rangle\langle b| + \mu_{ba}|b\rangle\langle a|)E(t),$$

where $\mu_{ab} = e\langle a|x|b\rangle$ is the matrix element of the dipole operator ex (we assume in this simple case to have an electrical field polarised in the x direction).

In the context of the dipole approximation it is useful to introduce the reduced Rabi frequencies¹. As we will see, the Rabi frequencies (their reciprocals) describe the timescale of the evolution of the atomic system under the influence of the external field and relate it to the intensity of the field itself. If one writes the electrical field in the form

$$E(t) = E_0 \cos(\omega t)$$

the reduced Rabi frequencies would be defined as²

$$\Omega = \frac{\mu E_0}{2\hbar}. \quad (1.1)$$

When one describes the system with the density operator in the way we have introduced here one makes very relevant assumptions. The most important of these assumptions is that the effect of the spontaneous emission in the processes described is completely neglected, as if it were not existing. To describe it, it is usually sufficient the further introduction of a phenomenological term in the Liouville-von Neumann equation. This can be done in an easy way (we follow here a suggestion of Arimondo [7]) introducing a relaxation operator R which describes several different relaxation processes taking place in the system. After this introduction, the Liouville-von Neumann equation becomes

$$\dot{\rho} = -\frac{i}{\hbar}[H, \rho] + R\rho. \quad (1.2)$$

Clearly, the form of the relaxation operator is a priori completely undetermined. The derivation of such an operator from more general concepts involves several assumptions about the way relaxation affects the system and on the physical mechanisms involved in it. Some assumptions regarding the spontaneous processes are sketched in the following section. In general the relaxation operator will account also for relaxation due to collisions or other effects. We will describe later (paragraph 1.4.4) how these additional terms can affect our system.

¹Unfortunately there is some inconsistency in the literature on what has to be called *Rabi frequency*. Sometimes the here defined reduced Rabi frequencies are called Rabi frequencies, some other times the value assumed for the Rabi frequencies is twice as big. Following some other authors I chose to call the smaller value of the two *reduced Rabi frequency*

²The reduced Rabi frequency introduced here are assumed to be real quantities.

1.4.2 Spontaneous processes within the density matrix formalism

It must be stressed that, when one introduces spontaneous emission terms into the Liouville-von Neumann equation, this is done for pure phenomenological reasons. This is in general true if the Schrödinger formalism is used, because in this description the electronic excited states are not subject to spontaneous processes. It is therefore impossible, within the formalism of the first quantisation and following strictly the approximations made here, to deduce spontaneous emission from general principles. We will soon see that, for level configurations more complicated than the two-level system, spontaneous emission is not the only effect which plays a relevant role in the evolution of the system.

In principle, if one wants to account for several other effects (including spontaneous emission), which emerge from time to time, a more appropriate Hamiltonian describing the interaction of the atom with an external field would be (see, for instance, [11])

$$H = H_0 + H_{\text{int}}(t) + H_R,$$

where the electric field included in $H_{\text{int}}(t)$ must be intended as the sum of the electric field due to the external field and the electric field associated with the quantum fluctuations of the vacuum (to which we will associate a Hamiltonian V), and H_R is the Hamiltonian of the quantum field accounting for all possible states of the vacuum. If in the Hamiltonian one neglects the coupling with the vacuum one obtains the usual Liouville-von Neumann equation for the evolution of the system. If, on the other side, one neglects the effect of the impinging radiation the vacuum can be interpreted as a reservoir of possible states coupled to the atom through electromagnetic interactions with it.

In this last case the density operator for the atomic system has to be intended as the partial trace of a more general density operator (accounting for the atom and the vacuum) over all possible states of the reservoir. In more mathematical terms if ρ is the density operator for the system composed by the atom and the vacuum, one introduces a "reduced" density operator of the form

$$\sigma = \text{Tr}_R \rho.$$

For a two level system this density matrix can be written as

$$\begin{pmatrix} \sigma_{aa} & \sigma_{ab} \\ \sigma_{ba} & \sigma_{bb} \end{pmatrix}.$$

In this formalism the diagonal elements of the density matrix are called *populations* and the off-diagonal terms *coherences*. For an ensemble of two-level atoms the diagonal terms represent indeed quantities proportional to the fraction of atoms being in one or another level, while the coherences are quantities oscillating at frequency $|\omega_a - \omega_b|$ which may be put in connection with physical variables such as the atomic dipole moment.

We want to show that, under the thermal interaction with the vacuum, the atom behaves in a way which is analogous to that of a particle in Brownian motion. Simultaneously, the vacuum will not be much affected by its interaction with the atom, therefore playing the

role of a *reservoir*. As it is the case for the Brownian motion, observing the evolution of the atom it is possible to identify two time-scales. There is a shorter time-scale (say of the order of τ) in which the system experiences one possible perturbation of the vacuum (i.e. is subject to one virtual transition). A longer time-scale (say of the order of T) describes the usual evolution of the atom or, in other terms, its variation of state induced by the interaction with the vacuum (e.g. a spontaneous emission process). It can be shown (see, for example, chapter IV in [11]) that the various fluctuations of the vacuum have a correlation which becomes neglectable very rapidly (timescale τ), much more rapidly than the time associated with spontaneous emission (which is given by $\frac{1}{\gamma_{ba}}$ and represents the timescale T) and still more rapidly than the period Δt associated to a typical atomic transition $\frac{2\pi}{\omega_a - \omega_b}$. Starting from these premises it can be also shown (ibid.) that for a two-level system interacting with other possible atomic levels (designed by general indices c and d) the density operator satisfies the following equation

$$\frac{d}{dt}\sigma_{ab}(t) \simeq -i\omega_{ab}\sigma_{ab}(t) + \sum_{c,d}^{(sec)} \mathcal{R}_{abcd}\sigma_{cd}(t).$$

Only those transitions which satisfy the relation $|\omega_{ab} - \omega_{cd}| \ll \frac{1}{\Delta t}$ (including of course the transition itself) are significant for the evolutions of coherences or populations involving levels $|a\rangle$ and $|b\rangle$. These transitions are called *secular* transitions and therefore the sum is restricted to the secular terms only. In principle the sum does not need to be limited to the secular terms. However, all other terms for which $|\omega_{ab} - \omega_{cd}| \gg \frac{1}{\Delta t}$ become negligible (it can be demonstrated [11] that each term which appears in \mathcal{R}_{abcd} contains a function of the form $\frac{\sin(\omega_{ab} - \omega_{cd})}{(\omega_{ab} - \omega_{cd})}$) while the terms for which $|\omega_{ab} - \omega_{cd}| \sim \frac{1}{\Delta t}$ can be proved to have only a weak effect if the condition $\Delta t \ll T$ is satisfied. The \mathcal{R}_{abcd} coefficients describe the interaction mediated by the reservoir and, within the approximation made, are independent of t and Δt and are of the order of $\frac{1}{T}$.

It is now clear that it can make a relevant difference if the system is degenerate or not. The equations for the non-degenerate two-level system can be rewritten in the form³ [11]

$$\frac{d}{dt}\sigma_{bb} = -\gamma_{ba}\sigma_{bb}, \tag{1.3a}$$

$$\frac{d}{dt}\sigma_{aa} = +\gamma_{ba}\sigma_{bb}, \tag{1.3b}$$

$$\frac{d}{dt}\sigma_{ba} = -i(\omega_{ba} + \Delta_{ba})\sigma_{ba} - \frac{\gamma_{ba}}{2}\sigma_{ba}. \tag{1.3c}$$

The γ_{ba} coefficients, representing the usual spontaneous emission processes, originate from coefficients of the form \mathcal{R}_{bbaa} while the coefficients \mathcal{R}_{baba} originate contributions of the form $-\gamma_{ba} - i\Delta_{ba}$. The shift Δ_{ba} is a radiative shift of the actual frequency of the transition induced by the interaction with the vacuum.

In the previous expressions all other \mathcal{R}_{abcd} coefficients have been neglected. For the population equations this approximation is justified by the fact that the atomic coherences

³We remark once more that the system is not subject to any other electromagnetic field than that of the vacuum; the processes emerging here are therefore sometimes called spontaneous processes.

typically evolve on a timescale of Δt which is the typical time for atomic transitions. For frequencies $\omega \ll \Delta t^{-1}$, i.e. interaction times much longer than Δt , these coherences do not play any further role in the evolution of the populations. In the equations for the coherences the only term of the form \mathcal{R}_{abcd} which still plays a relevant role is the one for which $a = c$ and $b = d$ (because we are in a non-degenerate situation but we have to take into account all transitions for which $|\omega_{ab} - \omega_{cd}| \ll \frac{1}{\Delta t}$, including the transition itself). As described above, this term causes the frequency radiative shift Δ_{ba} and is responsible for the damping Γ_{ba} of the coherences.

The previous considerations for the coherences are not true if one is in the presence of a degenerate two-level system. For a degenerate system \mathcal{R}_{abcd} contains also matrix elements of the electromagnetic interaction with the vacuum V which have the form $\langle a|V|c\rangle\langle d|V|b\rangle$ (where the states $|a\rangle$ and $|c\rangle$ are degenerate, as well as $|b\rangle$ and $|d\rangle$), and we assume $a \neq c$ and $b \neq d$). Those matrix elements cannot be neglected: they couple diverse degenerate levels and give rise to non-oscillating terms which do not disappear through the calculations. The effect of such terms is to enable a transfer of coherence between the coherence of the upper degenerate levels and that of the lower degenerate levels. Since this transfer can happen even in the absence of applied external fields it is sometimes called *spontaneous transfer of coherence*. This spontaneous transfer of coherence can often be neglected, especially because it does not usually change the phenomenology of the observed experimental results. In some cases, however, the effect induced by the spontaneous transfer of coherence may be very relevant. One of these cases is, as we will see in the following, electromagnetically induced absorption.

If we now go back to our two-level system, it is not completely uninteresting to see how the equations for its evolution change in the presence of a weak coupling field. In this case the equations can be rewritten as

$$\frac{d}{dt}\sigma_{bb} = -\gamma_{ba}\sigma_{bb} + \gamma'_{ba}(\sigma_{aa} - \sigma_{bb}), \quad (1.4a)$$

$$\frac{d}{dt}\sigma_{aa} = +\gamma_{ba}\sigma_{bb} + \gamma'_{ba}(\sigma_{bb} - \sigma_{aa}), \quad (1.4b)$$

$$\frac{d}{dt}\sigma_{ba} = -i(\omega_{ba} + \Delta_{ba} + \Delta'_{ba})\sigma_{ba} - \frac{\gamma_{ba} + 2\gamma'_{ba}}{2}\sigma_{ba}. \quad (1.4c)$$

Qualitatively speaking the external field changes the structure of the population equations only, which contain further terms accounting for induced absorption and emission. The populations equations assume then the known form of the Einstein equations. To recognise it it suffices to point out that the terms in γ'_{ba} are proportional to the intensity of the impinging field at the frequency ω_{ba} of the transition. The structure of the coherence equations does not change dramatically. A further radiative shift and a further damping are introduced by the radiation.

As for the case without radiation, further terms accounting for the spontaneous transfer of coherence have to appear in the equations for the coherences any time one has to do with degenerate systems.

Similar arguments can be extended to the case of an atom interacting with a strong

resonant electromagnetic field. We will see in the following sections that in this case it is possible to rewrite the equations in the form

$$\frac{d}{dt}\sigma_{bb} = -\gamma_{ba}\sigma_{bb} + i\Omega_{ba}(\sigma_{ba} - \sigma_{ab}), \quad (1.5a)$$

$$\frac{d}{dt}\sigma_{aa} = +\gamma_{ba}\sigma_{bb} - i\Omega_{ba}(\sigma_{ba} - \sigma_{ab}), \quad (1.5b)$$

$$\frac{d}{dt}\sigma_{ba} = -i\delta\sigma_{ba} - \frac{\gamma_{ba}}{2}\sigma_{ba} + i\Omega_{ba}(\sigma_{bb} - \sigma_{aa}), \quad (1.5c)$$

where

$$\delta = \omega - \omega_0$$

and $\omega_0 = \omega_{ba} + \Delta_{ba}$ is the transition frequency corrected with its radiative shifts. It is clear that even in this case the equations for the coherences are valid only for the non-degenerate case. For the degenerate case one has once again to introduce the spontaneous transfer of coherence.

The conclusion of this discussion is that the introduction in the Liouville-von Neumann equations of terms describing spontaneous transfer of coherence can be justified in the same way as the introduction into the Liouville-von Neumann equation of the supplementary term accounting for the spontaneous emission. For this reason we will at some point introduce spontaneous transfer of coherence in a form that, even if it seems quite arbitrary, is in no way more arbitrary than the introduction in the system of terms describing spontaneous emission.

1.4.3 Electromagnetically induced transparency

Let us return to the Liouville-von Neumann equation (1.2). In this section we want to discuss how equation (1.2) can be written when one operates with a Λ -system. To quantitatively treat the system it is important to characterise the Hamiltonian and the relaxation operator in their components. Calling $|a\rangle$ the upper level of the Λ -system (see Fig. 1.2) and calculating the energy differences with the upper level as a reference level for the energy the unperturbed Hamiltonian can be rewritten as

$$H_0 = -\hbar \begin{pmatrix} 0 & 0 & 0 \\ 0 & \omega_{ab} & 0 \\ 0 & 0 & \omega_{ac} \end{pmatrix}.$$

The interaction matrix describes the electric dipole transitions between the upper level $|a\rangle$ and the two lower levels $|b\rangle$ and $|c\rangle$. No electric dipole transitions are allowed between the levels $|b\rangle$ and $|c\rangle$. In terms of the Rabi frequencies one can write

$$H_{\text{int}} = -\hbar \begin{pmatrix} 0 & 2\Omega_{ab} \cos(\omega_{\text{probe}}t) & 2\Omega_{ac} \cos(\omega_{\text{coupl}}t) \\ 2\Omega_{ab} \cos(\omega_{\text{probe}}t) & 0 & 0 \\ 2\Omega_{ac} \cos(\omega_{\text{coupl}}t) & 0 & 0 \end{pmatrix}. \quad (1.6)$$

Ω_{ab} and Ω_{ac} are the reduced Rabi frequencies of the probe and the coupling beam, respectively, while ω_{probe} and ω_{coupl} are their frequencies.

When using an atomic beam, as it is the case in the experiments described in this work, there is a continuous refill of atoms into the interaction zone which compensate for atoms leaving the interaction zone. However, the refilled atoms are in the ground state(s) and substitute leaving atoms being either in the ground or the excited states, depending on the population distribution. If we call γ_0 the cumulative transient loss due to this process, i.e. the sum of the transient losses taking place at levels $|a\rangle$, $|b\rangle$, and $|c\rangle$, and we assume that the energy difference between the two ground system is negligible in terms of the population difference it generates, we can assign an injection rate of $\gamma_0/2$ to each ground level (one assumes that the population does not change during the experiment). This approximation is exact in case of a degenerate system where the ground level is repopulated with an injection rate γ_0 , the sum of the two values $\gamma_0/2$ previously considered.

One can easily show that the previous approximation is valid in the case of caesium atoms probed and coupled within the D_2 line, even when non-degenerate ground levels are considered (proper Λ configuration). Indeed, the energy differences corresponding to the atomic transitions are of the order of $h\nu_{bc} \approx 6.1 \times 10^{-24}$ J and $h\nu_{ac} \approx 2.3 \times 10^{-19}$ J, while the energy corresponding to the thermal excitation is of the order of $kT \approx 6.3 \times 10^{-21}$ J to 7.08×10^{-21} J depending on the temperature considered (here 453 K to 513 K). The calculated energies show that the temperature of the system is sufficient to consistently populate the $|b\rangle$ and $|c\rangle$ levels but not the level $|a\rangle$. Moreover, there can be a further thermalisation between the levels $|b\rangle$ and $|c\rangle$ caused by collisions between the atoms in the atomic beam that adjusts population differences between the levels $|b\rangle$ and $|c\rangle$. For this reason it is legitimate to assume that all atoms entering the interaction zone are equally distributed between one of the two ground levels.

It is also almost always a good approximation to work in the so-called *rotating wave approximation*, i.e. to neglect rapidly oscillating terms in the Hamiltonian. An easy way to do it is to rewrite equation (1.6) in the form

$$H_{\text{int}} = -\hbar \begin{pmatrix} 0 & \Omega_{ab}e^{i\omega_{\text{probe}}t} & \Omega_{ac}e^{i\omega_{\text{coupl}}t} \\ \Omega_{ab}e^{-i\omega_{\text{probe}}t} & 0 & 0 \\ \Omega_{ac}e^{-i\omega_{\text{coupl}}t} & 0 & 0 \end{pmatrix}.$$

Furthermore, since in our system the propagation direction of the electromagnetic fields is perpendicular to that of the atomic beam, it is a legitimate approximation to neglect the Doppler shift of the involved frequencies.

For the following calculations it is useful to quantify the spontaneous emission from level $|a\rangle$ with two spontaneous emission coefficients γ_{ab} and γ_{ac} and define the following detunings:

$$\begin{aligned} \Delta_{ab} &\doteq \omega_{\text{probe}} - \omega_{ab}, \\ \Delta_{ac} &\doteq \omega_{\text{coupl}} - \omega_{ac}, \\ \delta &\doteq \Delta_{ab} - \Delta_{ac}. \end{aligned}$$

Finally, to simplify the calculations one can change the coordinate system to a system corotating with the electromagnetic waves acting on the transitions. In this coordinate system the unperturbed Hamiltonian can be rewritten as

$$H_0 = \hbar \begin{pmatrix} 0 & 0 & 0 \\ 0 & \Delta_{ab} & 0 \\ 0 & 0 & \Delta_{ac} \end{pmatrix}.$$

In this coordinate system the interaction Hamiltonian is

$$H_{\text{int}} = \hbar \begin{pmatrix} 0 & \Omega_{ab} & \Omega_{ac} \\ \Omega_{ba} & 0 & 0 \\ \Omega_{ca} & 0 & 0 \end{pmatrix}.$$

The rotation of the coordinate system can be seen as a calculation in the interaction picture, where the atomic states of the unperturbed Hamiltonian remain unchanged but the operators evolve under the action of the interaction Hamiltonian.

To complete the description in this new coordinate system one needs to perform also the following substitutions

$$\begin{aligned} \rho_{ab} &\rightarrow \rho_{ab} e^{i\omega_{\text{probe}} t} \\ \rho_{ac} &\rightarrow \rho_{ac} e^{i\omega_{\text{coupl}} t} \\ \rho_{bc} &\rightarrow \rho_{bc} e^{i(\omega_{\text{probe}} - \omega_{\text{coupl}}) t}. \end{aligned}$$

If one defines the quantities

$$\begin{aligned} \Gamma_{ab} &\doteq \frac{1}{2}(2\gamma_0 + \gamma_{ab} + \gamma_{ac}) - i\Delta_{ab}, \\ \Gamma_{ac} &\doteq \frac{1}{2}(2\gamma_0 + \gamma_{ab} + \gamma_{ac}) - i\Delta_{ac}, \\ \Gamma_{bc} &\doteq \gamma_0 + i\delta, \end{aligned}$$

the Liouville-von Neumann equation (1.2) can be rewritten in term of its matrix elements as

$$\begin{aligned} \dot{\rho}_{aa} &= -(\gamma_0 + \gamma_{ab} + \gamma_{ac})\rho_{aa} - i(\Omega_{ab}\rho_{ba} - \Omega_{ba}\rho_{ab}) - i(\Omega_{ac}\rho_{ca} - \Omega_{ca}\rho_{ac}), \\ \dot{\rho}_{bb} &= \frac{\gamma_0}{2} - \gamma_0\rho_{bb} + \gamma_{ab}\rho_{aa} + i(\Omega_{ab}\rho_{ba} - \Omega_{ba}\rho_{ab}), \\ \dot{\rho}_{cc} &= \frac{\gamma_0}{2} - \gamma_0\rho_{cc} + \gamma_{ac}\rho_{aa} + i(\Omega_{ac}\rho_{ca} - \Omega_{ca}\rho_{ac}), \\ \dot{\rho}_{ab} &= -\Gamma_{ab}\rho_{ab} - i\Omega_{ab}(\rho_{bb} - \rho_{aa}) - i\Omega_{ac}\rho_{cb}, \\ \dot{\rho}_{ac} &= -\Gamma_{ac}\rho_{ac} - i\Omega_{ac}(\rho_{cc} - \rho_{aa}) - i\Omega_{ab}\rho_{bc}, \\ \dot{\rho}_{bc} &= -\Gamma_{bc}\rho_{bc} + i\Omega_{ac}\rho_{ba} - i\Omega_{ba}\rho_{ac}. \end{aligned}$$

The former equations are known in the literature as optical Bloch equations (sometimes abbreviated in OBE). One can, of course, write OBE for different level systems, starting from the simple case of the two-level system (see, for example, eqs. (1.5)). The name of

the OBE traces back to some equations written by F. Bloch for the evolution of a spin precessing in an oscillating magnetic field [9]. The optical Bloch equations completely characterise the evolution of an atomic system under the action of a strong electromagnetic field.

Typically, one is not interested in the transient response of the system but in its stationary state. To calculate the stationary response of the system it is sufficient to set the time derivatives of the density matrix components to zero in the OBE, thus obtaining the desired results. In this way it is easy to calculate quantities of experimental interest, such as the dispersion or the absorption of the atomic medium. In the present case one obtains the following stationary optical Bloch equations:

$$\begin{aligned}\rho_{aa} &= \frac{1}{(\gamma_0 + \gamma_{ab} + \gamma_{ac})} [-i(\Omega_{ab}\rho_{ba} - \Omega_{ba}\rho_{ab}) - i(\Omega_{ac}\rho_{ca} - \Omega_{ca}\rho_{ac})], \\ \rho_{bb} &= \frac{1}{\gamma_0} \left[\frac{\gamma_0}{2} + \gamma_{ab}\rho_{aa} + i(\Omega_{ab}\rho_{ba} - \Omega_{ba}\rho_{ab}) \right], \\ \rho_{cc} &= \frac{1}{\gamma_0} \left[\frac{\gamma_0}{2} + \gamma_{ac}\rho_{aa} + i(\Omega_{ac}\rho_{ca} - \Omega_{ca}\rho_{ac}) \right], \\ \rho_{ab} &= \frac{1}{\Gamma_{ab}} [-i\Omega_{ab}(\rho_{bb} - \rho_{aa}) - i\Omega_{ac}\rho_{cb}], \\ \rho_{ac} &= \frac{1}{\Gamma_{ac}} [-i\Omega_{ac}(\rho_{cc} - \rho_{aa}) - i\Omega_{ab}\rho_{bc}], \\ \rho_{bc} &= \frac{1}{\Gamma_{bc}} [i\Omega_{ac}\rho_{ba} - i\Omega_{ba}\rho_{ac}].\end{aligned}$$

Assuming identical spontaneous emission coefficients for the two transitions (i.e. $\gamma_{ab} = \gamma_{ac}$) it is convenient to define

$$\gamma \doteq \gamma_{ab} + \gamma_{ac},$$

or $\gamma_{ab} = \gamma_{ac} \doteq \frac{\gamma}{2}$. With this definition the Liouville-von Neumann equation can be rewritten in the compact form

$$\dot{\rho} = -\frac{i}{\hbar} [H_0 + H_{\text{int}}, \rho] - \frac{\gamma}{2} \{P_e, \rho\} + \gamma \sum_{q=1,2} Q_q^\dagger \rho Q_q - \gamma_0 \rho + \frac{\gamma_0}{2} P_g,$$

where $Q_1 = |a\rangle\langle c|$ and $Q_2 = |a\rangle\langle b|$ and the braces stay for the anticommutator. Furthermore, $P_e \doteq |a\rangle\langle a|$ is the projector on the excited state and $P_g \doteq |b\rangle\langle b| + |c\rangle\langle c|$ the projector on the ground states.

1.4.4 Electromagnetically induced absorption

Electromagnetically induced absorption can be considered as the experimental counterpart of electromagnetically induced transparency. However, while dark lines were discovered in the late seventies [6], bright states were firstly observed in the late nineties [1]. The reason for the delay is to be explained by the fact that stricter conditions had to

be satisfied to obtain electromagnetically induced absorption. Furthermore, since spontaneous transfer of light-induced anisotropy (coherence or, in other cases, population) is essential for the explanation of EIA, one has to abandon the simple three-level scheme in favour of a more complicated model which involves at least four atomic energy levels and three laser fields.

Electromagnetically induced absorption was firstly observed in a closed transition within the D_2 line of rubidium [1]. During these first observations it was stated that the occurrence of electromagnetically induced absorption is related to the following conditions:

1. The transition between the ground level and the excited level must be closed (i.e. no other electric dipole transitions are allowed so that spontaneous emission cannot play a relevant role).
2. The ground level must be degenerate (i.e. the condition $F > 0$ must be fulfilled).
3. The total angular momentum of the excited level F' must be greater than the angular momentum of the ground level (i.e. $F' > F$).

Similarly for rubidium, the D_2 line of caesium contains a closed transition which satisfies all three above mentioned conditions: the transition $F = 4 \longrightarrow F' = 5$. Furthermore, the line contains a second closed system which violates the third condition: the transition $F = 3 \longrightarrow F' = 2$.

It was later understood that the first condition must not be interpreted strictly. However, its fulfillment results in a good contrast of the signals, which is otherwise affected by spontaneous emission processes to other atomic levels.

Shortly after its discovery, an interpretation of electromagnetically induced absorption was developed for a four level scheme [39]. This interpretation explained electromagnetically induced absorption as an effect generated through spontaneous transfer of coherence. Such an interpretation was later supported through several numerical calculations. Unfortunately, the role of spontaneous transfer of coherence as a new effect has often been misinterpreted. Some authors have spoken of transfer of coherence induced by spontaneous emission, thus contributing to further confusion. It must be stressed once more that, even if spontaneous emission and spontaneous transfer of coherence both emerge because of interactions with the vacuum, their roles are not necessarily interlinked and each one is not caused by the other one.

It is opportune now to introduce the theory of electromagnetically induced absorption for a four level system in the N configuration. Subsequently we will see how this model can be extended to multilevel systems. This approach is justified by the fact that the measurements performed during this work were mostly conducted in degenerate two-level systems and that the simplest subsystem of a degenerate two-level system in which spontaneous transfer of coherence can appear is a so-called N-system. A pictorial representation of such a system is given in Fig. 1.5.

Following the approach given in reference [39] we write the Hamiltonian for the atom in

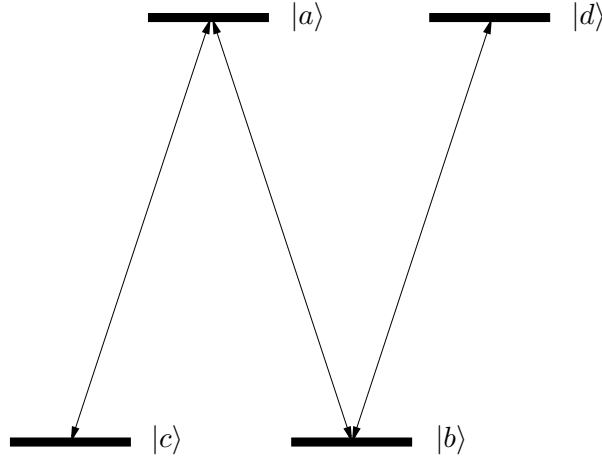


Figure 1.5: Energy diagram of an N-system.

the rotating frame as

$$H_0 = \hbar \begin{pmatrix} 0 & 0 & 0 & 0 \\ 0 & \Delta_{ab} & 0 & 0 \\ 0 & 0 & \Delta_{ac} & 0 \\ 0 & 0 & 0 & \delta \end{pmatrix}.$$

We assume that electric dipole transitions are not allowed between level $|d\rangle$ and levels $|a\rangle$ and $|c\rangle$. Using once more the rotating wave approximation the interaction matrix takes the form

$$H_{\text{int}} = \hbar \begin{pmatrix} 0 & \Omega_{ab} & \Omega_{ac} & 0 \\ \Omega_{ba} & 0 & 0 & \Omega_{bd} \\ \Omega_{ca} & 0 & 0 & 0 \\ 0 & \Omega_{db} & 0 & 0 \end{pmatrix}.$$

Since the transitions $|a\rangle \rightarrow |c\rangle$ and $|b\rangle \rightarrow |d\rangle$ are both coupled through the coupling laser, the ratio between Ω_{ac} and Ω_{bd} is determined by the atomic transition amplitudes.

In principle, for an atomic system interacting with several monochromatic electromagnetic fields, the description through the optical Bloch equations is sufficient to correctly predict its evolution. However, when writing the Bloch equations, the interaction between the system and the vacuum is usually neglected (spontaneous emission and spontaneous transfer of coherence). We have seen that the neglect of the spontaneous transfer of coherence is justified only when the system does not involve degenerate sublevels which, through the interaction with the vacuum, may introduce supplementary terms in the optical Bloch equations. If one assumes that the spontaneous emission coefficient and the spontaneous transfer of coherence coefficient have the same value γ one can write the Liouville-von Neumann equation for a four level system in the presence of spontaneous transfer of coherence in a compact way. In doing this I will follow, with small variations, the approach proposed in [39].

The Liouville-von Neumann equation for the N-system described here becomes, similarly to the Λ -system case,

$$\dot{\rho} = -\frac{i}{\hbar} [H_0 + H_{\text{int}}, \rho] - \frac{\gamma}{2} \{P_e, \rho\} + \gamma \sum_{q=1,2} Q_q^\dagger \rho Q_q - \gamma_0 \rho + \frac{\gamma_0}{2} P_g.$$

Clearly, in this case it is $P_e \doteq |a\rangle\langle a| + |d\rangle\langle d|$ and $P_g \doteq |b\rangle\langle b| + |c\rangle\langle c|$. Less intuitively the Q_q operators must be assumed of the form $Q_1 \doteq |a\rangle\langle c| + |d\rangle\langle b|$ and $Q_2 \doteq |a\rangle\langle b|$. In this way the term $\sum_{q=1,2} Q_q^\dagger \rho Q_q$ gives the correct expression for spontaneous emission arriving on the ground levels and introduces at the same time a spontaneous transfer of coherence from the upper levels to the lower ones, which has been qualitatively justified in paragraph 1.4.2.

It is possible to write explicitly the expression of the density matrix components. Since here we want to concentrate our attention on the probe laser absorption, to show that spontaneous transfer of coherence may induce electromagnetically induced absorption, we will focus on the equation for the coherence between $|a\rangle$ and $|b\rangle$. The probe absorption is actually proportional to the imaginary part of ρ_{ab} .

The evolution equation for ρ_{ab} is

$$\dot{\rho}_{ab} = -i [\Omega_{ab}(\rho_{bb} - \rho_{aa}) + \Omega_{ac}\rho_{cb} - \Omega_{db}\rho_{ad}] - \frac{\gamma}{2}\rho_{ab} + i\Delta_{ab}\rho_{ab} - \gamma_0\rho_{ab}.$$

In the stationary case the equation reduces to

$$\rho_{ab} = \frac{1}{\gamma_0 + \frac{\gamma}{2} - i\Delta_{ab}} [-i\Omega_{ab}(\rho_{bb} - \rho_{aa}) - i\Omega_{ac}\rho_{cb} + i\Omega_{db}\rho_{ad}].$$

The equation for the coherence between $|a\rangle$ and $|b\rangle$ contains one supplementary term with respect to the Λ -system case: $i\Omega_{db}\rho_{ad}$. This term, however, does not necessarily conduct to an enhanced absorption. It is the term which generates electromagnetically induced transparency in a V-system (where level $|c\rangle$ is not present). However, when the ρ_{ad} coherence "decays" into ρ_{cb} , electromagnetically induced absorption may appear. To see it let us write also the evolution equations for ρ_{cb} and ρ_{ad} :

$$\dot{\rho}_{cb} = -i [\Omega_{ca}\rho_{ab} - \Omega_{ab}\rho_{ca} - \Omega_{db}\rho_{cd}] + \gamma\rho_{ad} + i\delta\rho_{cb} - \gamma_0\rho_{cb}$$

and

$$\dot{\rho}_{ad} = -i [\Omega_{ab}\rho_{bd} + \Omega_{ac}\rho_{cd} - \Omega_{bd}\rho_{ab}] - \gamma\rho_{ad} + i\delta\rho_{ad} - \gamma_0\rho_{ad}.$$

It can be seen that, beside the terms which appear also in the evolution equations for the Λ -system or the V-system, the equations contain the term $\gamma\rho_{ad}$. This term describes the spontaneous transfer of coherence from the excited to the ground states. The stationary equations for ρ_{cb} and ρ_{ad} can be written in the form

$$\rho_{cb} = \frac{1}{\gamma_0 - i\delta} \{-i [\Omega_{ca}\rho_{ab} - \Omega_{ab}\rho_{ca} - \Omega_{db}\rho_{cd}] + \gamma\rho_{ad}\}$$

and

$$\rho_{ad} = \frac{1}{\gamma + \gamma_0 + i\delta} [i\Omega_{bd}\rho_{ab} - i\Omega_{ab}\rho_{bd} - i\Omega_{ac}\rho_{cd}].$$

To proceed in the expansion of the equation for ρ_{ab} we also need three further equations:

$$\begin{aligned} \dot{\rho}_{cd} &= -i[\Omega_{ca}\rho_{ad} - \Omega_{bd}\rho_{cb}] - \frac{\gamma}{2}\rho_{cd} - i(\Delta_{ac} - \delta)\rho_{cd} - \gamma_0\rho_{cd}, \\ \dot{\rho}_{aa} &= -i[\Omega_{ab}\rho_{ba} - \Omega_{ba}\rho_{ab} + \Omega_{ac}\rho_{ca} - \Omega_{ca}\rho_{ac}] - \gamma\rho_{aa} - \gamma_0\rho_{aa}, \\ \dot{\rho}_{bb} &= -i[\Omega_{ba}\rho_{ab} - \Omega_{ab}\rho_{ba} + \Omega_{bd}\rho_{db} - \Omega_{db}\rho_{bd}] + \gamma(\rho_{aa} + \rho_{dd}) - \gamma_0\rho_{bb}. \end{aligned}$$

In the stationary case the three previous equation become:

$$\begin{aligned} \rho_{cd} &= \frac{1}{\gamma_0 + \frac{\gamma}{2} + i(2\Delta_{ac} - \Delta_{ab})} [i\Omega_{bd}\rho_{cb} - i\Omega_{ca}\rho_{ad}], \\ \rho_{aa} &= \frac{1}{\gamma + \gamma_0} [i\Omega_{ba}\rho_{ab} - i\Omega_{ab}\rho_{ba} + i\Omega_{ca}\rho_{ac} - i\Omega_{ac}\rho_{ca}], \\ \rho_{bb} &= \frac{1}{\gamma_0} [i\Omega_{ab}\rho_{ba} - i\Omega_{ba}\rho_{ab} + i\Omega_{db}\rho_{bd} - i\Omega_{bd}\rho_{db} + \gamma(\rho_{aa} + \rho_{dd})]. \end{aligned}$$

Even if the equations are entangled with one another they can be disentangled in the low saturation approximation. One assumes that $\Omega_{ij} \ll \gamma$. In this case it is possible to neglect ρ_{aa} and ρ_{ad} any time they appear in the equations for the other coherences, because they are of the order of $\frac{\Omega_{ij}}{\gamma}$. On the other side, we have to keep terms like ρ_{cb} and ρ_{bb} because they contain contributions of the order of $\frac{\Omega_{ij}}{\gamma_0}$. Within this approximation the stationary equations for ρ_{ad} , ρ_{cb} , ρ_{ab} and ρ_{cd} can be reduced to

$$\rho_{ab} = \frac{1}{\gamma_0 + \frac{\gamma}{2} - i\Delta_{ab}} [-i\Omega_{ab}\rho_{bb} - i\Omega_{ac}\rho_{cb}], \quad (1.7a)$$

$$\rho_{cb} = \frac{1}{\gamma_0 - i\delta} [i\Omega_{ab}\rho_{ca} - i\Omega_{ca}\rho_{ab} + i\Omega_{db}\rho_{cd} + \gamma\rho_{ad}], \quad (1.7b)$$

$$\rho_{ad} = \frac{1}{\gamma + \gamma_0 + i\delta} [i\Omega_{bd}\rho_{ab} - i\Omega_{ab}\rho_{bd} - i\Omega_{ac}\rho_{cd}], \quad (1.7c)$$

$$\rho_{cd} = \frac{1}{\gamma_0 + \frac{\gamma}{2} + i(2\Delta_{ac} - \Delta_{ab})} [i\Omega_{bd}\rho_{cb}]. \quad (1.7d)$$

We can rewrite equation (1.7b) as

$$-i\Omega_{db}\rho_{cd} + (\gamma_0 - i\delta)\rho_{cb} - \gamma\rho_{ad} = -i\Omega_{ca}\rho_{ab} + i\Omega_{ab}\rho_{ca}.$$

Substituting the values for ρ_{cd} and ρ_{ab} expressed in (1.7d) and (1.7a) the previous equation becomes

$$\frac{\Omega_{db}\Omega_{bd}}{\frac{\gamma}{2} + \gamma_0 + i(2\Delta_{ac} - \Delta_{ab})}\rho_{cb} + (\gamma_0 - i\delta)\rho_{cb} - \gamma\rho_{ad} = -\frac{\Omega_{ca}\Omega_{ab}\rho_{bb} + \Omega_{ca}\Omega_{ac}\rho_{cb}}{\frac{\gamma}{2} + \gamma_0 - i\Delta_{ab}} + i\Omega_{ab}\rho_{ca}$$

which can be rewritten as

$$\begin{aligned} \left[\frac{|\Omega_{ac}|^2}{\frac{\gamma}{2} + \gamma_0 - i\Delta_{ab}} + \frac{|\Omega_{bd}|^2}{\frac{\gamma}{2} + \gamma_0 + i(2\Delta_{ac} - \Delta_{ab})} + \gamma_0 - i\delta \right] \rho_{cb} - \gamma\rho_{ad} = \\ = -\frac{\Omega_{ab}\Omega_{ca}}{\frac{\gamma}{2} + \gamma_0 - i\Delta_{ab}}\rho_{bb} + i\Omega_{ab}\rho_{ca}. \end{aligned} \quad (1.8)$$

Similarly, one can rewrite equation (1.7c) in the form

$$(\gamma + \gamma_0 + i\delta)\rho_{ad} = i\Omega_{bd}\rho_{ab} - i\Omega_{ab}\rho_{bd} - i\Omega_{ac}\rho_{cd},$$

substitute the value of ρ_{ab} and ρ_{cd} given by (1.7a) and (1.7d) and write

$$\begin{aligned} (\gamma + \gamma_0 + i\delta)\rho_{ad} = \frac{\Omega_{bd}\Omega_{ab}}{\frac{\gamma}{2} + \gamma_0 - i\Delta_{ab}}\rho_{bb} + \\ + \left[\frac{\Omega_{bd}\Omega_{ac}}{\frac{\gamma}{2} + \gamma_0 - i\Delta_{ab}} + \frac{\Omega_{ac}\Omega_{bd}}{\frac{\gamma}{2} + \gamma_0 + i(2\Delta_{ac} - \Delta_{ab})} \right] \rho_{cb} - i\Omega_{ab}\rho_{bd}. \end{aligned}$$

The term between square brackets in the previous equation corresponds to induced transfer of coherence (driven by the coupling laser) between the upper and the lower levels. It can be proven [39] that its contribution is negligible as long as one operates below the saturation regime (as we are doing at present). In this case the equation reduces to

$$(\gamma + \gamma_0 + i\delta)\rho_{ad} \approx \frac{\Omega_{bd}\Omega_{ab}}{\frac{\gamma}{2} + \gamma_0 - i\Delta_{ab}}\rho_{bb} - i\Omega_{ab}\rho_{bd}.$$

Calling D the term in square brackets in equation (1.8) and using the previous expression for ρ_{ad} it is finally possible to rewrite equation (1.7a) in the form

$$\begin{aligned} \rho_{ab} = \frac{-i\Omega_{ab}}{\frac{\gamma}{2} + \gamma_0 - i\Delta_{ab}} \left[\rho_{bb} - \frac{\Omega_{ac}}{\Omega_{ab}} \frac{1}{D} \frac{\Omega_{ab}\Omega_{ca}}{\frac{\gamma}{2} + \gamma_0 - i\Delta_{ab}} \rho_{bb} + \frac{\Omega_{ac}}{\Omega_{ab}} \frac{1}{D} (i\Omega_{ab}\rho_{ca} + \gamma\rho_{ad}) \right] \\ = \frac{-i\Omega_{ab}}{\frac{\gamma}{2} + \gamma_0 - i\Delta_{ab}} \left[\rho_{bb} - \frac{|\Omega_{ac}|^2}{D} \frac{1}{\frac{\gamma}{2} + \gamma_0 - i\Delta_{ab}} \rho_{bb} + i\frac{\Omega_{ac}}{D} \rho_{ca} \right. \\ \left. + \frac{\Omega_{ac}}{\Omega_{ab}} \frac{1}{D} \frac{\Omega_{bd}\Omega_{ab}}{\frac{\gamma}{2} + \gamma_0 - i\Delta_{ab}} \frac{\gamma}{\gamma + \gamma_0 + i\delta} \rho_{bb} - i\frac{\Omega_{ac}}{\Omega_{ab}} \frac{1}{D} \frac{\gamma}{\gamma + \gamma_0 + i\delta} \Omega_{ab}\rho_{bd} \right] \\ = \frac{-i\Omega_{ab}}{\frac{\gamma}{2} + \gamma_0 - i\Delta_{ab}} \left\{ \left[1 - \frac{\Omega_{ac} \left(\Omega_{ca} - \frac{\gamma}{\gamma + \gamma_0 + i\delta} \Omega_{bd} \right)}{\left(\frac{\gamma}{2} + \gamma_0 - i\Delta_{ab} \right) D} \right] \rho_{bb} + i\frac{\Omega_{ac}}{D} \left(\rho_{ca} - \frac{\gamma}{\gamma + \gamma_0 + i\delta} \rho_{bd} \right) \right\}. \end{aligned} \quad (1.9)$$

In the previous equation the terms having as a coefficient $\frac{\gamma}{\gamma + \gamma_0 + i\delta}$ are the ones generated by spontaneous transfer of coherence (as one can easily see tracking the original terms in the Liouville-von Neumann equation).

The probe laser absorption is proportional to the real part of $i\Omega_{ba}\rho_{ab}$. From the previous equation one obtains the following expression for the probe laser absorption coefficient

$$\alpha_{\text{probe}} \propto \left[1 - \frac{\Omega_{ac} \left(\Omega_{ca} - \frac{\gamma}{\gamma + \gamma_0 + i\delta} \Omega_{bd} \right)}{\left(\frac{\gamma}{2} + \gamma_0 - i\Delta_{ab} \right) D} \right] \rho_{bb}.$$

If the spontaneous transfer were absent the absorption would reduce to

$$\alpha_{\text{probe}} \propto \left[1 - \frac{|\Omega_{ac}|^2}{\left(\frac{\gamma}{2} + \gamma_0 - i\Delta_{ab}\right) D} \right] \rho_{bb}.$$

It is evident that the spontaneous transfer of coherence enhances the value of the absorption of the probe laser with respect to its absorption in the absence of transfer of coherence. One can easily see it considering the fact that D contains only positive contributions (apart from $i\delta$), that $\gamma + \gamma_0 + i\delta \approx \gamma$ and that Ω_{ac} and Ω_{bd} have the same order of magnitude, since both Rabi frequencies are generated by the coupling laser (their exact ratio depends on the transition probabilities between the atomic levels). Therefore, in the case of transfer of coherence, the contribution of the second term within the brackets becomes negligible with respect to the first one thus generating a supplementary absorption. The resulting enhanced absorption effect is what is generally called electromagnetically induced absorption.

1.4.5 Stationary solutions of the optical Bloch equations for a Λ -system

As we have seen in paragraph 1.4.3, stationary solutions of the optical Bloch equations can be obtained if one sets the time derivatives of the density matrix components to zero, thus reducing the system to a system of coupled linear equations.

Furthermore, it is known that the dispersion of the coupling and the probe fields are proportional to the real parts of the coherences of the coupled or the probed transition.

Under the assumption of a perfectly resonating coupling field ($\Delta_{ac} = 0$ and, therefore, $\Delta_{ab} = \delta$) the coupling refractive index results proportional to the following quantity

$$\frac{\partial}{\partial \delta} \left(\frac{\Re(\rho_{ac})}{\Omega_{ac}} \right) = \frac{\zeta_{\text{coupl}}}{\eta} \quad (1.10)$$

where

$$\begin{aligned} \zeta_{\text{coupl}} = 4\Omega_{ab}^2 \{ & \gamma_0(\gamma + \gamma_0)(\gamma + 2\gamma_0)(\gamma + 3\gamma_0) + \\ & + [4\gamma_{ab}(\gamma + 4\gamma_0) + 6\gamma_0^2]\Omega_{ac}^2 + [4(\gamma_{ac} + \gamma_0)(\gamma + 2\gamma_0) - 2\gamma_0^2]\Omega_{ab}^2 \} \end{aligned}$$

and

$$\eta = -(2\gamma_0 + \gamma)(2\gamma_0^2 + \gamma\gamma_0 + 2\tilde{\Omega}^2)^2 [\gamma_0(\gamma + \gamma_0)(\gamma + 2\gamma_0) + (4\gamma_{ac} + 8\gamma_0)\Omega_{ab}^2 + (4\gamma_{ab} + 8\gamma_0)\Omega_{ac}^2].$$

Similarly the probe refractive index is proportional to

$$\frac{\partial}{\partial \delta} \left(\frac{\Re(\rho_{ab})}{\Omega_{ab}} \right) = \frac{\zeta_{\text{probe}}}{\eta} \quad (1.11)$$

where

$$\begin{aligned} \zeta_{\text{probe}} = 2\gamma_0(\gamma + \gamma_0) [& \gamma_0(\gamma + 2\gamma_0) + 2\Omega_{ab}^2]^2 - 8(\gamma + 2\gamma_0)(\gamma_0 + 2\gamma_{ab})\Omega_{ac}^4 \\ & - 4\{ \gamma_0(\gamma + 2\gamma_0)(\gamma^2 + \gamma_0^2 + 4\gamma_0\gamma_{ac}) + 2[\gamma_0^2 - 2\gamma_0(\gamma_{ab} - 3\gamma_{ac}) + 2\gamma\gamma_{ac}]\Omega_{ab}^2 \} \Omega_{ac}^2. \end{aligned}$$

The previous results can be used as starting points for several approximations which reflect various experimental situations.

If we assume that $\gamma_0 \ll \gamma, \Omega_{ab}, \Omega_{ac}$ we can develop equation (1.10) grouping powers of γ_0 and neglecting terms of order γ_0^2 or higher.

$$\begin{aligned} \frac{\partial}{\partial \delta} \left(\frac{\Re(\rho_{ac})}{\Omega_{ac}} \right) &\approx - \left(\frac{\Omega_{ab}}{\tilde{\Omega}^2} \right)^2 \left(1 - \frac{\gamma_0 \gamma}{\tilde{\Omega}^2} \right) \\ &\times \left[1 + \frac{8\gamma_0 \gamma_{ab} \Omega_{ac}^2 - 4\gamma_0 \gamma \Omega_{ab}^2 - 8\gamma_0 \gamma \Omega_{ac}^2}{\gamma_0 \gamma^3 + \gamma(4\gamma_{ab} \Omega_{ac}^2 + 4\gamma_{ac} \Omega_{ab}^2) + 8\gamma_0(\gamma_{ac} \Omega_{ab}^2 + \gamma_{ab} \Omega_{ac}^2) + 8\gamma \gamma_0 \tilde{\Omega}^2} \right]. \end{aligned} \quad (1.12)$$

In case of a degenerate Λ -system the transitions $|a\rangle \rightarrow |b\rangle$ and $|a\rangle \rightarrow |c\rangle$ coincide. One can therefore assume that $\gamma_{ab} = \gamma_{ac} = \frac{\gamma}{2}$. This remains a very good approximation even if the Λ -system is non-degenerate (see paragraph 1.4.3). With the previous assumption equation (1.12) becomes

$$\begin{aligned} \frac{\partial}{\partial \delta} \left(\frac{\Re(\rho_{ac})}{\Omega_{ac}} \right) &\approx - \left(\frac{\Omega_{ab}}{\tilde{\Omega}^2} \right)^2 \left(1 - \frac{\gamma_0 \gamma}{\tilde{\Omega}^2} \right) \left[1 - \frac{4\gamma_0 \gamma (\Omega_{ab}^2 + \Omega_{ac}^2)}{\gamma_0 \gamma^3 + 2\gamma^2 (\Omega_{ab}^2 + \Omega_{ac}^2) + 12\gamma_0 \gamma (\Omega_{ab}^2 + \Omega_{ac}^2)} \right] \\ &\approx - \left(\frac{\Omega_{ab}}{\tilde{\Omega}^2} \right)^2 \left(1 - \frac{\gamma_0 \gamma^2 + 2\tilde{\Omega}^2}{\gamma \tilde{\Omega}^2} \right). \end{aligned} \quad (1.13)$$

It is interesting to evaluate the previous result in two extreme cases. One has

$$\frac{\partial}{\partial \delta} \left(\frac{\Re(\rho_{ac})}{\Omega_{ac}} \right) \approx \begin{cases} - \left(\frac{\Omega_{ab}}{\tilde{\Omega}^2} \right)^2 \left(1 - \frac{\gamma_0 \gamma}{\tilde{\Omega}^2} \right) & \text{if } \gamma^2 \gg \tilde{\Omega}^2, \\ - \left(\frac{\Omega_{ab}}{\tilde{\Omega}^2} \right)^2 \left(1 - \frac{2\gamma_0}{\gamma} \right) & \text{if } \tilde{\Omega}^2 \gg \gamma^2. \end{cases}$$

If one considers the equation 5.3 reported in [31] one can easily see that such an expression is valid only in the limit $\gamma^2 \gg \tilde{\Omega}^2$. Equation 5.3 in [31] is

$$n'_{\text{coupl}} \approx C_c \left(\frac{2\Omega_{ab}}{\gamma_0 \gamma + 2\tilde{\Omega}^2} \right)^2$$

and indeed one has

$$\left(\frac{2\Omega_{ab}}{\gamma_0 \gamma + 2\tilde{\Omega}^2} \right)^2 \xrightarrow{\gamma_0 \rightarrow 0} \left(\frac{\Omega_{ab}}{\tilde{\Omega}^2} \right)^2 \left(1 - \frac{\gamma_0 \gamma}{\tilde{\Omega}^2} \right),$$

which has the same asymptotical behaviour as the first of our limits (apart from a missing minus sign therein).

Similar conclusions can be derived starting from equation (1.11). The aim of the calculations is again to eliminate all the terms of $\mathcal{O}(\gamma_0^2)$ or higher. One has therefore

$$\begin{aligned} \frac{\partial}{\partial \delta} \left(\frac{\Re(\rho_{ab})}{\Omega_{ab}} \right) &\approx -\frac{1}{(\gamma_0\gamma + 2\tilde{\Omega}^2)^2} \\ &\times \frac{1}{\gamma_0\gamma^3 + \gamma[(4\gamma_{ac} + 8\gamma_0)\Omega_{ab}^2 + (4\gamma_{ab} + 8\gamma_0)\Omega_{ac}^2] + 2\gamma_0(4\gamma_{ac}\Omega_{ab}^2 + 4\gamma_{ab}\Omega_{ac}^2)} \\ &\times \left\{ 2\gamma\gamma_0(2\Omega_{ab})^2 - 4[\gamma_0\gamma^3 + (-4\gamma_0\gamma_{ab} + 12\gamma_0\gamma_{ac} + 4\gamma\gamma_{ac})\Omega_{ab}^2]\Omega_{ac}^2 \right. \\ &\quad \left. - 8\gamma\gamma_0\Omega_{ac}^4 - 16\gamma\gamma_{ab}\Omega_{ac}^4 - 8(4\gamma_0\gamma_{ab})\Omega_{ac}^4 \right\}. \end{aligned}$$

As we did for the coupling laser the previous expression can be simplified by putting $\gamma_{ab} = \gamma_{ac} = \frac{\gamma}{2}$. So finally one has

$$\frac{\partial}{\partial \delta} \left(\frac{\Re(\rho_{ab})}{\Omega_{ab}} \right) \approx \left(\frac{\Omega_{ac}^2}{\tilde{\Omega}^2} \right)^2 \left[1 - \frac{\gamma_0}{\tilde{\Omega}^2} \frac{\gamma^2\Omega_{ac}^2 + 2\tilde{\Omega}^2\Omega_{ac}^2 + (\tilde{\Omega}^2)^2}{\gamma\Omega_{ac}^2} \right]. \quad (1.14)$$

Similarly to what was done for the coupling laser it is interesting to analyse various limit cases:

$$\frac{\partial}{\partial \delta} \left(\frac{\Re(\rho_{ab})}{\Omega_{ab}} \right) \approx \begin{cases} \left(\frac{\Omega_{ac}}{\tilde{\Omega}^2} \right)^2 \left(1 - \frac{\gamma_0\gamma}{\tilde{\Omega}^2} \right) & \text{if } \gamma^2 \gg \tilde{\Omega}^2, \\ \left(\frac{\Omega_{ac}}{\tilde{\Omega}^2} \right)^2 \left(1 - \frac{3\gamma_0}{\gamma} \right) & \text{if } \tilde{\Omega}^2 \gg \gamma^2 \text{ and } \Omega_{ab} \ll \Omega_{ac} \text{ (weak probing),} \\ \left(\frac{\Omega_{ac}}{\tilde{\Omega}^2} \right)^2 \left(1 - \frac{\gamma_0}{\gamma} \right) & \text{if } \tilde{\Omega}^2 \gg \gamma^2 \text{ and } \Omega_{ab} \gg \Omega_{ac} \text{ (strong probing).} \end{cases}$$

One easily sees that the first of the previous expressions coincides with the approximation made in equation 5.4 in [31]. Equation 5.4 in [31] is

$$n'_{\text{probe}} \approx C_p \left(\frac{2\Omega_{ac}}{\gamma_0\gamma + 2\tilde{\Omega}^2} \right)^2$$

and indeed one has

$$\left(\frac{2\Omega_{ac}}{\gamma_0\gamma + 2\tilde{\Omega}^2} \right)^2 \xrightarrow{\gamma_0 \rightarrow 0} \left(\frac{\Omega_{ac}}{\tilde{\Omega}^2} \right)^2 \left(1 - \frac{\gamma_0\gamma}{\tilde{\Omega}^2} \right).$$

which asymptotically shares the same behaviour with our approximation for the case $\gamma^2 \gg \tilde{\Omega}^2$.

1.4.6 Stationary solutions of the optical Bloch equations for an N-system

In paragraph 1.4.4 we have introduced the formalism necessary to explain the emergence of EIA in an N-system. However, it is evident that in a real atomic system such as those

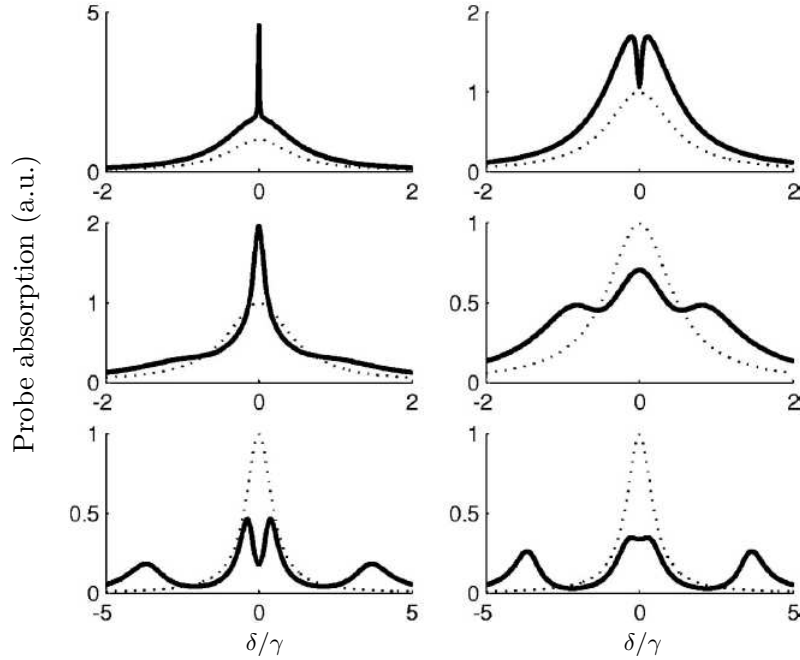


Figure 1.6: Probe absorption in an N-System with (left) and without (right) transfer of coherence for various coupling laser intensities. The dotted lines correspond to the one-photon Lorentzian probe absorption in the absence of coupling laser. The coupling intensity increases from top to bottom (as reported in [18]).

studied by Akulshin, Lezama and collaborators [1, 2, 3] the number of levels involved is much greater. If, in addition, supplementary effects are introduced (such as collisions or the effect of strong probing), the possibility to calculate exact solutions of the OBE (or even approximate ones) is reduced. One has to rely on numerical methods.

More detailed calculations than ours, involving such numerical calculations, were performed in recent years [17, 18]. They were mostly oriented to simulate the response of rubidium. These results can be extended to caesium if one is not interested in the exact behaviour of the atomic medium but in a qualitative explanation of the results experimentally obtained. We will report some of the results here.

First of all let us show how transfer of coherence modifies the absorption spectra of the probe laser. The experimental configuration analysed in [18] (and here presented) corresponds to a σ^+ circularly polarised coupling laser and a parallel π polarised probe laser, the intensity of which is negligible with respect to that of the coupling laser. Figure 1.6 gives the evolution of the absorption spectra of the probe laser in an N-system configuration. The right column represents the absorption in the absence of transfer of coherence. One can see that in the absence of transfer of coherence, at least for low coupling intensities (when the coupling Rabi frequency is much lower than the spontaneous decay coefficient γ), the probe laser would experience a reduced absorption at the two-photon resonance (a kind of EIT-like signal). When the transfer of coherence is introduced, the spectrum

of the probe laser at the two-photon resonance condition shows an enhanced absorption: this is the electromagnetically induced absorption we have calculated in the former paragraph. For increasing coupling laser intensity the electromagnetically induced absorption spectra change and, quite interestingly, the probe laser switches from enhanced absorption to enhanced transparency (at the two-photon resonance).

Before discussing how the absorption and the dispersion spectra in an N-system look like, it is opportune to give a retrospective concerning the probe and coupling spectra in a Λ - and a V-system. It has been proved both experimentally and theoretically [29, 30, 31] that in the case of electromagnetically induced transparency in Λ -systems the coupling laser parametric absorption has a profile which very much resembles the probe laser absorption (EIT). At the same time, while the probe laser experiences positive dispersion the parametric dispersion is negative.

Even if to my knowledge this has not been experimentally tested yet, according to the calculations performed in [18] the similarity between the absorption spectra of the coupling and the probe laser obtained in a Λ -system cannot be expected in a V-system, where, for a probe laser showing electromagnetically induced transparency the coupling laser gives rise to a broad transparency signal with a supplementary absorption peak at the two-photon resonance. We will call this feature *absorption within transparency*. Quite interestingly, absorption within transparency resembles closely the spectrum of the probe laser absorption changed of sign (and of course shifted to positive absorption values). In V-systems neither electromagnetically induced transparency nor absorption within transparency have the high contrast proper of Λ -systems even if the signals are supposed to have roughly the same width. The simulation shows also [ibid.] that the signal width is much broader than that of the signals originated in an N-system.

The description of the probe and coupling spectra changes drastically when one considers an N-system. In this case the coupling signals are not related to one transition alone, because the coupling laser drives simultaneously the two degenerate outer transitions of the N configuration. Since, however, it is impossible to distinguish between the contributions due to one or the other transition, the absorption and dispersion spectra generated by the two components contribute to cumulative absorption and dispersion spectra which summarise within themselves the characteristics of both transitions. This property may lead to quite unexpected spectra as those shown in Figs. 1.7, 1.8, and 1.9.

The calculations [18] also show that, like in a Λ system, the inner coupling laser component of the N-system (the one corresponding to a Zeeman transition between the levels with the lowest magnetic quantum numbers), which constitutes a Λ configuration together with the probe laser, has again an absorption spectrum which resembles that of the probe laser. Similarly, the outer component of the coupling laser, which constitutes a V-system with the probe laser, has an absorption spectrum which resembles that of the probe laser changed of sign.

Depending on the intensity of the coupling laser (in other words on the saturation level), the outer component of the N-system will play a more or less relevant role since one may expect that a high intensity coupling laser pumps most of the atoms in the outer

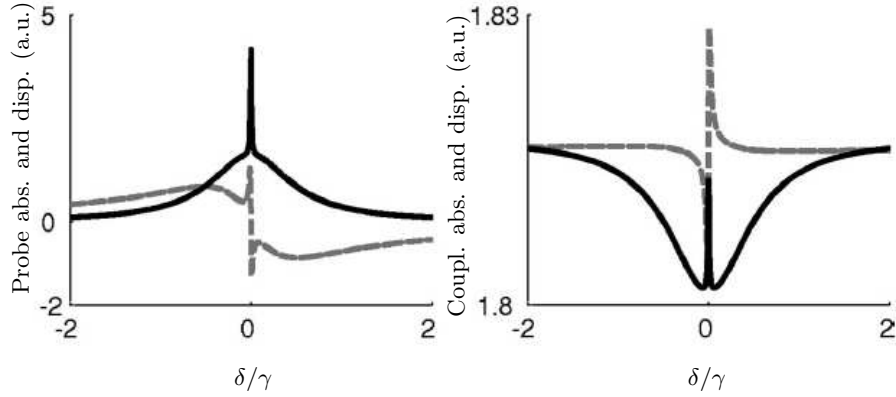


Figure 1.7: Probe (left) and coupling (right) absorption and dispersion in an N-system for low coupling intensity, below the saturation level (as reported in [18]).

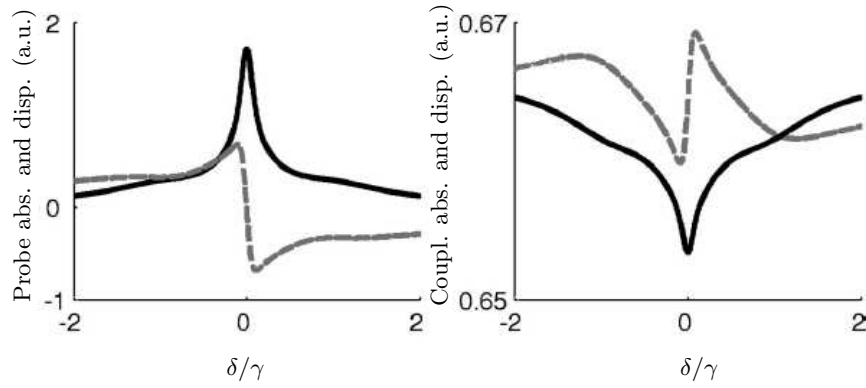


Figure 1.8: Probe (left) and coupling (right) absorption and dispersion in an N-system for moderate coupling intensity, around the saturation level (as reported in [18]).

transition in accordance with its highest transition probability. In this case most of the atoms interacting with the coupling laser are the atoms locked in the outer transition. This changes the ratio between the two coupling components in favour of the outer one (it is easy to show that under the saturation limit the ratio between the two components is almost unitary and it tends to 1 for increasing quantum numbers so that the situation for caesium is even more equilibrated than for rubidium). The effect of this rising unbalance between the two components is the reason of the quite dramatical change in the coupling spectra between Fig. 1.7 and Fig. 1.9 (which correspond to a coupling laser below and above the saturation limit).

Since most of the measurement performed in this experiment were obtained under the saturation limit one can concentrate on the spectra of Fig. 1.7. Here one can see that the probe laser experiences electromagnetically induced absorption and its dispersion is the combination of a broad negative dispersive signal with a narrower likewise negative dispersive signal. At the same time the coupling absorption shows absorption within transparency and a positive parametric dispersion signal. For rising coupling intensities

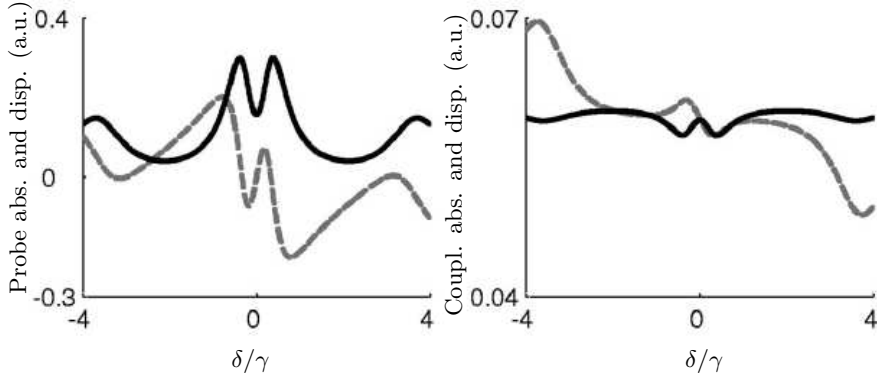


Figure 1.9: Probe (left) and coupling (right) absorption and dispersion in an N-system for high coupling intensity, above the saturation level (as reported in [18]).

(see Fig. 1.8) the probe signals still present an enhanced absorption of broader width while the probe dispersion evolves into a single negative dispersion curve. On the other side, the parametric dispersion of the coupling laser evolves into a broader curve while the absorption peak in the middle of the transparency tends to disappear.

It is interesting to note that at very high coupling laser powers the probe absorption evolves into a transparency signal while its dispersion changes sign (see Fig. 1.9). The change in sign in the dispersion deserves particular attention because media which can change their dispersion sign under the effect of an external parameter are good candidates for the development of opto-optical switches.

The simulations shown so far relate to a pure N-system. It is possible to extend the previous considerations to a realistic system (like the one adopted in this experiment) with a low-intensity σ polarised probe and a π polarised coupling laser [18]. In this case the probe laser absorption signal does not seem to evolve to a transparency signal even for high coupling laser powers (in the case of rubidium). However since the contribution of the coupling laser was not calculated these results are not of primary relevance for the results obtained in this research.

Other simulations [16] were stimulated by the experiment conducted in this research and closely related to it. In particular it was possible to calculate the effect of a weak σ polarised probe and a π polarised coupling laser in a closed two-level system of the kind $F = 1 \rightarrow F' = 2$. Apart from the different ratio between the two Rabi frequencies relative to the coupling laser components and the fact that the system contains a smaller number of N-like subsystems, the physics of this degenerate two-level system should also not differ too much from that of the $F = 4 \rightarrow F' = 5$ transition in caesium.

The results for the $F = 1 \rightarrow F' = 2$ transition with orthogonally linearly polarised laser are shown in Figs. 1.10, 1.11 and 1.12. The phenomenology of the spectra changes radically with respect to the N-system only for coupling intensities above the saturation limit, a regime which was not generally accessible by the measurement performed in this work. In this regime (see Fig. 1.12) the probe laser does not switch from absorption to

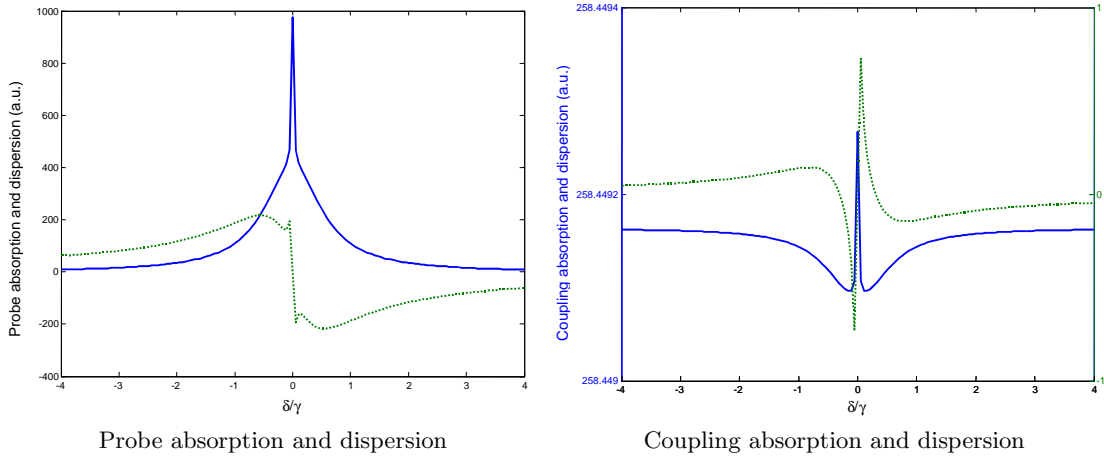


Figure 1.10: Probe and coupling absorption and dispersion for a closed degenerate $F = 1 \rightarrow F' = 2$ system with coupling laser under saturation intensity and negligible probe laser intensity. Courtesy of C. Goren [16].

transparency (unless probably at unreasonably high coupling laser intensities).

The extension of the previous results to caesium and to probe intensities comparable (if not higher) of those of the coupling laser involves the calculation of an even greater number of transitions due to the richer hyperfine structure of caesium with respect to rubidium and to the impossibility to neglect second-order contributions due to the probe laser. At present these calculations are still under development. We will discuss the results obtained together with the experimental results (chap. 3) since the calculations performed were directly related to intensity conditions corresponding to the performed experiments.

In any case, even if most of the previous results were obtained for an N system with transfer of coherence and negligible probing, they describe quite exactly the phenomenology of a degenerate two-level system satisfying the EIA-conditions. In the more general case one can qualitatively argue that it is the physics of the transitions with the higher magnetic quantum numbers which determines the physics of the whole system (these transition correspond indeed to those having the higher transition probabilities). In this spirit it can be argued that for a two-level system in which the degeneracy of the lower level is greater than that of the higher level (such as the $F = 3 \rightarrow F' = 2$ transition in the caesium D_2 line) the phenomenology will resemble that of a Λ -system, a hypothesis which will be experimentally verified in the following of this work.

1.5 Calculation of experimentally relevant quantities

Even if the theorists often express their calculations in terms of dimensionless quantities or ratios, when one wants to confront theory and experiment it is more convenient to

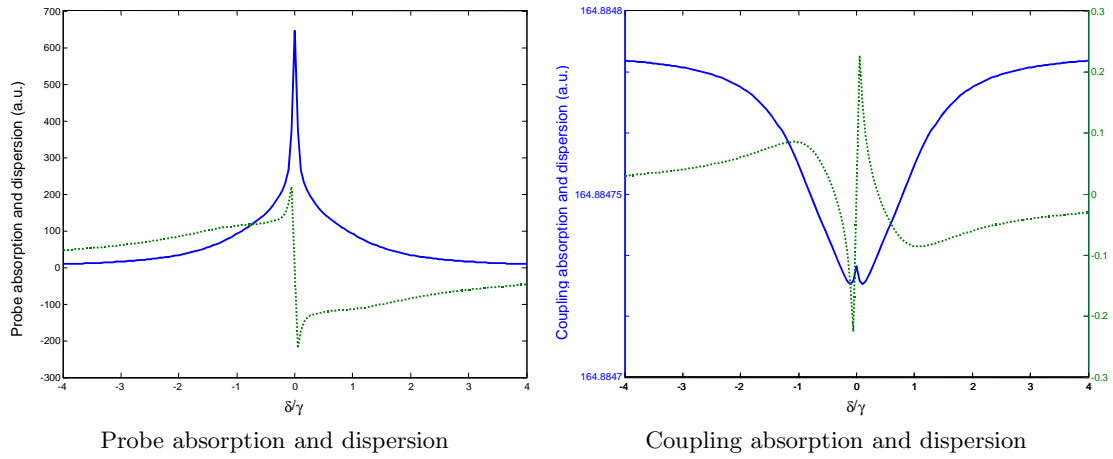


Figure 1.11: Probe and coupling absorption and dispersion for a closed degenerate $F = 1 \rightarrow F' = 2$ system with coupling laser around saturation intensity and negligible probe laser intensity. Courtesy of C. Goren [16].

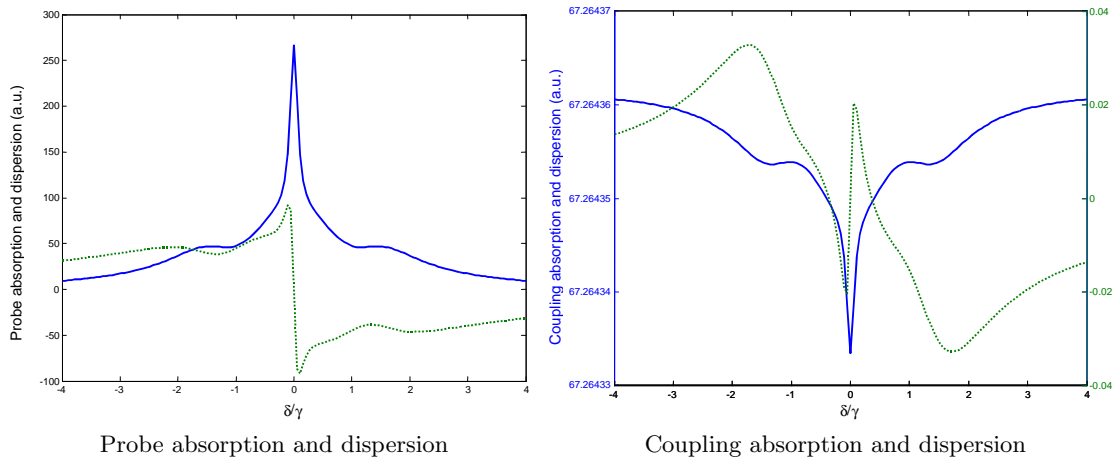


Figure 1.12: Probe and coupling absorption and dispersion for a closed degenerate $F = 1 \rightarrow F' = 2$ system with coupling laser above saturation intensity and negligible probe laser intensity. Courtesy of C. Goren [16].

calculate general expressions as a function of directly accessible experimental quantities. With this target in mind I will close this chapter with the calculation of some quantities which will prove useful when discussing the experimental results: Rabi frequencies and dispersion.

1.5.1 Calculation of the Rabi frequencies

The Rabi frequency for an arbitrary component of the fine structure of an atom can be written, according to equation (1.1), as

$$\Omega_{FS} = \frac{\mu E_0}{2\hbar}. \quad (1.15)$$

Since the intensity $I_{\text{e.m.}}$ of an electromagnetic wave impinging on a surface A is given by

$$I_{\text{e.m.}} \equiv \frac{P}{A} = \frac{c_0}{8\pi} E_0^2, \quad (1.16)$$

one can rewrite equation (1.15) as:

$$\Omega_{FS} = \frac{\mu}{2ea_0} \sqrt{\frac{e^2 a_0^2}{\hbar^2} \frac{8\pi P}{c_0 A}}.$$

It is often useful to compare the Rabi frequency with the spontaneous emission coefficient. This comparison clearly defines whether the atoms are subject to strong oscillating electromagnetic fields or not and thus identifies the regime in which it is possible to induce Rabi oscillations in the system. In a similar manner to the equation (1.15) for the Rabi frequency, it is possible to express the spontaneous emission coefficient relative to an arbitrary fine structure line in the form

$$\gamma_{FS} = \frac{e^2}{a_0 \hbar} \frac{4}{3} \left(\frac{2\pi a_0}{\lambda} \right)^3 \frac{\mu^2}{(ea_0)^2}.$$

The previous expression can be derived [24, chap. 5] from the expression of the Einstein coefficient A (expressed for simplicity in the Gaussian system of unity) which, as known, describes spontaneous emission in a semiclassical context.

After some algebra it is possible to express the Rabi frequency given by equation (1.15) as a function of the spontaneous emission coefficient in the form

$$\begin{aligned} \Omega_{FS} &= \frac{1}{2} \sqrt{\frac{a_0 \hbar}{e^2} \frac{3}{4} \frac{\lambda^3}{(2\pi a_0)^3} \frac{e^2 a_0^2}{\hbar^2} \frac{8\pi P}{c_0 A} \gamma_{FS}} \\ &= \frac{1}{4} \sqrt{\frac{3\lambda^3}{c_0 \hbar \pi^2} \frac{P}{A} \gamma_{FS}} \\ &= \frac{\lambda}{4\pi R} \sqrt{\frac{3\lambda}{c_0 \hbar \pi} P \gamma_{FS}} \end{aligned}$$

where we have factorised the dimensionless quantity $\frac{\lambda}{4\pi R}$ and expressed the interaction area as $A = \pi R^2$ (with R as the radius of the laser beam impinging on the medium).

However, a more natural way to compare the Rabi frequency and the spontaneous emission coefficient is to calculate the ratio

$$\frac{\Omega_{FS}}{\gamma_{FS}} = \frac{\lambda}{4\pi R} \sqrt{\frac{3\lambda}{c_0 \hbar \pi} \frac{P}{\gamma_{FS}}},$$

which simplifies slightly to

$$\frac{\Omega_{FS}}{\gamma_{FS}} = \frac{\lambda}{4\pi R} \sqrt{\frac{6\lambda}{c_0 h} \frac{P}{\gamma_{FS}}}. \quad (1.17)$$

Since γ_{FS} and λ are known for the transition in analysis the only remaining variables are R and P . Usually the radius R is given for a specific experiment (we changed it only once during the duration of this work). The remaining variable is then P , the power of the electromagnetic field exciting the transition.

1.5.2 Calculation of the Rabi frequency for the transition $4 \rightarrow 5$

In this section we calculate the Rabi frequency relative to the single $F = 4 \rightarrow F' = 5$ hyperfine transition of the caesium D_2 line, which constituted the object of most of the measurements described in this work.

To calculate the Rabi frequency for the $4 \rightarrow 5$ transition one has to start from the general expression of the Rabi frequency for the fine structure Ω_{FS} given in equation (1.15) and derive the correct expression for the desired transition through some Clebsch-Gordan coefficients algebra. It results [36, chap. 6] in

$$\begin{aligned} \Omega_{4 \rightarrow 5} &= \sqrt{\Omega_{FS}^2 \sum_{M_F, M_{F'}, q} (2F+1)(2F'+1) \left\{ \begin{matrix} J & F & I \\ F' & J' & 1 \end{matrix} \right\}^2 \left(\begin{matrix} F & 1 & F' \\ -M_F & q & M_{F'} \end{matrix} \right)^2} \\ &= \Omega_{FS} \sqrt{(2F+1)(2F'+1)} \left\{ \begin{matrix} J & F & I \\ F' & J' & 1 \end{matrix} \right\} \sqrt{\sum_{M_F, M_{F'}, q} \left(\begin{matrix} F & 1 & F' \\ -M_F & q & M_{F'} \end{matrix} \right)^2}, \end{aligned} \quad (1.18)$$

where $\Omega_{FS} \equiv \Omega_{J \rightarrow J'}$ is connected to the reduced matrix element between the ground and excited state of the line.

Since $F' = 5$ and $F = 4$ one has

$$\sqrt{(2F+1)(2F'+1)} = 3\sqrt{11}.$$

It is known from the addition rules for angular momenta that $\mathbf{F} = \mathbf{I} + \mathbf{J}$. Since in our system the ground level is a $^2S_{1/2}$ state and the excited level a $^2P_{3/2}$ state, one has

$J = 1/2$ and $J' = 3/2$, which gives

$$\begin{aligned} \left\{ \begin{array}{ccc} J & F & I \\ F' & J' & 1 \end{array} \right\} &= \left\{ \begin{array}{ccc} 1/2 & 4 & 7/2 \\ 5 & 3/2 & 1 \end{array} \right\} \\ &= \sqrt{\frac{1}{2^2 \times 3^2}} \\ &= \frac{1}{6}. \end{aligned}$$

Let us now calculate the sum which appears as an argument of the square root in equation (1.18)

$$\sum_{M_F, M_{F'}, q} \left(\begin{array}{ccc} F & 1 & F' \\ -M_F & q & M_{F'} \end{array} \right)^2$$

assuming that $F = 4$ and $F' = 5$ (q can only be $-1, 0$, or $+1$). We first calculate the Clebsch-Gordan coefficients for the case $q = 0$.

$$\begin{aligned} \left(\begin{array}{ccc} 5 & 4 & 1 \\ 0 & 0 & 0 \end{array} \right)^2 &= \frac{5}{3^2 \times 11} \\ \left(\begin{array}{ccc} 5 & 4 & 1 \\ 1 & -1 & 0 \end{array} \right)^2 &= \left(\begin{array}{ccc} 5 & 4 & 1 \\ -1 & 1 & 0 \end{array} \right)^2 = \frac{2^3}{3 \times 5 \times 11} \\ \left(\begin{array}{ccc} 5 & 4 & 1 \\ 2 & -2 & 0 \end{array} \right)^2 &= \left(\begin{array}{ccc} 5 & 4 & 1 \\ -2 & 2 & 0 \end{array} \right)^2 = \frac{7}{3 \times 5 \times 11} \\ \left(\begin{array}{ccc} 5 & 4 & 1 \\ 3 & -3 & 0 \end{array} \right)^2 &= \left(\begin{array}{ccc} 5 & 4 & 1 \\ -3 & 3 & 0 \end{array} \right)^2 = \frac{2^4}{3^2 \times 5 \times 11} \\ \left(\begin{array}{ccc} 5 & 4 & 1 \\ 4 & -4 & 0 \end{array} \right)^2 &= \left(\begin{array}{ccc} 5 & 4 & 1 \\ -4 & 4 & 0 \end{array} \right)^2 = \frac{1}{5 \times 11} \end{aligned}$$

Summing the coefficients for $q = 0$ one has

$$\sum_{M_F, M_{F'}, q=0} \left(\begin{array}{ccc} F & 1 & F' \\ -M_F & q & M_{F'} \end{array} \right)^2 = \frac{1}{3}.$$

For the case $q = 1$ one has

$$\begin{aligned} \left(\begin{array}{ccc} 5 & 1 & 4 \\ -5 & 1 & 4 \end{array} \right)^2 &= \frac{1}{11} \\ \left(\begin{array}{ccc} 5 & 1 & 4 \\ -4 & 1 & 3 \end{array} \right)^2 &= \frac{2^2}{5 \times 11} \\ \left(\begin{array}{ccc} 5 & 1 & 4 \\ -3 & 1 & 2 \end{array} \right)^2 &= \frac{2^2 \times 7}{3^2 \times 5 \times 11} \end{aligned}$$

$$\begin{aligned} \begin{pmatrix} 5 & 1 & 4 \\ -2 & 1 & 1 \end{pmatrix}^2 &= \frac{7}{3 \times 5 \times 11} \\ \begin{pmatrix} 5 & 1 & 4 \\ -1 & 1 & 0 \end{pmatrix}^2 &= \frac{1}{3 \times 11} \\ \begin{pmatrix} 5 & 1 & 4 \\ 0 & 1 & -1 \end{pmatrix}^2 &= \frac{2}{3^2 \times 11} \\ \begin{pmatrix} 5 & 1 & 4 \\ 1 & 1 & -2 \end{pmatrix}^2 &= \frac{2}{3 \times 5 \times 11} \\ \begin{pmatrix} 5 & 1 & 4 \\ 2 & 1 & -3 \end{pmatrix}^2 &= \frac{1}{3 \times 5 \times 11} \\ \begin{pmatrix} 5 & 1 & 4 \\ 3 & 1 & -4 \end{pmatrix}^2 &= \frac{1}{3^2 \times 5 \times 11}. \end{aligned}$$

Therefore it results

$$\sum_{M_F, M_{F'}, q=1} \begin{pmatrix} F & 1 & F' \\ -M_F & q & M_{F'} \end{pmatrix}^2 = \frac{1}{3}.$$

Similarly one has

$$\sum_{M_F, M_{F'}, q=-1} \begin{pmatrix} F & 1 & F' \\ -M_F & q & M_{F'} \end{pmatrix}^2 = \frac{1}{3}.$$

Summarising the results obtained one obtains

$$\begin{aligned} \Omega_{4 \rightarrow 5}^{q=0} &= \Omega_{FS} \times 3\sqrt{11} \times \frac{1}{6} \sqrt{\frac{1}{3}} \\ &= \frac{1}{2} \sqrt{\frac{11}{3}} \Omega_{FS} \end{aligned}$$

and

$$\begin{aligned} \Omega_{4 \rightarrow 5}^{q=\pm 1} &= \Omega_{FS} \times 3\sqrt{11} \times \frac{1}{6} \sqrt{\frac{2}{3}} \\ &= \frac{1}{2} \sqrt{\frac{22}{3}} \Omega_{FS}. \end{aligned}$$

The apparent discrepancy in the results obtained above for the two different linear polarisations (corresponding to the cases $q = 0$ and $q = \pm 1$) has to be related to the definition of the Rabi frequencies used in this context. Indeed the use of circular polarised components of the light in the calculation of the matrix elements requires the use of complex instead of real vectors. For normalisation reasons these vectors involve a further normalisation factor of $\frac{1}{\sqrt{2}}$ in front of the expression for the Rabi frequency. This

factor reestablishes the symmetry between the two different polarisations and gives—for the two linearly polarised components of a laser driving the $F = 4 \rightarrow F' = 5$ line of caesium—the following expressions for the Rabi frequencies:

$$\Omega_{4 \rightarrow 5}^{\parallel} = \frac{1}{2} \sqrt{\frac{11}{3}} \Omega_{FS}^{\parallel}$$

$$\Omega_{4 \rightarrow 5}^{\perp} = \frac{1}{2} \sqrt{\frac{11}{3}} \Omega_{FS}^{\perp}.$$

Because Ω_{FS} is a function of the laser power (see equation (1.15)), in general it must be distinguished as to whether one is operating with the probe or with the coupling laser, thus discriminating between $\Omega_{FS}^{\text{coupl}}$ and $\Omega_{FS}^{\text{probe}}$.

1.5.3 Calculation of the dispersion profile

In chap. 3 we will focus our attention on the dispersive signals obtained when simultaneously driving and probing the $F = 4 \rightarrow F' = 5$ in caesium. In order to be able to make a comparison between the measured dispersion value and some theoretical predictions we will calculate an explicit expression for the dispersion of either the coupling or the probe laser acting on the $F = 4 \rightarrow F' = 5$ line. To do this, since no explicit expression of the dispersion has been calculated for a system subject to electromagnetically induced absorption, we will refer to the calculations of the dispersion figures performed for a Λ -system. In this case one can assume a degenerate Λ -system (one in which the two ground states coincide).

The values for the dispersion φ' calculated for a Λ -system in [31] are given by (e.g. caption to Fig. 8 in ref. [31])

$$\varphi'_{\text{coupl}} = n'_{\text{coupl}} \omega_{\text{coupl}} \frac{l}{c_0}$$

and

$$\varphi'_{\text{probe}} = n'_{\text{probe}} \omega_{\text{probe}} \frac{l}{c_0},$$

where n' is the refractive index for the involved laser and l the interaction length. As explained in section 1.4.5 an approximation which fits n'_{coupl} and n'_{probe} better than that given in [31] is given by

$$n'_{\text{coupl}} \approx C_{\text{coupl}} \left(\frac{\Omega_{ab}}{\tilde{\Omega}^2} \right)^2 \left[1 - \frac{\gamma_0}{\gamma} \frac{\gamma^2 + 2\tilde{\Omega}^2}{\tilde{\Omega}^2} \right]$$

and

$$n'_{\text{probe}} \approx C_{\text{probe}} \left(\frac{\Omega_{ac}}{\tilde{\Omega}^2} \right)^2 \left[1 - \frac{\gamma_0}{\gamma} \frac{\gamma^2 \Omega_{ac}^2 + 2\tilde{\Omega}^2 \Omega_{ac}^2 + (\tilde{\Omega}^2)^2}{\tilde{\Omega}^2 \Omega_{ac}^2} \right],$$

Variable	Symbol	Value
Coherence decay	γ_0	0.1 MHz
Spontaneous decay	γ	$2\pi \times 5.22$ MHz
Atomic density	N	10^{15} m ⁻³
Interaction length	l	5 mm
Laser beam radius	R	2.2 mm (or 1.1 mm)

Table 1.2: Typical values of experimental quantities used throughout the experiment

where

$$C_{\text{coupl}} = -\frac{2\pi N}{\hbar} \mu_{ac}^2 \text{ and } C_{\text{probe}} = \frac{2\pi N}{\hbar} \mu_{ab}^2.$$

Remembering the definition of the Rabi frequency given in equation (1.15) one can write

$$\Omega_{ab} = \mu_{ab} \frac{E_0^{\text{probe}}}{2\hbar} \text{ and } \Omega_{ac} = \mu_{ac} \frac{E_0^{\text{coupl}}}{2\hbar}.$$

Extracting the dipole moments from the previous equation one obtains

$$\mu_{ab}^2 = \frac{4\hbar^2 \Omega_{ab}^2}{(E_0^{\text{probe}})^2} \text{ and } \mu_{ac}^2 = \frac{4\hbar^2 \Omega_{ac}^2}{(E_0^{\text{coupl}})^2}.$$

Therefore, one has

$$\begin{aligned} \varphi'_{\text{coupl}} &\approx -4\hbar \frac{2\pi N}{(E_0^{\text{coupl}})^2} \omega_{\text{coupl}} \frac{l}{c_0} \left(\frac{\Omega_{ab} \Omega_{ac}}{\tilde{\Omega}^2} \right)^2 \left[1 - \frac{\gamma_0}{\gamma} \frac{\gamma^2 + 2\tilde{\Omega}^2}{\tilde{\Omega}^2} \right], \\ \varphi'_{\text{probe}} &\approx 4\hbar \frac{2\pi N}{(E_0^{\text{probe}})^2} \omega_{\text{probe}} \frac{l}{c_0} \left(\frac{\Omega_{ab} \Omega_{ac}}{\tilde{\Omega}^2} \right)^2 \left[1 - \frac{\gamma_0}{\gamma} \frac{\gamma^2 \Omega_{ac}^2 + 2\tilde{\Omega}^2 \Omega_{ac}^2 + (\tilde{\Omega}^2)^2}{\tilde{\Omega}^2 \Omega_{ac}^2} \right]. \end{aligned}$$

Remembering that the intensity of the laser is described by equation (1.16) one easily obtains

$$\varphi'_{\text{coupl}} \approx -N(lA) \frac{\hbar \omega_{\text{coupl}}}{P_{\text{coupl}}} \left(\frac{\Omega_{ab} \Omega_{ac}}{\tilde{\Omega}^2} \right)^2 \left[1 - \frac{\gamma_0}{\gamma} \frac{\gamma^2 + 2\tilde{\Omega}^2}{\tilde{\Omega}^2} \right]$$

and

$$\varphi'_{\text{probe}} \approx N(lA) \frac{\hbar \omega_{\text{probe}}}{P_{\text{probe}}} \left(\frac{\Omega_{ab} \Omega_{ac}}{\tilde{\Omega}^2} \right)^2 \left[1 - \frac{\gamma_0}{\gamma} \frac{\gamma^2 \Omega_{ac}^2 + 2\tilde{\Omega}^2 \Omega_{ac}^2 + (\tilde{\Omega}^2)^2}{\tilde{\Omega}^2 \Omega_{ac}^2} \right].$$

The previous expressions can be evaluated with a simple substitution of the experimental quantities measured during the experiment. A typical set of experimental values for the measurements performed within this work is given in table 1.2.

Let us evaluate the various factors which are involved in the calculation of the dispersion. One has

$$\begin{aligned} \frac{\Omega_{ab}\Omega_{ac}}{\tilde{\Omega}^2} &= \frac{\frac{1}{2}\sqrt{\frac{11}{3}}\Omega_{FS}^{\parallel}\frac{1}{2}\sqrt{\frac{11}{3}}\Omega_{FS}^{\perp}}{\frac{11}{12}\left(\Omega_{FS}^{\parallel}\right)^2 + \frac{11}{12}\left(\Omega_{FS}^{\perp}\right)^2} \\ &= \frac{\Omega_{FS}^{\parallel}\Omega_{FS}^{\perp}}{\left(\Omega_{FS}^{\parallel}\right)^2 + \left(\Omega_{FS}^{\perp}\right)^2}. \end{aligned}$$

To calculate the other factors let us make some assumptions regarding the transition on which we operate; in the following it will be assumed that:

- $\gamma_{FS} = \gamma_{ab} = \gamma_{ac} \equiv \gamma$
- $\omega_{\text{coupl}} = \omega_{\text{probe}}$.

Under these assumptions one can write

$$\begin{aligned} \left(\frac{\Omega_{ab}\Omega_{ac}}{\tilde{\Omega}^2}\right)^2 &= \left(\frac{\sqrt{P_{\text{coupl}}P_{\text{probe}}}}{P_{\text{coupl}} + P_{\text{probe}}}\right)^2 \\ &= \frac{P_{\text{coupl}}P_{\text{probe}}}{(P_{\text{coupl}} + P_{\text{probe}})^2}, \end{aligned}$$

$$\begin{aligned} \frac{\tilde{\Omega}^2}{\Omega_{ac}^2} &= 1 + \frac{\Omega_{ab}^2}{\Omega_{ac}^2} \\ &= 1 + \frac{P_{\text{probe}}}{P_{\text{coupl}}} \end{aligned}$$

and, remembering equation (1.17),

$$\begin{aligned} \frac{\gamma^2}{\tilde{\Omega}^2} &= \frac{\gamma^2}{\Omega_{ab}^2 + \Omega_{ac}^2} \\ &= \gamma \frac{1}{\left(\frac{\lambda}{4\pi R}\right)^2 \frac{6\lambda}{c_0 h} \frac{11}{12}(P_{\text{coupl}} + P_{\text{probe}})}. \end{aligned}$$

One has, therefore,

$$\left[1 - \frac{\gamma_0 \gamma^2 + 2\tilde{\Omega}^2}{\gamma \tilde{\Omega}^2}\right] = \left\{1 - \frac{\gamma_0}{\gamma} \left[2 + \gamma \frac{1}{\left(\frac{\lambda}{4\pi R}\right)^2 \frac{6\lambda}{c_0 h} \frac{11}{12}(P_{\text{coupl}} + P_{\text{probe}})}\right]\right\}$$

and

$$\begin{aligned}
 & \left[1 - \frac{\gamma_0 \gamma^2 \Omega_{ac}^2 + 2\tilde{\Omega}^2 \Omega_{ac}^2 + (\tilde{\Omega}^2)^2}{\tilde{\Omega}^2 \Omega_{ac}^2} \right] = \\
 & = \left[1 - \frac{\gamma_0}{\gamma} \left(\frac{\gamma^2 + 2\tilde{\Omega}^2}{\tilde{\Omega}^2} + \frac{\tilde{\Omega}^2}{\Omega_{ac}^2} \right) \right] \\
 & = \left\{ 1 - \frac{\gamma_0}{\gamma} \left[3 + \gamma \frac{1}{\left(\frac{\lambda}{4\pi R}\right)^2} \frac{1}{\frac{6\lambda}{c_0 h} \frac{11}{12} (P_{\text{coupl}} + P_{\text{probe}})} + \frac{P_{\text{probe}}}{P_{\text{coupl}}} \right] \right\}.
 \end{aligned}$$

So, finally, one can write an expression for the coupling and probe laser dispersion as a function of experimentally accessible parameters and known physical constants in the form

$$\varphi'_{\text{coupl}} \approx \frac{-NlA\hbar\omega_{\text{coupl}}P_{\text{probe}}}{(P_{\text{coupl}} + P_{\text{probe}})^2} \left\{ 1 - \frac{\gamma_0}{\gamma} \left[2 + \gamma \frac{1}{\left(\frac{\lambda}{4\pi R}\right)^2} \frac{1}{\frac{6\lambda}{c_0 h} \frac{11}{12} (P_{\text{coupl}} + P_{\text{probe}})} \right] \right\} \quad (1.19)$$

and

$$\varphi'_{\text{probe}} \approx \frac{NlA\hbar\omega_{\text{probe}}P_{\text{coupl}}}{(P_{\text{coupl}} + P_{\text{probe}})^2} \left\{ 1 - \frac{\gamma_0}{\gamma} \left[3 + \gamma \frac{1}{\left(\frac{\lambda}{4\pi R}\right)^2} \frac{1}{\frac{6\lambda}{c_0 h} \frac{11}{12} (P_{\text{coupl}} + P_{\text{probe}})} + \frac{P_{\text{probe}}}{P_{\text{coupl}}} \right] \right\} \quad (1.20)$$

which constitute the desired expressions for the dispersion of the probe laser or the parametric dispersion of the coupling laser as a function of the probe and coupling laser powers and of the laser beam radius.

Chapter 2

Experimental Setup

Introduction

In this chapter I will introduce the experimental setup used to investigate the physics of coherent phenomena in two-level, three-level, and four-level systems. The experimental apparatus chosen to perform the measurements included a modified version of a heterodyne interferometer proposed several years ago by Guido Müller *et al.* [27, 28] and subsequently developed by Mario Müller *et al.* [30, 31]. Considering the fact that some improvements of the experimental setup have been introduced in recent years [37], I will give here a full description of the experimental setup. For further details on some aspects of the experiment the reader should also refer to [27, 29].

2.1 Laser

Experiments involving phase locks between different lasers greatly profit from a short-term narrow linewidth of the laser output (the noise at high Fourier frequencies can only be poorly handled by phase-locked loops). At the same time the purpose of investigating a specific set of atomic transitions fixes the working frequency and therefore puts several restraints on the selectable sources. A typical light source at 852 nm linewidth, which has the economical advantage of being easily affordable, is constituted by diode lasers. Diode lasers, however, do not provide the desired linewidth. To reduce it several feedback schemes have been developed, involving coupled resonators or gratings, such as the Littman or the Littrow setup.

In this experiment we followed a design proposed in Dahmani, Hollberg, and Drullinger [13], which suggests the use of an external optical feedback from a separate cavity to reduce the linewidth to few kilohertz. Some researchers refer to this scheme by calling it *external cavity diode laser* or, with an acronym, ECDL.

Even if external cavity diode lasers have a low frequency noise at high Fourier frequency, they present several other disadvantages; they have a smaller tuning range than other lasers with feedback configurations and, moreover, their frequency output is not easily repeatable, since it involves the competing and somewhat concurring effect of at least four actuators: the current driver, the temperature driver, an etalon inserted in the

laser system, and the external cavity itself, the coupling of which is determined by the position of a coupling mirror. Because the demand for repeatability constituted one of the major problems of our experimental setup, if not the most relevant one, it was decided to tackle this aspect on a separate project, which led to the development of a new laser setup scheme, somehow summarising within itself the advantages of extended cavity diode lasers (also known as *grating lasers* or Littman lasers) and external cavity diode laser [45, 42, 21]. Regrettably, the new setup does not yet support the powers needed to perform a complete analysis of our system. Therefore it has not been implemented in the apparatus; nevertheless, its study and development are going to play a crucial role in improving the performance of the system. Furthermore, it is interesting to note that such a laser could be implemented in a so-called *master-slave configuration*.

2.1.1 Laser diodes

The lasers used in the experiment were constructed with JDS Uniphase's SDL-5400 series single-mode laser diodes (Fig. 2.1).

Their single-mode performance is achieved through an index-guided single-mode waveguide. The best laser diodes compatible with the needs of the experiment had a wavelength precision of 852 ± 4 nm. The output power of the diodes did not exceed 150 mW. During the experiment diodes with 100 mW (model SDL-5410-C) and 150 mW (model SDL-5420-C) output power were tested. Diode lasers with 200 mW output power were available in former times but were retired from the market since they did not offer enough reliability, especially concerning their single-mode performance, at the desired frequency. They remain unavailable at present time.

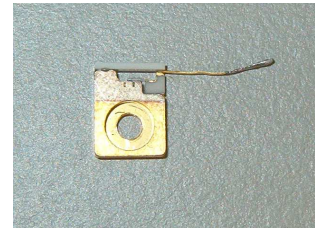


Figure 2.1: Laser diode in open heatsink package

We decided to choose laser diodes with an open heatsink package mainly for geometrical reasons. The rectangular shaped form helped the positioning of the laser diode in the laser construction and, therefore, facilitated the directioning of the laser beam. The emitting dimensions of the laser diode are $3 \mu\text{m} \times 1 \mu\text{m}$. The small dimensions of the laser emitting surface caused a relevant divergence of the beam. To improve the directionality of the beam a collimator with a focal length of 5 mm was put along the direction of propagation. The collimator was built in the laser emitting block and did not need to be further adjusted once the block had been fixed to its position.

The different dimensions of the emitting surface caused also ellipticity of the emitted laser beam profile. Since mode-matching to a Gaussian mode is required only where the measurement is performed we decided to avoid mode-cleaning at the laser output. As we will see in the following paragraphs, mode-cleaning can be obtained through single-mode fibres which were used in the experiment for purposes of geometrical alignment.

To further improve the control capabilities on the laser output three actuators were added to the laser construction: a tuneable current supply for the diode, a temperature controller

based on a Peltier device to heat or cool it, and a glass plate working as an etalon after the laser diode output and before the collimator.

2.1.2 External cavity diode laser

The wavelength precision offered by the diode lasers was widely insufficient for the purposes of the experiment: 852 ± 4 nm. Through the coupling of a fraction of the laser output with an external resonator and its feedback to the laser diode it was possible to radically narrow the width of the outgoing light. This configuration is known in the literature as external cavity diode laser or ECDL[13]. In such a scheme a small fraction (about 4%) of the output light is extracted through a beam splitter. The extracted light reflects on a mirror surface and enters a confocal collimator to build up a V-like resonance mode. Part of the light which enters the resonator exits through the input port. It can then go back to the laser diode through the same path followed for entering the cavity, thus feeding back to the laser.

A picture of the ECDL configuration adopted in this experiment is shown in Fig. 2.2

In this figure the confocal resonator is sketched in blue on the right side of the picture (since it is not to be seen in the figure). The laser infrared light is represented with a red beam. Part of the laser light (about 4%) coming from the lower part of the structure (where the laser diode is accommodated) is extracted from the main beam through a beam splitter and is then reflected to the cavity via the small mirror on the left side. This mirror is curved and its surface has a curvature radius of 200 mm. The curvature facilitates the mode-matching with the Fabry-Perot cavity. For further control, the position of this mirror can be additionally adjusted through a piezoelectrical controller. The main output of the laser is shown with an arrow in the upper part of the picture.

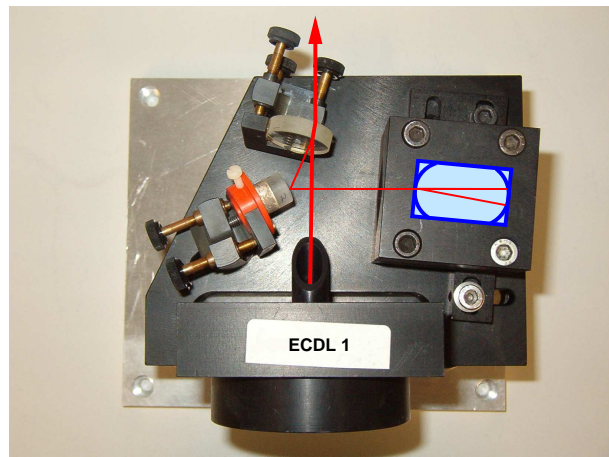


Figure 2.2: ECDL

The glass plate used as an etalon and placed directly over the laser diode block also constitutes an important part of our construction of an ECDL. Together with the back-facet of the diode, the glass plate builds up a resonator of low finesse and wide free-spectral-range. Through its control it is possible to tune the laser frequency to various frequency intervals separated in frequency of about 50 GHz. Once the desired frequency interval is reached the other three actuators (current, temperature, and coupling mirror to the resonator) can be used for the fine tuning to the frequency of interest.

The external optical resonator possesses a finesse of about 50 and a narrow free-spectral-range (1.5 GHz). It is 50 mm long. With its help it is possible for the ECDL to reach narrow linewidths, below 1 kHz. The complete accessible frequency range amounts to about 1 GHz. To enhance the tunability through the selection of the desired resonance frequency for the cavity, a further piezoelectrical controller operates directly on the back-mirror of the resonator.

Even if the ECDL emits very narrow linewidths, the concurring interaction of the several built-in resonators calls for an efficient electronic stabilisation. In any case, the ECDL can become instable on timescales longer than some minutes, because various drifts in the actuators can lead to the selection of another frequency in the resonator. This problem, which constituted the most severe constraint to the repeatability of the measurement conducted in this research, was tackled on a separate project [45, 42, 21] which is still under development. The underlying idea is that of performing a preselection of the light entering the resonator through a grating. For this reason the new scheme developed was called GEECDL, an acronym which stands for *grating enhanced extended cavity diode laser*[45].

2.2 Heterodyne interferometer

With the purpose of measuring the phase of either the probe or the coupling laser, the experimentalists headed towards two set-ups slightly different from each other to perform their measurements. In both schemes, the underlying structure of the apparatus was constituted by a heterodyne interferometer. In such a configuration the sensitivity to acoustical noise and vibrations could be kept orders of magnitudes below the ones typical for homodyne interferometers while retaining a comparable signal strength. The two experimental set-ups are shown in Fig. 2.3a and Fig. 2.3b.

Instead of the more usual configuration involving two lasers, this particular kind of heterodyne interferometer was constructed with three lasers; we called them coupling, probe, and reference laser. The names given to the lasers mirrored their function throughout the experiment. The coupling laser coupled two levels of the caesium hyperfine structure. It operated at a fixed frequency which could be tuned to match the frequency of the desired transition. Its frequency was locked to that of the desired transition by means of the frequency modulation spectroscopy. The probe laser probed a second hyperfine transition which could be either the same transition coupled by the coupling laser or another one; its polarisation was orthogonal to that of the coupling laser; its detuning constituted the independent variable during the data acquisition. The reference laser was an auxiliary laser which enabled the dispersion measurement of one of the other two lasers (namely the one with which it shared the polarisation). Its frequency was detuned from that of the other two lasers of about 1 GHz, so that no interaction could be assumed between the light generated by the reference laser and levels under analysis in caesium.

At its output, each laser beam went through a Faraday isolator which protected the laser system from back-reflections coming from other optical components. A polariser and a

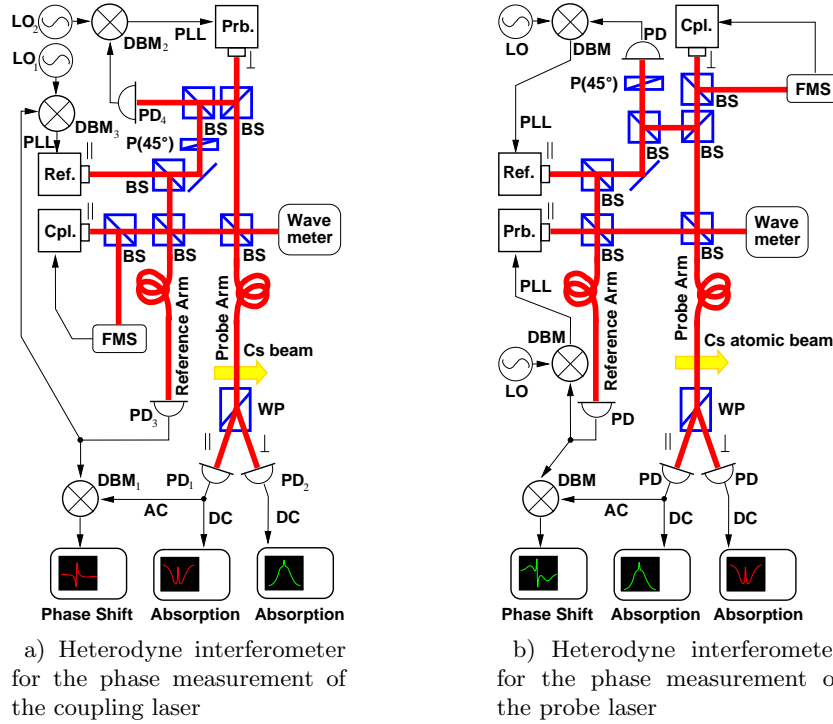


Figure 2.3: Different interferometer configurations for the phase measurement — **Cpl.**, **Ref.**, **Prb.**: coupling, reference, and probe laser; **LO**: local oscillator; **PD**: photodiode; **DBM**: double balanced mixer; **BS**: beam splitter; **WP**: Wollaston prism; **P(45°)**: polariser oriented at 45° with respect to the impinging laser beam; **FMS**: frequency modulation spectroscopy; **PLL**: phase-locked loop.

half-wave plate followed each Faraday isolator; with their help the polarisation of each laser could be adjusted to the desired value at the interaction zone with a negligible loss of output power (less than 1%).

The experiment required a strong phase correlation between all the lasers involved; for this reason, the three lasers were connected in a chain of two consecutive phase-locked loops. Since there were slight differences depending on the phase of the laser one wished to measure, and on the system one wanted to measure, we will describe the optical paths and the design of the phase-locked loops in separate sections. In either case, even if other configuration were occasionally tried, the configuration commonly used involved a first phase-locked loop between coupling and reference laser, and a second one between reference and probe laser.

To minimise the relative phase noise between the lasers caused by mechanical and acoustical perturbations of the optical setup, the laser fields coming from the three laser sources were superimposed well before the interaction zone. Once superimposed, and before passing through the atomic beam (in the probe arm) or reaching the photodiodes (in the reference arm or in the other control arms), all lasers were guided through single mode

fibres, allowing us to achieve extremely good alignment and mode matching (about 96% with a gaussian profile) between the beams, which was accompanied by a loss in power of about 50%. The fibres adopted in the experiment were single mode fibres (model 1234 of the company New Focus) with a gradient-index (GRIN) lens at the input. Since the output of the fibres was characterised by a divergence of 5° the outcoming beam was collimated through achromatic lenses to the desired beam radius (mostly 2.2 mm but in certain measurements, to test the effect of stronger intensities, 1.1 mm). To avoid thermal or acoustical disturbances of the fibres—which affected particularly the dispersion measurements—the fibres placed in the probe and reference arm had to be thermally and mechanically isolated from the environment through a protective external shield built around them.

After the interaction zone a Wollaston prism separated the two orthogonally polarised components propagating in the probe arm. Starting from this point, the reference laser shared its path only with the laser the phase of which one wanted to measure, and continued its way to a 1 GHz photodiode with a DC and an AC output. With these DC and AC signals it was possible to reconstruct the absorption and dispersion signals of either the probe or the coupling laser (depending on which one shared its polarisation with the reference laser). Meanwhile, the second beam coming from the Wollaston prism reached a 40 MHz photodiode where the absorption measurement of the perpendicularly polarised laser could be carried out.

To increase the signal-to-noise ratio of the transmitted intensities we separated a small component of the input laser light by means of a glass plate (GP) situated just before the vacuum chamber (see Fig. 2.4). The uncoated glass plate generated two reflexes which could be used as secondary auxiliary beams. With two polarisers we set the polarisation of the two beams to either horizontal or vertical (respectively) and were therefore able to separately measure a signal proportional to the sum of the reference laser intensity and of that of the laser sharing the same polarisation of the reference laser (at the photodiode PD₅), and another one proportional to the signal of the laser having the orthogonal polarisation (at photodiode PD₆) immediately before the interaction area. Due to this proportionality, the signals carried information regarding the noise accumulated in the interferometer by the two polarisation channels before reaching the vacuum tank. Keeping the optical paths for the transmitted intensities as short as possible after the interaction area, and dividing the signals generated by the transmitted intensities with the signals generated by the derived beams having the corresponding polarisation (i.e. filtering out the common noise), the procedure resulted in a drastic improvement of the signal-to-noise ratio, especially at low transmitted intensities. An example of such an improvement is commented in section 3.2.

2.3 Frequency lock

The proximity of several different atomic levels in the caesium D_2 line and the necessity to distinguish between them were the reasons to look for a stable frequency reference

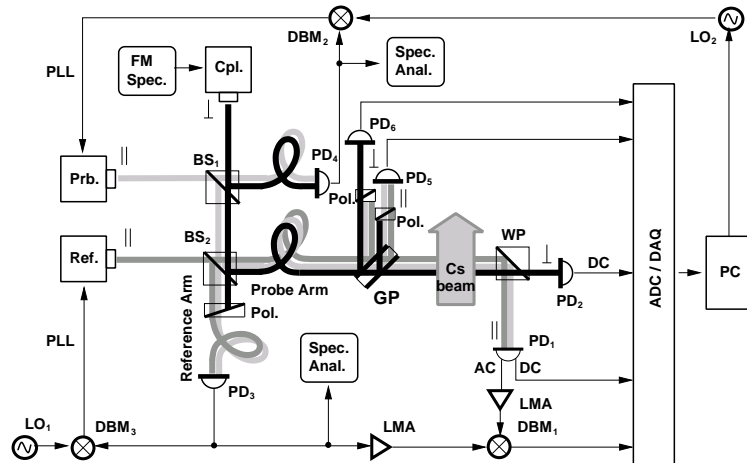


Figure 2.4: Working scheme of the experimental setup — **Cpl.**, **Ref.**, **Prb.**: coupling, reference, and probe laser; **LO**: local oscillator; **PD**: photodiode; **DBM**: double balanced mixer; **BS**: beam splitter; **Pol.**: polariser; **WP**: Wollaston prism; **GP**: glass plate; **FM Spec.**: frequency modulation spectroscopy; **LMA**: limiting amplifier; **Spec. Anal.**: spectrum analyser; **PLL**: phase-locked loop; **ADC/DAQ**: AC and DC data acquisition; **PC**: computer.

signal. Moreover, such a reference signal was crucial in stabilising the phase measurements which had to be performed. The stabilisation of the laser frequency to a known one was realised combining different techniques: Doppler-free saturation spectroscopy to pick out the desired frequency from the Doppler-broadened caesium absorption spectrum; frequency modulation spectroscopy to obtain instead of an absorptive a dispersive signal which could then be used as an error signal for the frequency stabilisation; lock-in detection to clean the obtained spectra from the residual Doppler shift which was still present even after the frequency modulation spectroscopy.

2.3.1 Doppler-free saturation spectroscopy

To obtain a stable frequency reference signal within the caesium D_2 line we locked the output of the laser to one of the atomic frequencies available in the D_2 line itself. The procedure involved the use of a glass cell containing caesium in gaseous form. To access the target atomic transition frequency it was necessary to filter out the Doppler broadening which affected the whole spectrum. The Doppler shift was caused by the thermal movement of the caesium atoms inside the cell. At room temperature the Doppler shift amounted to about 380 MHz (as we will see in section 2.6). The various accessible atomic lines are separated only of an amount included between 150 MHz and 250 MHz. The Doppler broadening led, therefore, to overlapping of the lines and to their indistinguishability.

It was possible to separately pick out the various atomic transitions with the aid of the so-called saturation spectroscopy. This technique involves the utilisation of two laser

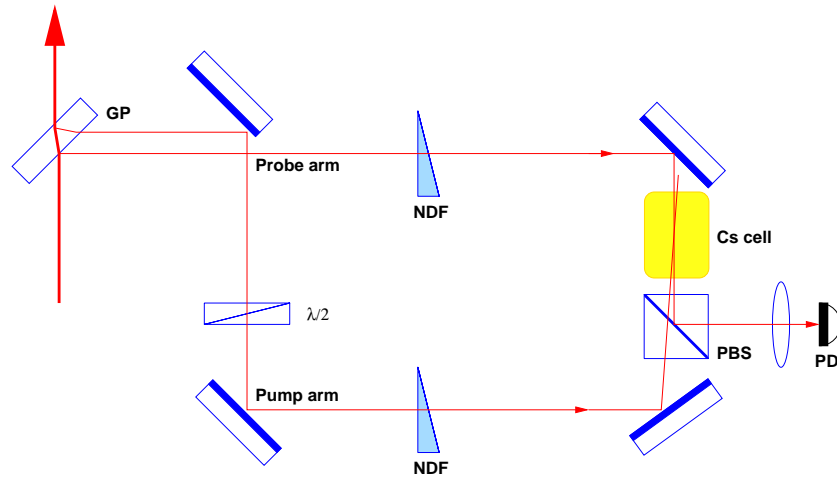


Figure 2.5: Heterodyne interferometer for saturation spectroscopy — **NDF**: neutral density filter; **PD**: photodiode; **PBS**: polarising beam splitter; **GP**: uncoated glass plate; $\lambda/2$: half-wave plate.

beams counterpropagating through an atomic medium (here caesium). The two beams constituted a second heterodyne interferometer, auxiliary to the main one (the one with which the measurement were performed). A sketch of this second interferometer is shown in Fig. 2.5.

Saturation spectroscopy measures the absorption signal of a probe laser beam probing the caesium optical ensemble while the medium is pumped by a second laser beam (called the pump beam). Two auxiliary beams (pump and probe) were therefore extracted from the main beam coming from the coupling laser by passing it through an uncoated glass plate. The two reflected beams originating at the glass-air separation surface constituted the probe and the pump beams of the auxiliary interferometer. The intensity of the probe and the pump beam could be adjusted to maximise the absorption signal from the desired line with the help of two variable neutral density filters. To facilitate the signal extraction, the polarisation of the pump beam was rotated by 90° through a half-wave plate. The probe signal was extracted through a polarising beam splitter and could be detected through a photodiode.

With saturation spectroscopy it was possible to obtain a Doppler-free spectrum of the hyperfine transitions constituting the caesium D_2 line. Depending on the ground level considered (which can have a total angular momentum of $F = 3$ or $F = 4$) it was possible to measure two different absorption spectra in which the permitted hyperfine transitions emerged as dips (so called Lamb-dips) or peaks in the profile. These peaks or dips were generated by atoms which had a negligible velocity component in the propagation direction of the laser beams and therefore were not affected by the Doppler shift. Only such atoms could interact simultaneously and coherently with the pump and the probe laser on the same atomic transition. The coherent interaction produced the enhanced or reduced absorption of the probe beam. Together with the expected lines, the spectra

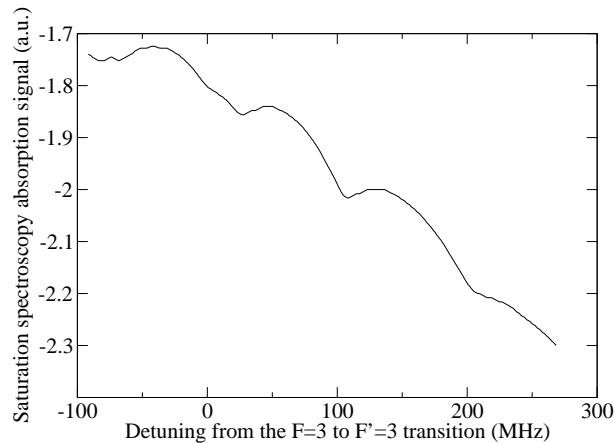


Figure 2.6: Saturation absorption transitions from the $F = 3$ level. One can recognise the absorption signal corresponding to the transitions to the $F' = 3$ and $F' = 4$ levels and the three cross-over resonances. The transition to the $F' = 2$ level lies out of the range of the frequency axis.

showed also some other transitions. These supplementary signals could be explained as cross-over resonances, i.e. resonances in which one laser excited one velocity class of atoms corresponding to one hyperfine transition while the other one excited a velocity class corresponding to a different hyperfine transition. Depending on the external magnetic fields, cross-over resonances might have an intensity which becomes comparable with that of the actual hyperfine transitions. Nevertheless, since it was always possible to distinguish between the different cross-over and hyperfine transition lines it was decided not to apply a compensation magnetic field around the caesium cell.

An example of a saturation spectroscopy signal obtained for transitions from the ground level with $F = 3$ is shown in Fig. 2.6. From Fig. 2.6 it is easy to recognise that saturation spectroscopy signals are absorptive signals. As such, they do not present a zero point and are, therefore, not suited to be used as an error signal for locking purposes. The corresponding dispersive signals would offer the desired profile. To obtain them, we implemented into the interferometer a technique called frequency modulation spectroscopy.

2.3.2 Frequency modulation spectroscopy

Frequency modulation spectroscopy (shortly FMS) was firstly proposed in [8]. It is a method of heterodyne spectroscopy which is sensitive to the absorption and the dispersion of narrow spectral features. The basic principle of FMS is the use of sidebands which are impressed on the carrier frequency (here the laser frequency of the probe beam in the auxiliary interferometer) through a frequency modulation. This idea traces back to the Pound microwave frequency stabiliser [34] and has also been implemented for optical resonators in the so-called Pound-Drever-Hall technique [14].

It can be demonstrated that, if the frequency gap between the carrier and the sidebands is

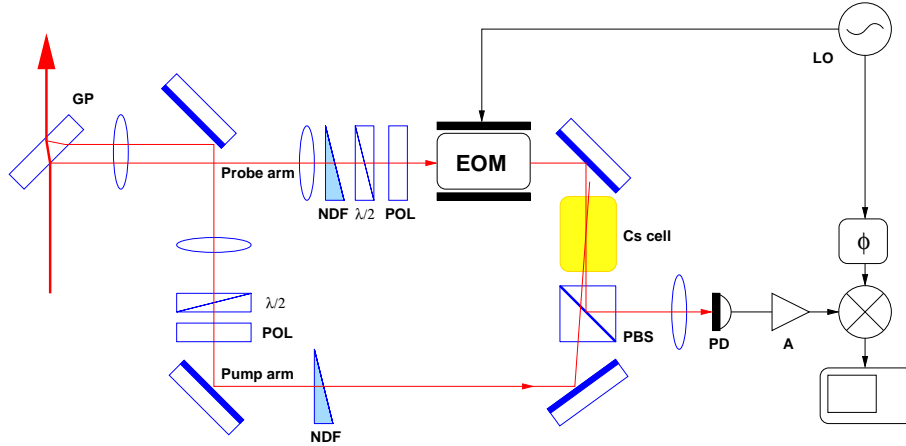


Figure 2.7: Experimental scheme for frequency modulation spectroscopy — **NDF**: neutral density filter; **PD**: photodiode; **PBS**: polarising beam splitter; **GP**: uncoated glass plate; **POL**: polariser; $\lambda/2$: half-wave plate; **EOM**: electro-optical modulator; **LO**: local oscillator at 26 MHz; **A**: amplifier (chain); Φ : phase shifter.

bigger than the width of the signal to be measured, the intensity of the modulated signal contains two components oscillating at the frequency of the modulation and proportional to either the absorption or the dispersion of the spectral feature to be measured.

An easy method to impress the modulation on the carrier is to use an electro-optical modulator (shortly EOM). In our experiment an EOM model 4001 of the company New Focus was used: a resonant modulator which generated sidebands detuned from the carrier of 26 MHz. Resonant modulators offer a higher modulation depth than broadband modulators. For this reason it was possible to obtain a high modulation even if the modulator was operated at low voltage. In our experiment the half-wave voltage V_π , i.e. the voltage needed to produce a π phase shift, amounted to 16 V. This corresponded to a modulation depth of 0.2 rad/V. The EOM was driven at 26 MHz by an ultrastable local oscillator (a voltage controlled crystal oscillator VCXO 3627 S19 of the company Bürger).

Since the detected signal of the auxiliary heterodyne interferometer originates from the probe arm the EOM was inserted in the probe arm, before the caesium cell. To match the aperture of the EOM (which amounts to 2 mm) a telescope was built before the EOM. This reduced the beam radius to about 300 μm . Furthermore, to obtain a proper phase modulation, the polarisation of the beam entering the EOM had to be set perpendicular to the experiment surface. This was made possible through a polariser and a half-wave plate. Through a fine adjustment of the polarisation it was possible to reduce the residual amplitude modulation to less than -60 dB. After the implementation of the FMS the experimental setup of the auxiliary interferometer changed as shown in Fig. 2.7.

The signal coming from the probe arm was detected at a 26 MHz-resonant photodiode. The amplitude of the modulation was small enough to neglect higher order sidebands. Since the modulation frequency was much bigger than the width of the spectral feature

to analyse, the spectral feature could be probed by one sideband alone. In fact, calling ω_c the carrier frequency and ω_m the modulation frequency one can express the intensity reaching the photodiode as

$$I_{PD} = I_0 e^{-\alpha_0 L} \left(1 - \frac{L}{2} M \Delta\alpha \cos \omega_m t + M \Delta\phi \sin \omega_m t \right)$$

where α_0 is the absorption coefficient of the (off-resonant) carrier, M the modulation amplitude, L the length of the caesium cell and $\Delta\alpha$ and $\Delta\phi$ are the deviations from the background absorption coefficient and phase shift induced by the caesium spectral feature(s).

After amplification the signal was mixed with the signal coming from the local oscillator (the phase of which could be shifted on the way to the mixer to extract $\Delta\phi$ from the mixed signal) and could be read, as a dispersive signal, on an oscilloscope.

Despite the use of saturation spectroscopy, the demodulated dispersion signal was still affected by the Doppler broadening. This was due to the fact that the gap between the carrier and the modulated wave was indeed bigger than the width of signal to measure but smaller than the width of the Doppler broadening. In this case the FMS was not capable to completely circumvent the Doppler broadening and the demodulated signal showed an undesired offset.

This offset could be cancelled through a lock-in procedure using the property of the Doppler-free absorption signals generated in the saturation spectroscopy profile to appear only when the pump beam is active on the medium (i.e. in case of a coherent interaction). Switching periodically on and off the pump beam (with the insertion of an acousto-optical modulator), the generated signals appeared and disappeared with the same frequency, while the Doppler background remained constant. Demodulating the signal at this new periodical frequency (in the present case 70 kHz), with the aid of a lock-in amplifier, it was possible to extract a clean dispersive signal which was free of the supplementary Doppler background noise. This further modification of the experimental setup is shown in Fig. 2.8. For further control it was decided to monitor also the original Doppler-affected saturation signal, decoupling (after the mixer) a part of the signal through a divider, letting it through a low-pass filter, and finally detecting it on an oscilloscope.

An example of dispersive signal which could be obtained at the output of the lock-in amplifier and subsequently used as a proper error signal to lock the frequency of the coupling laser to the desired transition is shown in Fig. 2.9

2.4 Phase lock

As already mentioned, the heterodyne interferometer adopted in this experiment was developed to perform dispersion measurements of either the coupling or the probe laser. Depending on whether one aimed at measuring the dispersion within a degenerate or a non-degenerate atomic system, the measurement had to be approached with two different

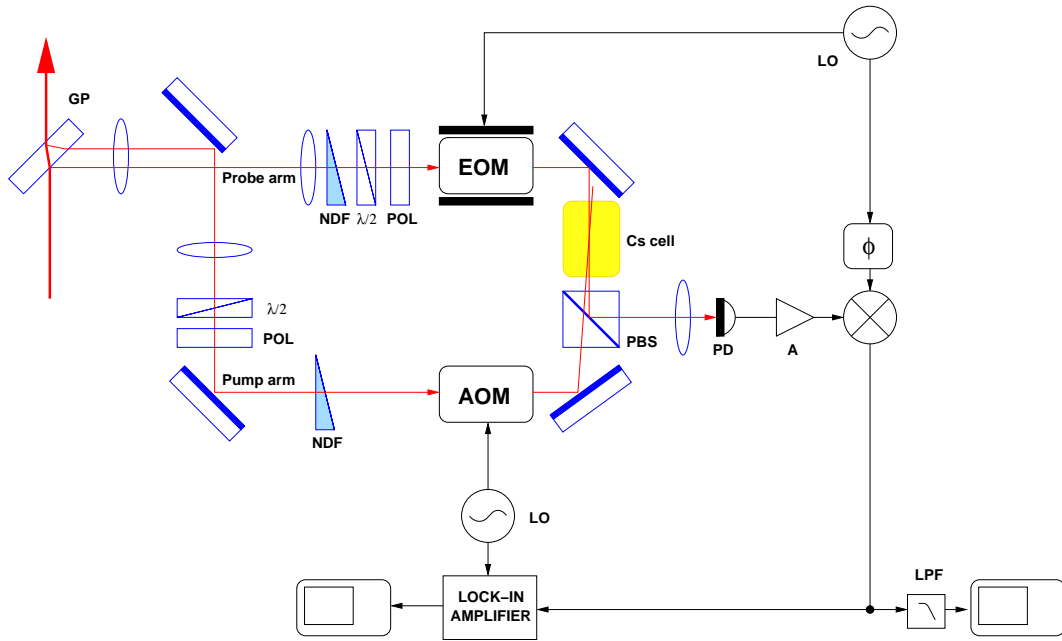


Figure 2.8: Experimental scheme for frequency modulation spectroscopy with lock-in amplification — **NDF**: neutral density filter; **PD**: photodiode; **PBS**: polarising beam splitter; **GP**: uncoated glass plate; **POL**: polariser; $\lambda/2$: half-wave plate; **AOM**: acousto-optical modulator; **EOM**: electro-optical modulator; **LO**: local oscillator; **A**: amplifier (chain); Φ : phase shifter; **LPF**: low-pass filter.

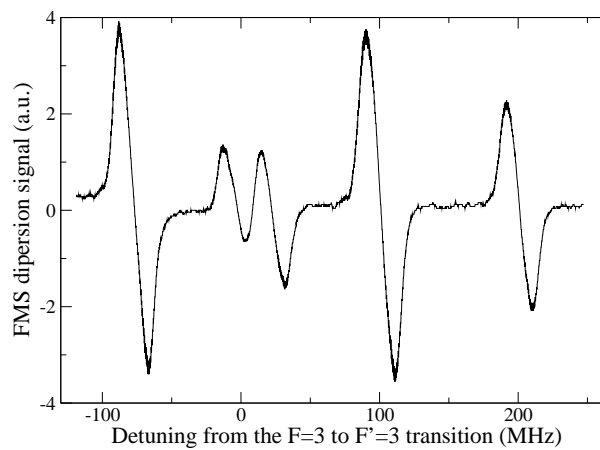


Figure 2.9: Example of error signal obtained after frequency modulation spectroscopy and lock-in amplification. The dispersive signals correspond to the absorptive signals of Fig. 2.6.

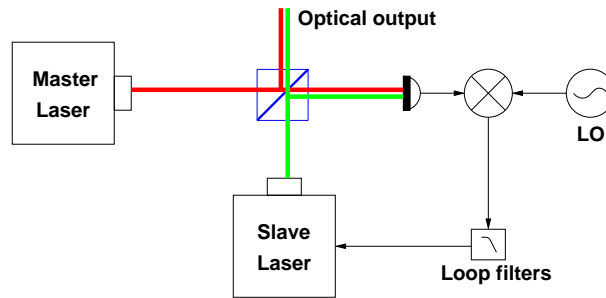


Figure 2.10: Working principle of a phase-locked loop — **LO**: local oscillator.

methods, each of which was tailored to the specific case. In both situations a stable phase difference between all lasers involved was necessary to perform the measurements. Such a phase relationship was needed not only to obtain dispersion measurement but also to be able to conduct coherent measurements at all, since any coherent measurements can be performed only when the involved fields are coherent to one another (i.e. the phase difference between the respective fields does not change in time).

2.4.1 Phase coherence adjustment

To realise the desired phase coherence between the fields it is possible to follow two approaches. The simplest one involves the use of modulators to generate detuned sidebands of the main field; these sidebands are intrinsically coherent with the generating field. This approach was the one used (at least partially) in the auxiliary interferometer (FMS). Another approach involves the use of phase-locked loops to lock the phase of fields originating from different sources.

A schematic of an optical phase-locked loop is presented in Fig. 2.10. The figure shows how through electronic subtraction of a signal generated at an ultrastable local oscillator from the beat signal originated by beating two optical fields at a photodiode, it is possible to obtain a phase-error signal which can be fed back to the slave laser to lock it in phase to the master one. In fact, the slave laser is forced to follow the master laser at a frequency offset determined by the local oscillator. Properly setting the frequency of the local oscillator one can obtain an error signal which is, for small dephasings, proportional to the dephasing itself, i.e. the desired error signal for the actuator feedbacking the slave laser.

In this experiment we used three different lasers. To perform the desired measurements of absorption and dispersion all three had to be phase-locked with one another. This was achieved by building a chain of subsequent phase-locked loops. However, the phase-locked loops had to be designed following two different schemes, depending on the transition under analysis. In the following sections we will present the underlying schemes and their main differences.

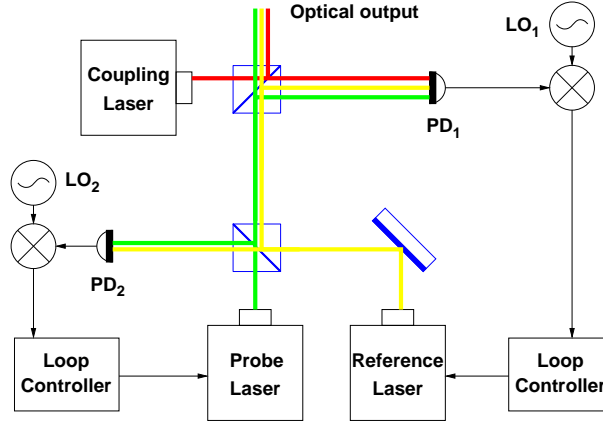


Figure 2.11: Phase-locked loop setup used for the measurements in a three-level system.

2.4.2 Phase lock for a three-level configuration

In a non-degenerate atomic configuration all lasers could be distinguished by means of their frequency. This characteristic constituted an advantage for the practical realisation of the interferometer and the design of the phase-locked loops. Lasers of different frequencies generated different beat signals even when they reached the same photodiode. The use of resonant amplifiers at the frequency needed for the phase-locked loop gave the possibility to filter out the undesired beat signals and keep only the one relevant for the feedback.

For the realisation of the heterodyne interferometer it was necessary to superimpose the light coming from three different lasers. This was in general obtained through the insertion of beam splitters. Since each beam splitter has two outputs it was always possible to use the second port of the beam splitter for phase-locked loops purposes. In this way no auxiliary beams had to be extracted from the laser paths before their superimposition in order to realise the loops. This reduced the amount of optics and alignment required and resulted in a less complicate measurement preparation.

A schematic of the phase-locked loop configuration used for three-level systems is shown in Fig. 2.11. In this case the coupling laser was driving the $F = 4 \rightarrow F' = 4$ transition. The reference laser was locked to the coupling laser with the help of the local oscillator LO_1 . We chose 1 GHz as output frequency of LO_1 . In this way the detuning of the reference laser from the resonance frequencies of atomic transition within the D_2 line was such that no residual interaction with the atomic system could be assumed. The reference laser frequency gap was indeed too large to stimulate a hyperfine transition from the level $F = 4$ to any F' excited level and too small to stimulate a hyperfine transition from the level $F = 3$.

Subsequently the probe laser was locked to the reference laser with the help of the local oscillator LO_2 . The output frequency of LO_2 amounted to about 10.193 GHz, i.e. the sum of the detuning of the reference laser and the hyperfine splitting between the two

ground states of the caesium D_2 line. In this way the probe laser resulted automatically driving the $F = 3 \rightarrow F' = 4$ transition.

Depending on whether we aimed at measuring the phase of the probe or of the coupling laser we were able to sweep both phase-locked loops through their central frequency via a computer controlled system acting on the desired local oscillator (LO₂ for the coupling phase measurement and LO₁ for the probe phase measurement). Furthermore, in case of a coupling laser phase measurement (when coupling laser and reference laser shared the same polarisation, orthogonal to that of the probe laser), it was useful to insert a polariser on the optical path leading to PD₁ to completely filter out the probe laser light.

The photodiodes PD₁ and PD₂ were 25 GHz photodetectors (*InGaAs* photodiodes with single-mode fibre-optic coupler; New Focus model 1431). The signal outputs of the photodiodes were amplified through low-noise microwave amplifiers before reaching the mixer (the amplification not shown in the figure). The local oscillators were Rohde and Schwarz signal generators model SMT06 (LO₁) and SMP02 (LO₂).

2.4.3 Phase lock for a degenerate two-level configuration

In case of a measurement in a degenerate system the frequency shift between the coupling and the reference laser must be the same (in absolute value) as the frequency shift between the reference and the probe laser. Only in this case it is possible to force the coupling and the probe laser to drive the same transition. In this situation, if one has all three lasers in an optical channel used for a phase-locked loop, it is impossible to distinguish between the beat signal originating from the coupling and the reference laser and that originating from the reference and the probe laser. For this reason one had to extract part of the light coming from the coupling and the reference laser with two beam splitters and superimpose them to a photodiode to get a clean beat signal there. Since not very much intensity of the laser was needed for a phase-locked loop (usually 0.5 mW for each laser was sufficient) it sufficed to extract only a small part of the laser intensity with 4% beam splitter cubes (or simply a glass pick-up plate). The design adopted in our experiment is shown in Fig. 2.12.

It is worthy of note that the design adopted for the phase-locked loops in the three level system could be in principle adopted even in the two-level system case at least in the case of a dispersion measurement of the coupling laser. The insertion of a polariser blocking the probe laser light would transform a three-laser channel into a two-laser channel, thus opening the possibility of a phase-locked loop between coupling and reference laser despite their superimposition with the probe laser. This possibility was exploited in first stages of the experiment. However the extinction of the probe laser achievable with the available polarisers amounted to about 0.5%. This value was sufficient to avoid cross-talk between the two beats when the intensity of the probe laser was lower than that of the coupling laser. However, since in this experiment we conducted also measurements in which the intensity of the probe laser was comparable or higher than that of the coupling laser, it resulted convenient to look for a new setup, which had to be found anyway to perform

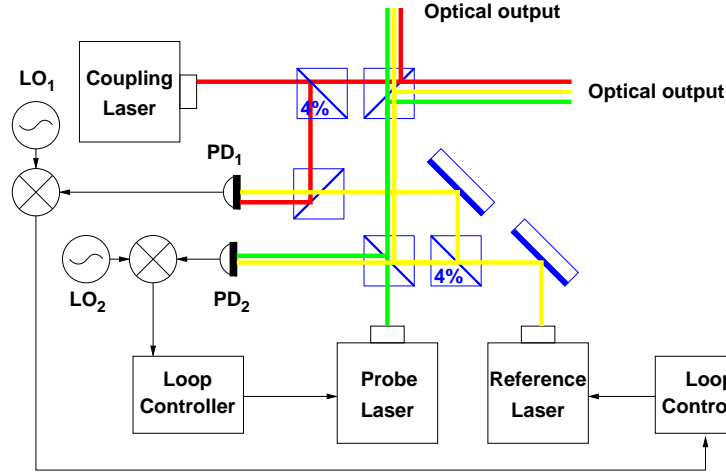


Figure 2.12: Phase-locked loops setup used for measurements in two-level systems

dispersion measurements of the coupling laser.

The photodiodes adopted in the experiment were the same used for the three-level system. Before reaching the mixer their output was amplified through microwave amplifiers (not shown in the figure) to a level comparable to the output of the local oscillators. The local oscillators LO_1 and LO_2 were in this case Rohde and Schwarz signal generators model SMT06 and SMT03.

2.5 Dispersion measurements with the heterodyne interferometer

In this paragraph I will briefly sketch how it is possible to perform a dispersion measurement with the heterodyne interferometer described in section 2.2. Since the working principle of a dispersion measurement remains the same if one measures the coupling or the probe dispersion and if one operates in a two-level or a three-level system I will describe the dispersion measurement of the coupling laser in a two-level system. The corresponding setup is shown in Fig. 2.3a.

The coupling laser was locked to the desired two-level atomic transition using frequency modulation spectroscopy. The reference laser was phase-locked to the coupling laser (via the local oscillator LO_1) with a fixed offset $\Delta\nu_{\text{off}} \approx 1$ GHz; the probe laser was phase-locked to the reference laser with a tuneable offset $\Delta\nu \approx \delta + 1$ GHz (via the local oscillator LO_2). The offsets $\Delta\nu_{\text{off}}$ and $\Delta\nu$ had opposite sign, so that the residual offset between the coupling and probe laser amounted to exactly δ . Since coupling and probe laser drove the same transition, δ corresponded to the probe detuning from the resonance frequency.

Let E_0^j be the amplitude of the electrical field of the j -th laser (with j being c, p, and r for coupling, probe, and reference laser) and let ω_{coupl} , ω_{probe} and ω_{ref} be the laser angular

frequencies. The signals produced at the photodiodes PD₂ and PD₃ had the following dependence:

$$S_{\text{PD}_3} \propto (E_0^c)^2 + (E_0^r)^2 + 2E_0^c E_0^r \cos \left[(\omega_{\text{coupl}} - \omega_{\text{ref}}) - \frac{L_{\text{ref}}}{c_0} \right],$$

$$S_{\text{PD}_2} \propto (E_0^c)^2 e^{-\alpha_c l} + (E_0^r)^2 + 2E_0^c E_0^r e^{-\frac{\alpha_c l}{2}} \cos \left[(\omega_{\text{coupl}} - \omega_{\text{ref}}) - \frac{L_{\text{probe}}}{c_0} + \Delta\varphi_c(\delta) \right],$$

where L_{probe} and L_{ref} were the arm lengths of the probe and the reference arms of the interferometer, $\Delta\varphi_c(\delta)$ the phase shift induced on the coupling laser by the variation of the refractive index in the proximity of the resonance as a function of the detuning δ of the probe laser, α_c the absorption coefficient for the coupling laser, l the length of the interaction area (i.e. the width of the atomic beam).

Neglecting the higher frequency terms, the output signal at the double balanced mixer DBM₁ could be written as:

$$S_{\text{mix}}(\delta) \propto (E_0^c E_0^r)^2 e^{-\frac{\alpha_c(\delta)l}{2}} \cos[\Delta\varphi_c(\delta) - \phi].$$

In the previous expression $\phi = 2\pi\Delta\nu_{\text{off}}(L_{\text{probe}} - L_{\text{ref}})/c_0$ could be set to $(k + \frac{1}{2})\pi$ (with $k \in \mathbb{N}$) by an appropriate tuning either of the reference laser frequency (which was the solution adopted in this experiment) or of the arm lengths L_{probe} and L_{ref} . One obtains, therefore,

$$S_{\text{mix}}(\delta) \propto (E_0^c E_0^r)^2 e^{-\frac{\alpha_c(\delta)l}{2}} \sin[\Delta\varphi_c(\delta)].$$

The proportionality constant depends on several parameters, including the efficiency of the photodiodes and the amount of intensity reaching them. It could be determined through calibration. To avoid the repetition of the calibration procedure any time the intensities of the lasers were changed, the signal output of the photodiodes PD₂ and PD₃ were amplified with two chains of microwave amplifiers ending with two limiting amplifiers (Miteq model AMF-5F-009011-30-10P-LM), which ensured a stable input to the mixer DBM₁ over a wide laser intensity range and simultaneously a constant calibration factor.

The coupling and probe beams absorption signals could be extracted from the intensity of the light impinging on the photodiodes PD₁ and PD₂. As the reference laser was not interacting with the medium its power contributed only with a constant offset. Since this power remained unchanged during a whole measurement set, it could be easily measured and subtracted at the end of a measurement session. Calling I_i^{DC} the non-oscillating component of the intensity reaching the i -th photodiode, one could write

$$I_{\text{PD}_1}^{\text{DC}}(\delta) \propto (E_0^p)^2 e^{-\alpha_p(\delta)l}, \quad (2.1)$$

$$I_{\text{PD}_2}^{\text{DC}}(\delta) \propto (E_0^c)^2 e^{-\alpha_c(\delta)l} + (E_0^r)^2, \quad (2.2)$$

where α_c and α_p were the absorption coefficients for the coupling and the probe laser. From the previous relationships, known l and the efficiency of the photodiodes (or more easily through a further calibration), one could extract α_c and α_p .

2.6 Atomic source

2.6.1 Doppler broadening

The precision of spectroscopical measurements is often limited by Doppler effect. Since through the spectroscopical measurements aiming at measuring electromagnetically induced transparency and absorption the experimentalists wanted to detect signals having a half-width well below the natural width of the lines (about 20 kHz to 100 kHz against a natural line of about 5.3 MHz), it was meaningful to construct an experimental setup which prevented, or at least strongly reduced, the contributions to the line width caused by Doppler effects.

In this experiment it was chosen to utilise an atomic beam generated by an oven instead of an atomic cell, which is included in the standard setup of the greatest part of competing experiments. The atoms forming the beam moved in a direction which was orthogonal to that of the laser beams; therefore their contribution to the shifts of the line was limited to that coming from the beam misalignment with respect to the orthogonal direction and to that relative to the natural divergence of the beam. Collisions between the atoms had to be minimised in order to reduce the motion orthogonal to the main propagation axis. Such collisions limited the possibility to increase the oven temperature above 250 °C because their effect was greater than the advantage obtained through the temperature-dependent increase of the atomic density.

To quantify the atom movement at different temperatures we schematise the gas as a perfect gas. Starting from the Maxwellian velocity distribution for perfect gases

$$dn = 4\pi N \left(\frac{m}{2\pi kT} \right)^{\frac{3}{2}} v^2 \exp \left(-\frac{mv^2}{2kT} \right) dv \quad (2.3)$$

one can extract the most probable velocity of the gas molecules:

$$v_p = \sqrt{\frac{2kT}{m}}. \quad (2.4)$$

For the caesium isotope in use one has $m = 133$ u and, consequently, at a room temperature of 25 °C,

$$v_p = 193 \text{ m/s}. \quad (2.5)$$

With this value one can calculate the most probable Doppler line broadening (full width at half maximum) as [see 36, chap. 1.6]

$$\Delta\nu_D = \frac{\nu_0}{c_0} v_p 2\sqrt{\ln 2} \approx 377 \text{ MHz}$$

Such a large Doppler broadening with respect to the frequencies of the transitions to be measured made it impossible to use a pure caesium cell. One alternative could have been

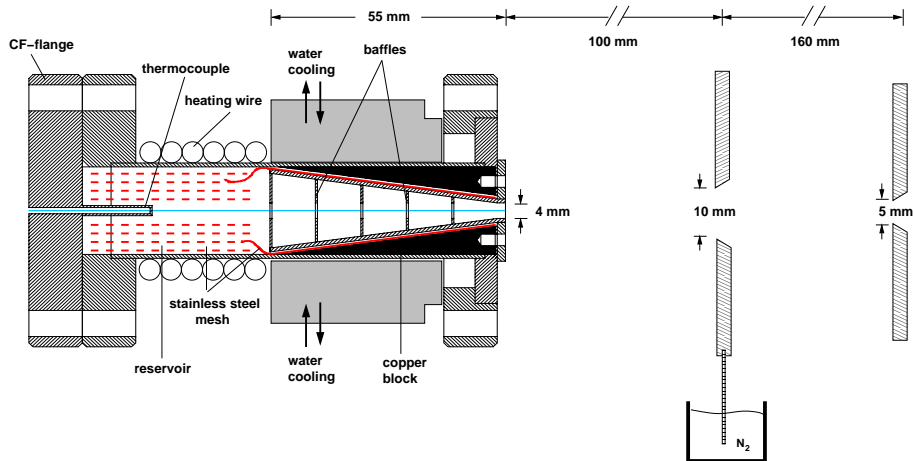


Figure 2.13: Reflux oven and baffling system.

to use a cell containing a buffer gas but through the use of atomic beams the experimentalists could operate on one more degree of freedom: the atomic density. Furthermore, since the interaction volume between lasers and medium in case of an atomic beam is more compact than a cell, the adoption of an atomic beam resulted in a simplification of the procedures needed to compensate the environmental magnetic field around the interaction zone.

2.6.2 Reflux oven

As known, caesium is the most electropositive of all stable elements and has the lowest first ionisation potential. It is, therefore, an extremely reactive material and explodes if put in contact with water, even in the form of water vapour in air; its hydroxide CsOH can easily attack glass and even more easily human tissues. The desire to prevent physical damage to the experimentalists, combined with the practical need of a caesium source stable in its performance over a long time scale (months or, possibly, years), suggested the search for an oven design in which some kind of caesium recycling was possible. A good solution was found in the so-called reflux oven, which could be continuously used over a period of several months without substituting the caesium source. For this reason, throughout the whole experiment, we adopted the reflux oven.

The first design of such an oven, suited for ultrahigh-vacuum performances, is given in [38]. A schematic representation of the oven is given in Fig. 2.13. The oven combines baffling to obtain the desired collimation and capillarity to ensure the caesium circulation.

The oven structure was separated into two sections: a hot part and a cold part. The hot section contained the caesium reservoir; it was the area where the caesium reached the needed temperature and, subsequently, the desired effusive velocity. The heat was generated through a heating wire surrounding the walls of the reservoir, thus keeping the system at the desired temperature. For control purposes a second independent thermo-

meter (a thermocouple) could be inserted in an aperture leading to the middle of the reservoir.

The reservoir was filled with a rolled stainless steel mesh, on which the caesium distributed because of capillarity. This helped to improve the energy transfer between the hot walls of the reservoir and caesium, and prevented the accumulation of caesium in a liquid pool at the lower end of the reservoir, which could eventually affect the effusion process.

The cold section of the oven combined within itself the recycling and the collimation. The beam had to pass through five different baffles that performed the collimation process, each with an aperture of 4 mm. The baffles were milled in a conical structure, the lateral surface of which was connected to the collimating canal through several apertures of 1 mm to 2 mm calibre. Through these apertures the caesium blocked by the baffles flew onto a second stainless steel mesh, which was rolled two times around the lateral surface of the conical structure, and finally came back, because of capillarity, to the reservoir section.

The conical structure and the surrounding mesh were inserted in a copper block of cylindrical form, which was cooled through a water cooling mechanism to roughly 310 K, a temperature above the solidification temperature of caesium (301.59 K) to ensure recirculation but still low enough to avoid that caesium deposited on the baffles acted as a secondary source of effusive beams.

The oven was loaded with 10 g of caesium with a purity of 99.98%. It has to be noted that at least 5 g of caesium were necessary to activate the recirculation process. The filling process was carried out within a glove box under argon atmosphere. It was made possible by a CF-flange, which was located at the backside of the oven and could be opened when necessary.

The oven effusive aperture could be shut with a UHV valve which sealed the oven during transportation and when no measurements were performed.

Behind the effusive aperture two more baffles, with an aperture of 10 mm and 5 mm and at a distance from the effusive aperture of 100 mm and 160 mm respectively, filtered out further caesium atoms propagating in unwanted directions. In this last case no more recycling was used. To minimise the evaporation of the caesium deposited on these baffles during the measurements, we cooled the first baffle down connecting it through a metallic bar to a liquid nitrogen reservoir, which, however, needed continuous filling (at a rate of about 2 l/h) throughout the whole measurement. The second baffle remained at room temperature.

2.7 Interaction volume

The interaction between caesium and light took place in a vacuum chamber under ultra-high-vacuum specifications. To achieve such a low pressure one had to provide a pre-vacuum of at least 10^{-2} mbar to the turbomolecular pumps, to ensure their operation. For the major part of the experimental results discussed within this work, the prevacuum

was produced with a rotary vane pump, ensuring a prevacuum of at least 10^{-3} mbar. This design was abandoned after having rebuilt the experiment in a new experimental facility, where a central prevacuum of 4×10^{-3} mbar provided in the laboratories permitted the direct utilisation of turbomolecular vacuum pumps to achieve ultra-high vacuum. Two turbomolecular pumps (Leybold Turbovac 50 and Leybold Turbovac 361) produced a vacuum of at least 10^{-8} mbar. During the measurements, the caesium flux did not substantially reduce this value.

As we have seen in the previous section, the caesium atomic beam was collimated through a series of baffles before reaching the interaction zone. The last baffle had a collimation hole of 5 mm, so we assumed an interaction length $l = 5$ mm in which the atomic ensemble could interact with the electromagnetic radiation coming from an orthogonal direction through antireflection-coated windows built in the vacuum chamber.

Around the interaction zone the environmental magnetic field (including the terrestrial magnetic field) was compensated through a system of six coils. The coils were oriented to be orthogonal to the direction of propagation of the atomic beam, to that of the laser beam, and in the third spatial direction (perpendicular to the previous two). Since the laser beam in the interaction zone was collimated to a radius of 2.2 mm (or smaller) the adoption of the coils was sufficient to compensate the external DC magnetic fields to a level below $0.5 \mu\text{T}$ so that no significant interaction of the magnetic field with the Zeeman substructure of the lines could be assumed. No AC magnetic field compensation was performed: the opportunity to perform such a compensation with the standard techniques adopted in the field of scanning electron microscopy was discussed. Since the AC magnetic field compensation was not the limiting factor of the measurement resolution, its implementation in the experimental apparatus was abandoned.

Chapter 3

Experimental Results

In this chapter I present the experimental results obtained from investigating various Λ -systems and degenerate two-level systems in caesium. Beginning with the results in Λ -systems, I show how it was possible to improve the detected absorption signals through the insertion of supplementary optical channels leading to reference photodiodes. This improvement leads to measurements of electromagnetically induced transparency in a Λ -system in which the transparency obtained is greatly improved with respect to [29]. Through a discussion of the off-resonant absorption level for the coupling laser I present some curious dispersive-like signals which were obtained in the absorption spectra of the coupling laser. These signals are explained in terms of light-induced birefringence. After this I move to the results obtained in two different closed degenerate two-level systems. Depending on the two-level system considered, it is illustrated how the spectra change from electromagnetically induced transparency to electromagnetically induced absorption. In this context I give a deeper insight on the characteristics of the absorption and dispersion spectra of the coupling laser in the presence of electromagnetically induced absorption for the probe laser. Such spectra were measured for the first time in this research and enrich the known phenomenology of electromagnetically induced absorption. They also experimentally confirm theoretical predictions based on spontaneous transfer of coherence. Finally, I close the chapter with some results concerning the giant Kerr effect achievable in media affected by electromagnetically induced transparency and absorption.

3.1 Optimisation of the detected signal in a Λ -system

As already discussed, it was possible to dramatically improve the signal-to-noise ratio of the heterodyne interferometer by dividing the signals recorded after the interaction zone with signals picked-up immediately before the interaction zone. We want to show here how effective this solution was. To do it we will refer to the experimental setup shown in Fig. 3.1.

Let PD_1 be the photodiode which measured the absorption and dispersion of the coupling laser after the coherent interaction with the caesium beam and let PD_2 be the photodiode which measured the probe laser absorption (also after the coherent interaction). Let PD_5 be the photodiode which measured the intensity extracted from the main beam through a glass plate (before the interaction area) and shared the polarisation of the coupling laser;

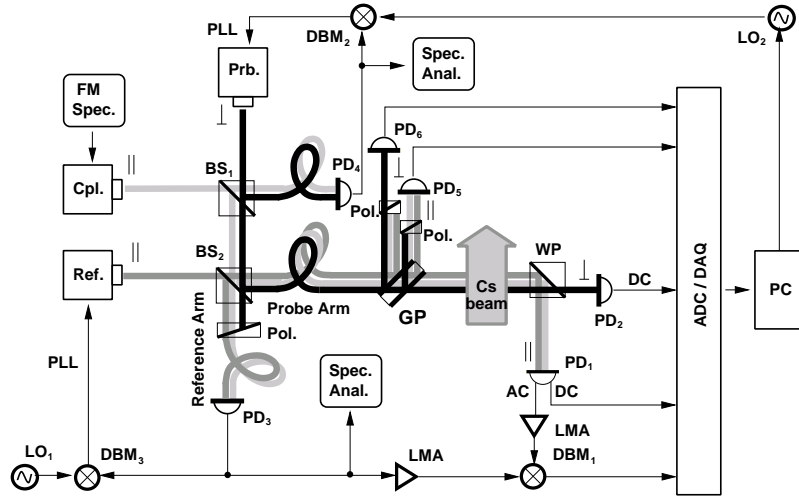


Figure 3.1: Experimental setup with reference photodiodes — **Cpl.**, **Ref.**, **Prb.**: coupling, reference, and probe laser; **LO**: local oscillator; **PD**: photodiode; **DBM**: double balanced mixer; **BS**: beam splitter; **Pol.**: polariser; **WP**: Wollaston prism; **GP**: glass plate; **FM Spec.**: frequency modulation spectroscopy; **LMA**: limiting amplifier; **Spec. Anal.**: spectrum analyser; **PLL**: phase-locked loop; **ADC/DAQ**: AC and DC data acquisition; **PC**: computer.

similarly let PD_6 be the photodiode which measured the intensity extracted from the main beam and shared the polarisation of the probe laser. It is evident that the signals recorded at PD_1 and PD_5 carried information on the noise accumulated in the probe arm by laser light of one polarisation (that of the coupling laser) and the signals recorded at PD_2 and PD_6 carried information on the noise accumulated by light of the orthogonal polarisation. For this reason, dividing the two corresponding signals, i.e. calculating the ratios I_1/I_5 and I_2/I_6 (where I_i represents the intensity at the i -th photodiode), one could eliminate the common noise accumulated along the probe arm.

An example of the improvement obtainable with such a procedure is given in Fig. 3.2, where the original and the noise-filtered data of a single simultaneous measurement of the coupling and the probe absorption are shown. The whole procedure of division of the signals was automated through the computer program—a Labview code—which controlled the data acquisition card. For completeness this figure also includes the simultaneously taken dispersive signal which corresponds to a measurement of the coupling laser parametric dispersion.

With the measurement shown in Fig. 3.2 we demonstrated the capability of the heterodyne interferometer to simultaneously detect (i.e. in one single measurement) the absorption of the probe and the coupling laser together with the dispersion of the coupling laser. At the same time we demonstrated the improvement of the output signal obtained by scaling with respect to the reference photodiodes (this is the name given to photodiodes PD_5 and PD_6).

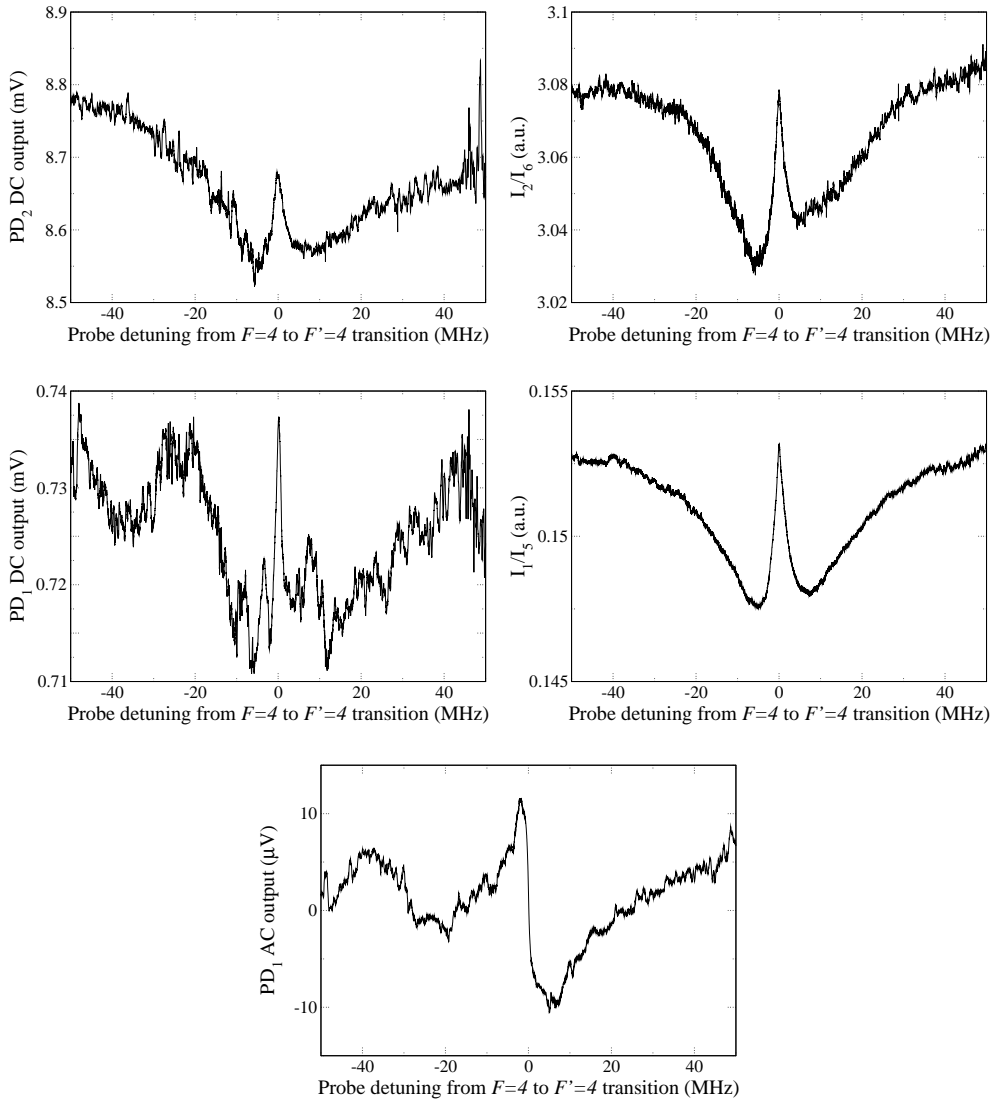


Figure 3.2: Simultaneously measured DC transmission signals at PD₁ (centre left) and PD₂ (top left), corresponding noise-filtered signals (centre and top right) and AC signal at PD₁ (corresponding to the phase shift of the coupling laser). The photodiodes correspond to those described in Fig. 3.1.

It is interesting to note that the better signal optimisation was not obtained when the glass plate was inserted with an angle of $\frac{\pi}{4}$ rad with respect to the incident beam (the angle needed to obtain an extracted beam perpendicular to the probe arm). The best pick-up angle had to be empirically determined. In the present case it resulted in an angle between probe arm and extracted beam of about 1.25 rad instead of $\frac{\pi}{2}$ rad ($\simeq 1.57$ rad).

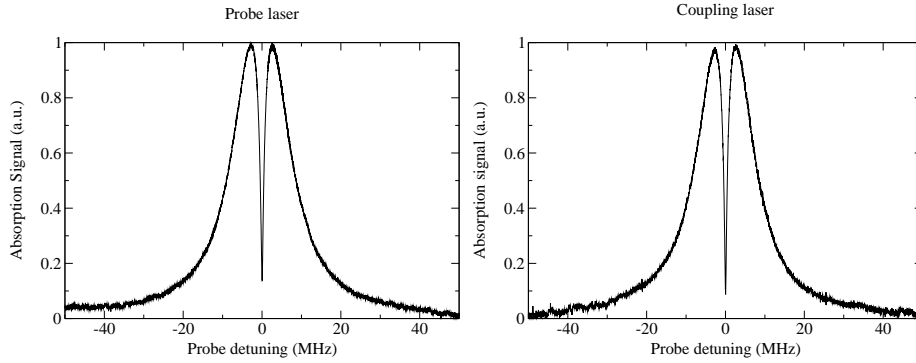


Figure 3.3: Simultaneously measured coupling and probe laser absorption in a Λ -system as a function of the probe laser detuning. The maximum absorption has been normalised to 1. The measurements were taken at a coupling laser intensity of 4.1 mW/cm^2 and a probe laser intensity of 1.3 mW/cm^2 .

3.2 Measurements in a Λ -system

Through a careful adjustment of the laser polarisations and an efficient control of the magnetic field in the interaction volume it was possible to perform measurements of absorption in a Λ -system in which the dark resonance could be resolved with a very high contrast.

An example of simultaneous measurement, obtained for the coupling laser driving the transition $F = 3 \rightarrow F' = 4$ and the probe laser probing the transition $F = 4 \rightarrow F' = 4$ is shown in Fig. 3.3. The probe laser signal shows that the obtained electromagnetically induced transparency at the two-photon resonance had a level comparable to the transparency which the probe laser experienced when it was driven off resonant (this level can be assumed to be roughly the level of the tails of the broad resonance curve). The transparency obtained here was about 86% of the off-resonant value¹.

The coupling laser signal shows an even more impressive extinction of the absorption (the value is approximately 92% with respect to the tails). It must be noted, however, that the off-resonant value of the tails of the coupling laser absorption spectrum corresponds to the one-photon absorption level of a *resonant* coupling laser. The absorption here presented is a parametric absorption spectrum which describes the variation of the absorption of the coupling laser induced by the nonlinear medium once the medium is swept with a probe laser. For this reason it is even possible to obtain a value of parametric absorption which lies below the off-resonant value of the spectrum (we stress once again that this corresponds to a situation in which the probe laser is off-resonant). Neglecting this may lead (and has led) to a misinterpretation of the measured coupling laser spectra.

¹The values would have to be compared with the one-photon probe absorption on the same system. Since the absorption maximum in the two-photon case, which was assumed as the reference value for normalising the absorption, lies below the one-photon absorption maximum value, the extinction given above has to be taken as a lower limit

3.3 Broad spectral measurements within the caesium D_2 line

In the previous section we have stated that the parametric absorption signal of the coupling laser may present an enhanced transparency with respect to the absorption level due to one-photon resonance. In doing this we have assumed the one-photon absorption for the coupling laser to be the level given by the tails of the two-photon resonance curve. Since these tails extend theoretically over an infinite range of frequencies but experimentally only a finite number of points can be measured, we had to put a cut-off at specific detunings of the probe laser from the two-photon resonance. Experimentally, it was impossible to continuously sweep the probe laser over a range of more than 150 MHz. To have some extra freedom in the choice of the sweep range, the frequency window adopted to perform the measurements was fixed to 100 MHz (sometimes, to resolve particularly narrow features it was reduced to 20 MHz).

To be able to determine if the tails of the coupling absorption curve had a further decrease at frequencies of the probe laser detuned of more than ± 50 MHz from the Λ -system two-photon resonance, we extended the range of the measured data moving the central frequency of the probe laser in the direction of the other hyperfine transitions (in the Λ -system the probe laser probed the $F = 4 \rightarrow F' = 4$ transition; the new target transitions were $F = 4 \rightarrow F' = 5$ and $F = 4 \rightarrow F' = 3$). The measurement of the whole hyperfine splitting of level $6p \ ^2P_{3/2}$ requires a frequency tuning range of about 550 MHz. Since our laser system allowed only stable tuning ranges of about 100 MHz, we measured the splitting by overlapping ten 100 MHz scans, each of which was detuned from the previous one by 50 MHz to ensure a good overlap. During these measurements we kept the reference laser off, thus not performing any dispersion measurements. Apart from this, the experimental setup coincides with the one shown in Fig. 2.3a. In Fig. 3.4 the intensities measured PD₁ and PD₂ are shown; these intensities correspond to transmission signals. The excited transitions relative to each measured signal are sketched above it. The measurements also show the reference transparency signal obtained when the atomic beam was shut. The reference level of transparency shown in the figure was the maximum achievable in this experiment; the small residual absorption due to the optical components could not be avoided.

We found strong differences between the two spectra. With PD₂ we observed two regular absorption profiles and an absorption signal with a narrow feature at the line centre, corresponding to EIT; with PD₁ a regular absorption profile, an EIT-like signal and a signal resembling a dispersion profile. These signals will be explained in the immediately following paragraphs.

Absorption signal

PD₂ recorded the intensity of the probe laser transmitted through the nonlinear medium. When the probe laser frequency was resonant with the hyperfine transition $6s \ ^2S_{1/2} F =$

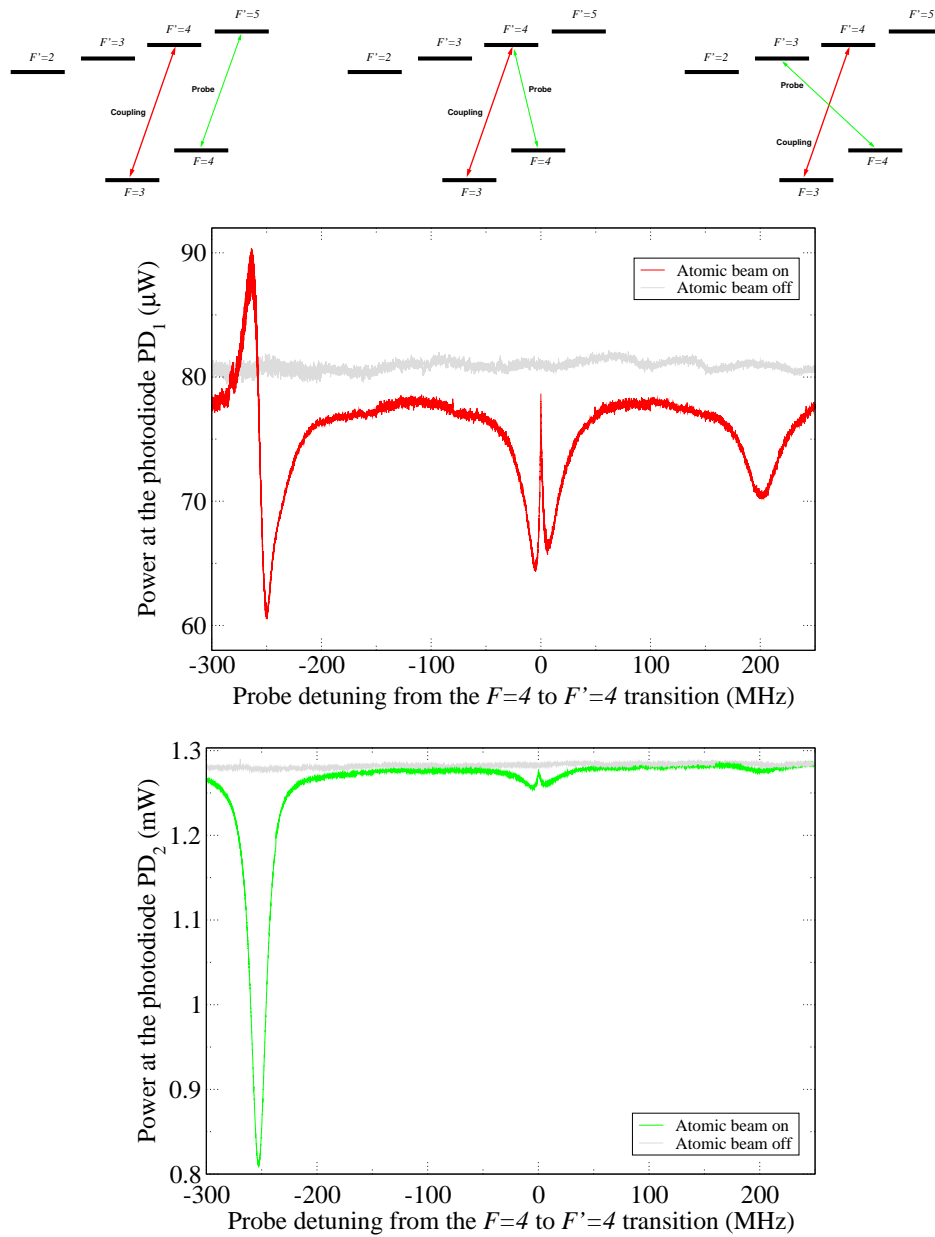


Figure 3.4: Transmitted powers observed at PD₁ and PD₂ as a function of the probe laser detuning. PD₂ detected the probe laser intensity and PD₁ the light orthogonally polarised to the probe laser polarisation. Above each resonance feature the figure shows the corresponding hyperfine transitions which are coupled and probed with the two lasers. The probe laser is shown in green and the coupling laser in red.

$3 \rightarrow 6p \ ^2P_{3/2} \ F' = 3 \text{ or } F' = 5$ we measured a normal absorption profile. This is the behaviour that one could expect since, generally, laser light passing through an atomic sample will be strongly absorbed if the laser frequency nears a transition frequency of the

atoms.

PD₁ detected the transmitted intensity of the light which was orthogonally polarised with respect to the polarisation of the probe laser as, for example, the intensity of the coupling laser. The amount of transmitted intensity changed as a function of the probe detuning: when the probe laser was resonant, it induced transitions which modified the former constant absorption level of the resonant coupling laser (the absorption which is responsible for the off-resonant gap between the measured values with and without the atomic beam). The energy level diagram in Fig. 3.4 (top right) explains why an absorption profile was detected at PD₁ on the right hand side of the spectrum. The coupling laser depopulated the $6s^2S_{1/2} F = 3$ hyperfine level and, as a result of the optical hyperfine pumping, the population in the $6s^2S_{1/2} F = 4$ level increased. When the probe laser was in the vicinity of the transition to the excited hyperfine level $6p^2P_{3/2} F' = 3$ a re-pumping from the $6s^2S_{1/2} F = 4$ level took place and the population in the $6s^2S_{1/2} F = 3$ level increased; this led to an increase in the coupling laser field absorption and to the absorption profile detected with PD₁.

Electromagnetically induced transparency signal

When the probe laser frequency was scanned around the hyperfine transition $6s^2S_{1/2} F = 4 \rightarrow 6p^2P_{3/2} F' = 4$ a signal with a dip in the centre was recorded both at PD₁ and at PD₂. In this case the coupling and the probe laser transitions formed a three level Λ -system (Fig. 3.4, top centre). The measured signals are then an example of EIT signals. We pointed out in the previous section that in the presence of EIT, the coupling laser might lead to a transparency level higher than that experienced with an off-resonant probe laser. The signal measured at PD₁ confirmed this possibility.

Light-induced birefringence

The signals detected with the probe laser on the $F = 4 \rightarrow F' = 5$ and the coupling laser on the $F = 3 \rightarrow F' = 4$ were characterised by a huge absorption of light of the same polarisation as the probe laser light and a curious dispersive-like signal which showed a gain of transmission of light polarised orthogonally to that of the probe laser. The first time these signals were measured we believed them to be due to some accidental rotation of a polariser but this possibility was excluded.

Furthermore, through the experimental setup adopted in this experiment we could fully resolve the hyperfine structure in the ground and in the excited states of the caesium D_2 line. Thanks to temperatures of about 210 °C we could neglect the effects of collisions in the ground as well in the excited states (see section 2.7) and the laser intensity was sufficiently low so as to ignore the stimulated emission.

From the level diagram in Fig. 3.4 (top left), we could argue that no influence of the probe laser field should have been present on the coupling laser field when the probe laser field was resonant with the hyperfine transition $F = 4 \rightarrow F' = 5$, because no electric dipole

transition was possible from the excited level $F' = 5$ to the ground level $6s\ ^2S_{1/2}\ F = 3$. In addition, we could not detect any dispersion signal when we tried to measure the AC contribution of the light orthogonally polarised to that of the probe laser, i.e. the light which, in the case of EIT, gave origin to the so-called parametric dispersion.

The explanation of the measured signals could be reduced to *light-induced birefringence*. We will explain briefly how such an effect can explain the measured signals. Since the discussion of these signals is not very relevant for the main subject of this work the following discussion will be kept to a simplified level.

The coupling and probe fields were linearly polarised and of orthogonal polarisation. The coupling field populated the Zeeman sublevels of the excited $6p\ ^2P_{3/2}\ F' = 4$ hyperfine level differently, in accordance with the transition probabilities. The population of each of these levels decayed at a rate corresponding to its branching ratio and created an alignment in the $6s\ ^2S_{1/2}\ F = 4$ level [32]; the defined polarisation of the coupling laser is responsible for this alignment and thus for an induced anisotropy of the medium [22]. Hence, the absorption coefficients and the refractive indices for the left and right circularly polarised probe laser light (in which the probe polarisation could be decomposed) became different. The difference in the refractive index resulted in optical birefringence while the anisotropy in the absorption made the polarisation of the probe beam elliptical.

Let us now consider the polarisation of the probe laser. After the interaction with the atomic sample the linearly polarised light of the probe laser crossed a Wollaston prism and was consequently decomposed into two linear polarisations perpendicular to each other. On account of the optical sample birefringence the polarisation axis was rotated and extra intensity coming from the probe laser was detected on the photodetector PD₁.

The linear polarisation of the probe could be decomposed into a left and a right circular polarisation with the same transition frequency. Since the frequency dependence of the refractive index due to birefringence was dispersive-like for each polarisation, the difference led to a dispersive signal. Following [47] the contribution of the intensity of the probe light on PD₁ could be expressed (up to the second order) as

$$I(\Phi) = \{\sin^2 \Phi + \Delta\theta \sin 2\Phi + [(\Delta\theta)^2 + (\Delta\alpha l/4)^2] \cos^2 \Phi\} I_{pr} \exp(-\alpha l),$$

where Φ is the small angle deviation from the axis perpendicular to the polarisation axis of the probe light and $\Delta\theta = (n_+ - n_-)k_0 l/2$ the phase difference between the two circularly polarised components; l is the interaction length of the probe laser with the atomic sample; $\Delta\alpha$ and α represent the difference and the sum of the absorption coefficients for left and right circularly polarised components, respectively.

If the axis of the analyser had been exactly perpendicular to the direction of the polarisation ($\Phi = 0$) then no dispersion shape could have been measured. A small deviation from the perpendicular adjustment was needed, so that the term $\Delta\theta \sin 2\Phi$ gave the main contribution to the signal, while $\sin^2 \Phi$ contributed to the signal with a bare offset.

As a counterproof for our explanation we also measured the dependence of the laser light-induced birefringence on the intensity of both lasers. We observed no significant

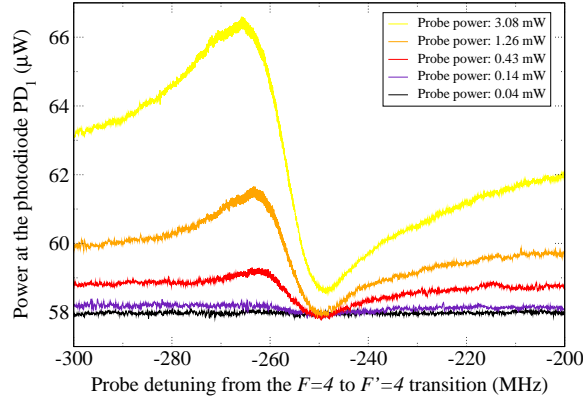


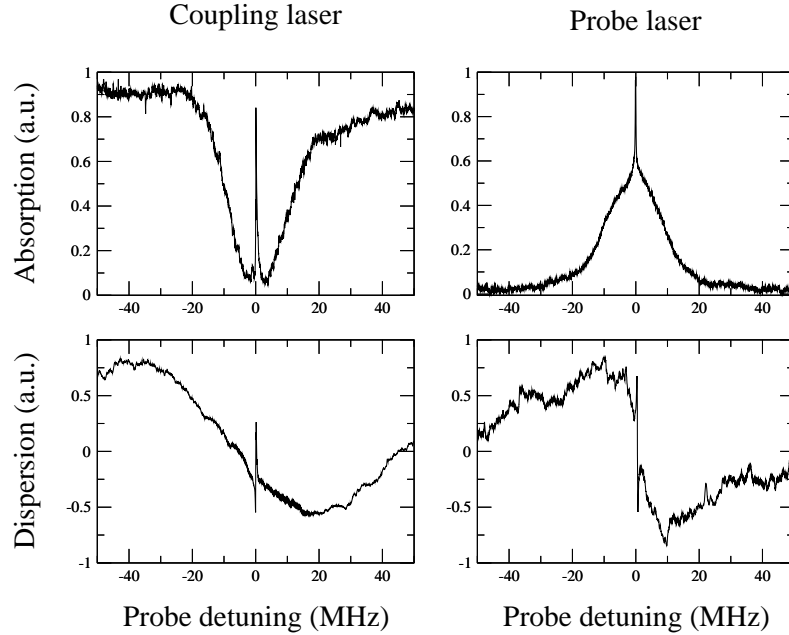
Figure 3.5: Transmitted power detected at PD₂. Light-induced birefringence as a function of the power of the probe laser.

dependence of the dispersion-like absorption profile measured with PD₁ on the coupling laser intensity when the probe laser power was kept constant. Conversely, as shown in Fig. 3.5, the light-induced birefringence amplitude showed a strong variation as a function of the probe laser power (keeping the coupling laser power constant). For increasing probe laser intensity the light induced birefringence increased because a greater amount of probe light could be rotated in its polarisation through the effect of the medium. This corroborated the hypothesis that the signals were originated through an anisotropy in the propagation of the probe laser light and confirmed the explanation given above.

3.4 Degenerate two-level systems

In chap. 1 we saw how the introduction of spontaneous transfer of coherence affects the spectra of closed degenerate two-level systems. In this section I present the results obtained in the two closed two-level systems available within the caesium D_2 line: the $F = 4 \rightarrow F' = 5$ transition, where EIA was observed, and the $F = 3 \rightarrow F' = 2$ transition, where EIT was observed.

In Fig. 3.6 typical spectra obtained on the $F = 4 \rightarrow F' = 5$ transition are shown. One can see that the probe laser experienced electromagnetically induced absorption while the coupling laser was characterised by what we called *absorption within transparency*, i.e. a narrow induced absorption peak appearing in the middle of a broad enhanced transparency profile. In correspondence with these absorption patterns, the probe dispersion curve followed a broad profile with a narrow central feature; both features were characterised by to negative (anomalous) dispersion. Contrarily, the parametric dispersion was positive. All results were in accordance with the simulations presented in chap. 1 for coupling intensities below saturation. The parametric absorption and dispersion measurements were the first performed on a two-level system satisfying EIA-conditions. Because they confirm the results obtained with the numerical simulations they support the hypothesis

Figure 3.6: Typical EIA spectra for the $F = 4 \rightarrow F' = 5$ transition

that spontaneous transfer of coherence is essential for the explanation of EIA².

Figure 3.7 shows similar spectra obtained in the closed two-level system $F = 3 \rightarrow F' = 2$. This system does not satisfy the EIA-condition requiring a higher degeneracy of the excited state with respect to the ground state. In this case the hyperfine structure had to be considered a superposition of Λ -systems rather than N-systems. This resulted in absorption spectra which resembled those of non-degenerate Λ -systems such as those measured in [29, 30, 31] or presented in Fig. 3.3. As usual for EIT, the probe dispersion could be described by a broad negative dispersion curve (corresponding to the one-photon probe resonance) with a narrow positive dispersion signal superimposed to it in correspondence with the two-photon resonance. The coupling laser parametric dispersion showed only a central feature at the two-photon resonance (negative parametric dispersion). The width of the signals appeared to be narrower than that measured in Λ -systems (or at least comparable) with a similar value of induced transparency (for the probe laser, a value of about 98% of the off-resonant transparency was obtained). These results made the degenerate closed two-level system a good candidate for the appearance of high Kerr-coefficients in the presence of transparency.

²It is known to the author that in case of equal polarisations of probe and coupling laser the theory predicts EIA as a consequence of transfer of population [17]. We refer here to the experimental configuration corresponding to the experiment performed: two linearly polarised probe and coupling laser of orthogonal polarisation. This is the configuration in which EIA was discussed for the first time [23].

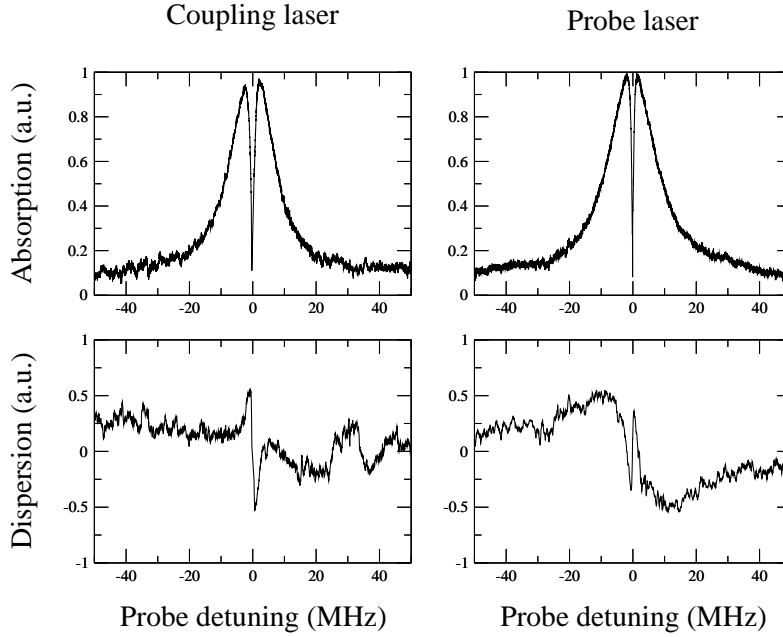


Figure 3.7: Typical EIT spectra for the $F = 3 \rightarrow F' = 2$ transition

To deepen our understanding of degenerate closed two-level systems in the presence of spontaneous transfer of coherence we want to see how the measured spectra change as a function of the coupling and probe laser intensities and compare the results with the simulations described in chap. 1. Figure 3.8 presents five probe absorption spectra obtained at various coupling laser intensities. The width of the central induced absorption peak at the two photon resonance broadens while the absorption decreases for increasing coupling intensities. This is in accordance with the numerical simulations presented in section 1.4.6. For the highest coupling laser intensity the probe spectrum develops two further absorption enhancements at about ± 10 MHz detuning from the two-photon resonance. These supplementary sidebands can be explained through a splitting of the hyperfine transitions induced by the coupling laser, which arises naturally in the formalism of second quantisation. Since this splitting is a function of the coupling laser intensity the corresponding quasi-degenerate levels can only be resolved at high coupling laser powers.

When the probe laser intensity was changed it was not possible to resolve the signals from the background with enough contrast over such a large intensity window as when varying the coupling laser intensity. However, at coupling intensities much greater than the probe intensities the variation of the spectra could be followed over at least one intensity decade. The corresponding results are shown in Fig. 3.9. Even at probe intensities of about $30 \mu\text{W}/\text{cm}^2$ the enhanced absorption is still recognisable.

Similar spectra can be obtained for the coupling laser parametric absorption, i.e. for the variation of the coupling laser absorption as a function of the probe laser detuning. In this

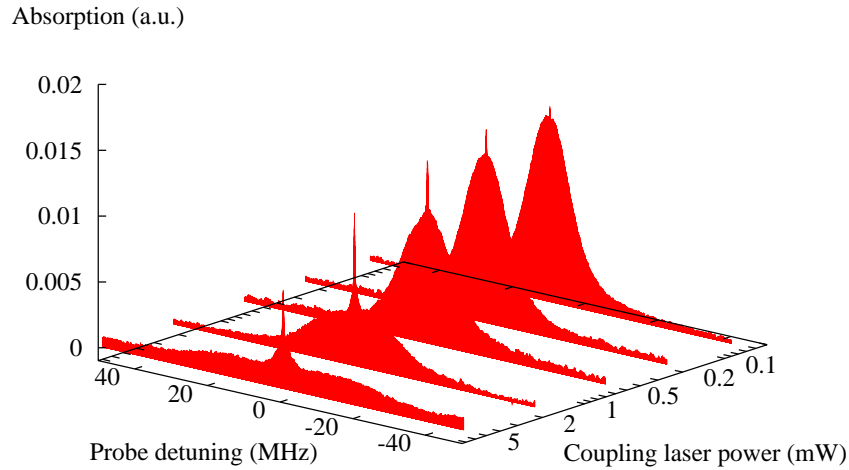


Figure 3.8: $F = 4 \rightarrow F' = 5$ transition: modification of the probe absorption spectra as a function of the coupling laser power. The probe laser power is $250 \mu\text{W}$. The laser beam radius amounts to 2.2 mm

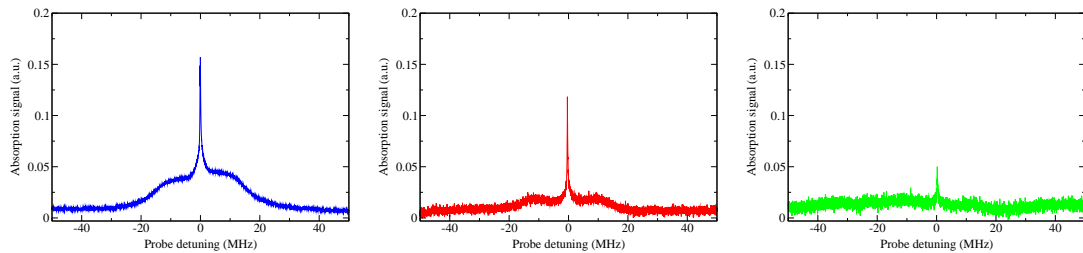


Figure 3.9: $F = 4 \rightarrow F' = 5$ transition: modification of the probe absorption spectra as a function of the probe laser power. The probe laser power amounts to $160 \mu\text{W}$ (left), $16 \mu\text{W}$ (centre), and $5 \mu\text{W}$ (right). The coupling laser power is 1.5 mW . The laser beam radius amounts to 2.2 mm

case it was the change of probe laser intensity which could be followed with more ease. The results are shown in Fig 3.10 and illustrate measurements obtained at a coupling intensity lower than those corresponding to the probe laser spectra of Fig. 3.8. In this regime it was possible to follow the variation of the parametric absorption spectra over an interval of almost three probe laser intensity decades. However, since for most of these measurements the probe laser intensity lay above the coupling intensity, one could not properly compare the spectra obtained in this case with the simulations described in section 1.4.6. More complex simulations would have been needed for such spectra, because

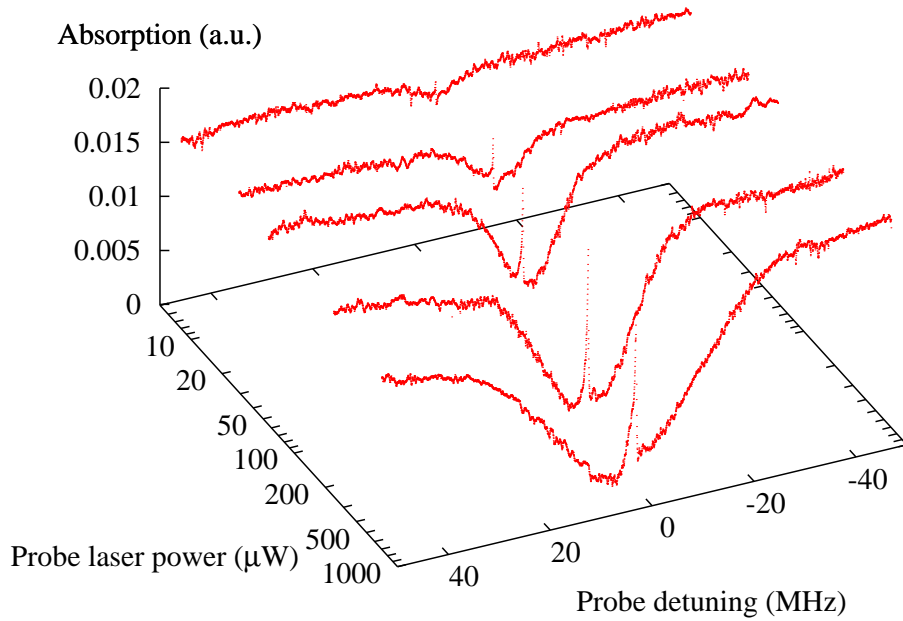


Figure 3.10: $F = 4 \longrightarrow F' = 5$ transition: modification of the coupling parametric absorption spectra as a function of the probe laser power. The coupling laser power is $120 \mu\text{W}$. The laser beam radius amounts to 1.1 mm

the probe laser effect could not be neglected by an approximation. These simulations are currently still under development. It has not yet been possible to calculate such spectra for linearly polarised laser of orthogonal polarisation. However preliminary results [46] exist for the case of a π polarised coupling laser and a σ^+ polarised probe laser and for circularly polarised lasers of orthogonal polarisation. In both cases the coupling laser only exhibits *absorption within transparency*, which is consistent with the measured data. The parametric absorption spectra for the two cases are shown in Fig. 3.11.

Figure 3.6 shows that the dispersion of the probe laser was characterised by a broad negative dispersion signal with a narrow superimposed negative dispersion feature. We have seen that the numerical simulations expect this behaviour only for low intensities of the coupling laser. We confirmed this prediction with our measurements as it can be seen from Fig. 3.12, where we show the probe dispersion spectra corresponding to EIA signals obtained at four different coupling laser intensities. The broader dispersive signal can be clearly identified at low coupling intensities. At high coupling intensities only the central feature at the two-photon resonance remains. At the same time the amplitude of the central feature tends to diminish. Both results are in qualitative accordance with the expectations of the numerical simulations.

To investigate the dependence of the probe phase shift (which is a function of the probe dispersion) on the laser powers, we fitted the central dispersion profile obtained at various

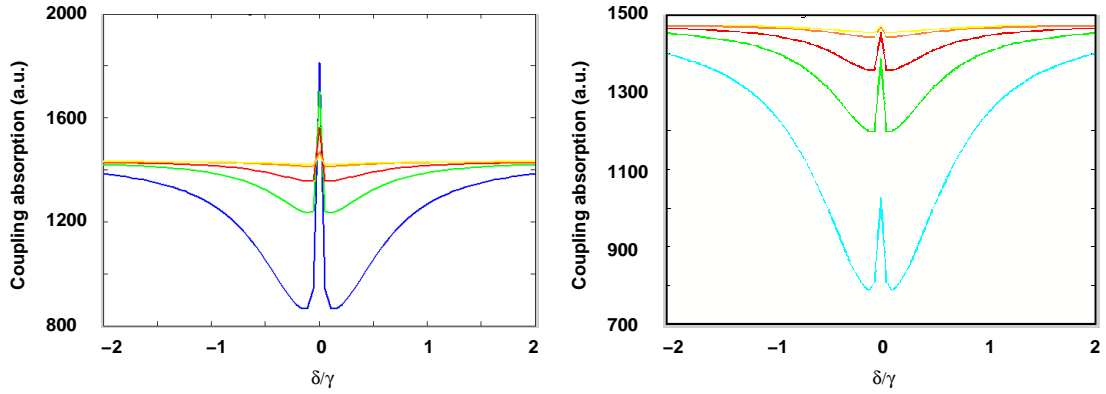


Figure 3.11: $F = 4 \rightarrow F' = 5$ transition: simulation results for a π polarised coupling laser and a σ^+ polarised probe laser (left) and for a σ^- polarised coupling laser and a σ^+ polarised probe laser (right). The coupling laser has a power of $170 \mu\text{W}$. The probe laser powers are $41 \mu\text{W}$ (yellow), $69 \mu\text{W}$ (orange), 0.27 mW (red), 0.71 mW (green), and 2.6 mW (blue or light blue). The beam radius is 2.2 mm . Courtesy of Arlene Wilson-Gordon [46].

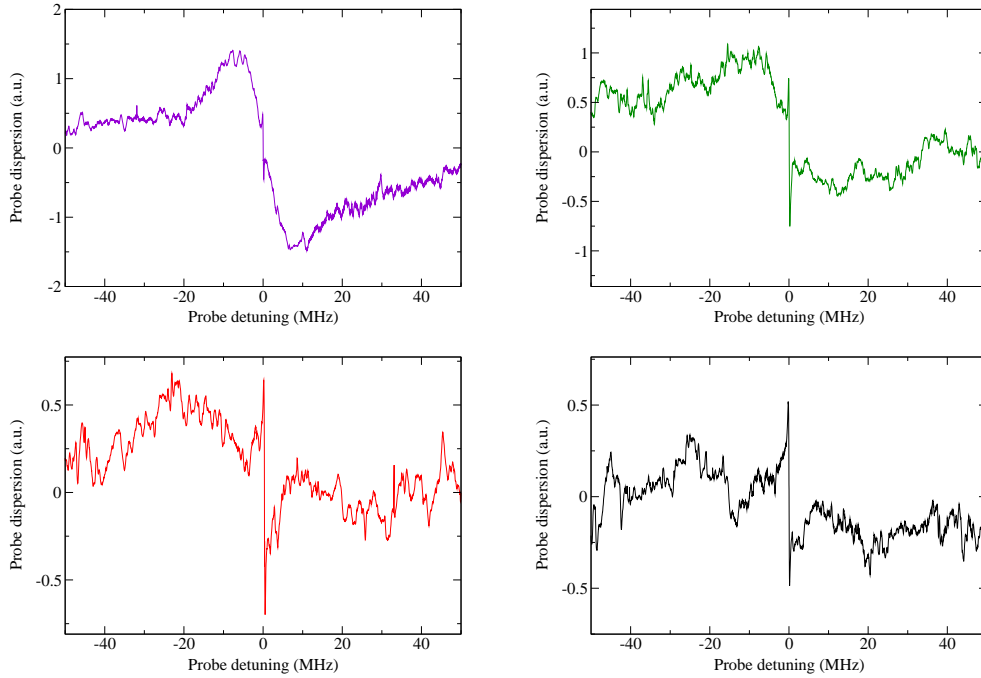


Figure 3.12: $F = 4 \rightarrow F' = 5$ transition: probe laser dispersion spectra for various coupling laser intensities. Probe power: 0.35 mW . Coupling power: 0.18 mW (blue), 0.64 mW (green), 3.0 mW (red), 4.5 mW (black). Laser beam radius: 2.2 mm .

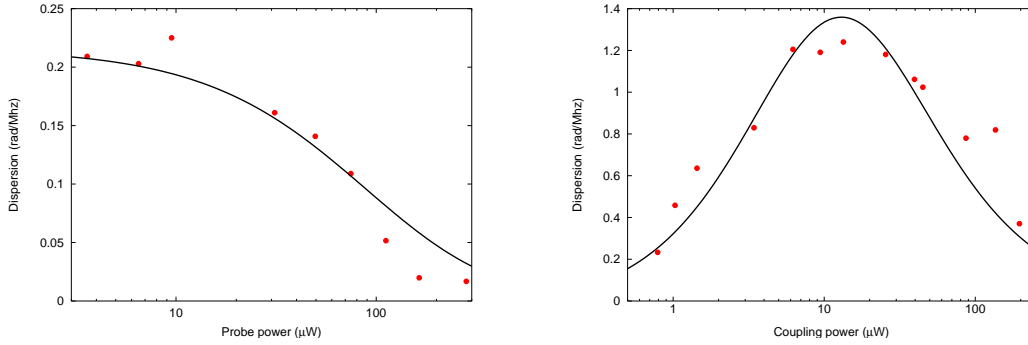


Figure 3.13: $F = 4 \rightarrow F' = 5$ transition. Probe laser dispersion (absolute value) as a function of the probe power variation at a constant coupling power of $535 \mu\text{W}$ (left) and probe laser dispersion as a function of the coupling laser power at a constant probe laser power of $20 \mu\text{W}$. The laser beam radius amounts to 2.2 mm . The solid lines are the results of a simulation of the system under comparable experimental conditions.

powers to a phenomenological dispersion curve of equation

$$D(\nu) = d + \frac{c(\nu - a)}{1 + \left(\frac{\nu - a}{b}\right)^2},$$

thus obtaining information on the width and steepness of the signals. In doing this we neglected the effect of the broader dispersion profile which characterises the spectra at low coupling laser intensities. The a and d parameters describe an offset which might be contained in the measurements because of systematic errors in the measurement procedure (for an ideal measurement one would assume $a = 0$ and $d = 0$). The parameter b contains information on the width of the curve and c on the steepness of the curve at the two-photon resonance, i.e., in the first approximation, on the phase shift induced by the medium.

It is possible to follow the change of such a phase shift as a function of either the coupling laser power (at constant probe power) or vice versa. The obtained experimental results covered two to three laser-power decades and are shown in Fig. 3.13. Because the measured probe dispersion was negative, the results presented in Fig. 3.13 have to be understood as absolute values. While the probe dispersion decreases as a function of the probe laser power it presents a maximum as a function of the coupling laser power. This maximum corresponds to coupling intensities well below the saturation intensity and roughly comparable to those of the probe laser.

Unfortunately, a general explicit expression for the probe dispersion (or the coupling parametric dispersion) in terms of experimentally accessible parameters has neither been published nor calculated so far. Nevertheless, inspired from the approach used by the discoverers of EIA [2], we compared the results obtained in this research with the analytical expression calculated in paragraph 1.5.3 for the probe dispersion in an ideal degenerate Λ configuration. In this case the dispersion was calculated for experimental conditions of

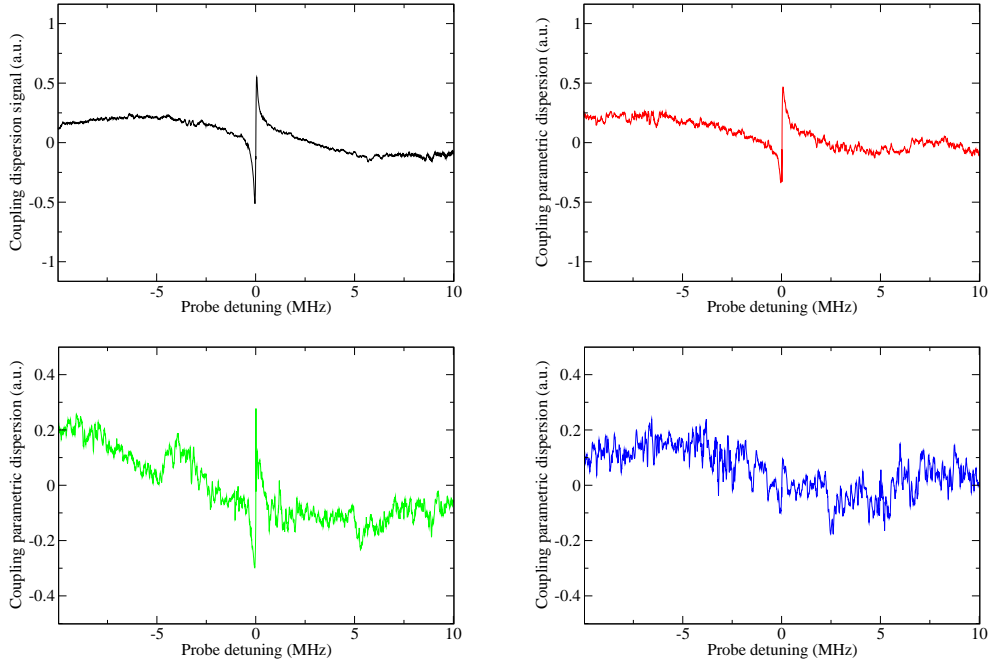


Figure 3.14: $F = 4 \longrightarrow F' = 5$ transition: coupling laser parametric dispersion spectra for various coupling laser intensities. Probe power: 0.26 mW. Coupling power: 4 μW (black), 23 μW (red), 80 μW (green), 0.33 mW (blue). Laser beam radius: 2.2 mm.

laser intensity, atomic density and interaction length comparable with those experimentally tested. Even if one could expect only a qualitative agreement between theory and experiment, the calculated values of the dispersion are comparable with the measured ones. The results of the calculations are shown as a solid curve in Fig. 3.13.

As was shown for the probe dispersion, it is also possible to perform an analysis of the behaviour of the coupling parametric dispersion as a function of the intensity of both lasers. These results are of particular interest because no measurement of the coupling laser dispersion in a degenerate two-level system has been hitherto performed. First of all let us compare the measured dispersion curves with the simulation results of chap. 1. Four parametric dispersion spectra which were obtained at increasing coupling laser power are illustrated in Fig. 3.14. The figure shows that it was possible to obtain very clear dispersive signals only at relatively low coupling laser intensities because the signal-to-noise ratio diminished for increasing coupling laser power. This seems to confirm the expectations of theoretical predictions even if those were performed for a much lower probe laser intensity. The simulation calculated a decrease of a factor between 50 and 100 in the amplitude of the dispersive signal for increasing coupling laser power. Since for higher coupling intensities the detection noise at the photodiode was also increased, this resulted in an overly unfavourable signal-to-noise ratio at high coupling powers.

Nevertheless, it was again possible to follow the variation of the parametric dispersion as a function of the laser intensities over a range of more than two power decades. The proced-

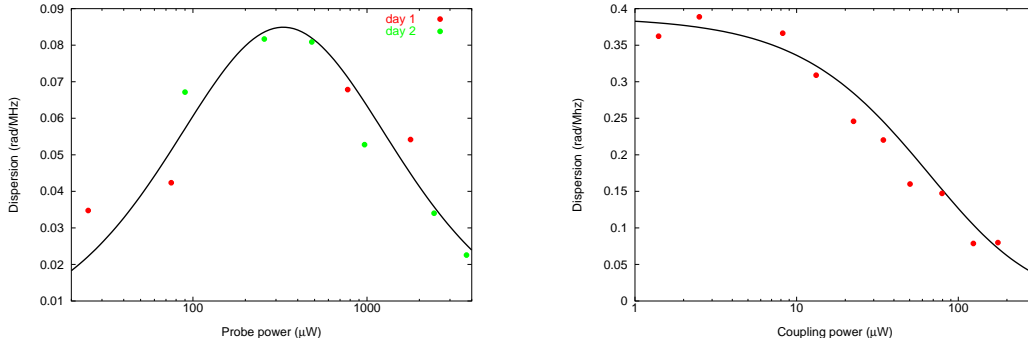


Figure 3.15: $F = 4 \rightarrow F' = 5$ transition. Coupling laser parametric dispersion as a function of the probe power variation at a constant coupling power of 0.16 mW (left) and probe laser dispersion as a function of the coupling laser power at a constant probe laser power of 0.26 mW. The laser beam radius amounts to 2.2 mm. The solid lines are the results of a simulation of the system under comparable experimental conditions.

ure used was similar to the one adopted for the probe dispersion. Each signal was fitted to a phenomenological dispersion curve. From the fit we extracted the information on the steepness and width of the dispersion. The results are shown in Fig. 3.15. Once again the solid curves are the results of a simulation performed on the system under comparable experimental conditions and based on the approximation of treating the dispersion as if it were generated in a Λ -system. Again, despite the lack of a proper analytical description of the expected dispersion signals, the measurements and the simulations show a qualitative satisfactory agreement.

At first we varied the probe field power from 25 μ W to 3.2 mW whilst keeping the coupling power constant (0.16 mW). We repeated this last measurement on two different days under identical experimental conditions. The coupling laser parametric dispersion showed a maximum as a function of the probe laser power. Again, the maximum appears in a range where the two lasers have roughly the same intensity. Conversely, when the coupling laser power was changed, we observed a decrease in the dispersion value with increasing power.

We measured signals with a half-width-at-half-maximum (HWHM) starting from about 10 kHz and remaining under 150 kHz for various laser powers. Figure 3.16 shows the width of the dispersion curve when keeping the coupling laser power fixed at 16 μ W. The observed half-widths were well below the half-widths of parametric dispersion curves observed in Λ -systems in Caesium. A similar result for the regular probe absorption spectra in the EIA and EIT configurations has been discussed in [4].

Finally, since some predictions of a transition from absorption to transparency or of a change of sign in the dispersion were made (see, for example, the simulations presented in Fig. 1.12 relative to a regime above saturation and the general case described in [18]), we tried to verify whether it was possible to observe any change in the absorption or dispersion spectra once coupling the system with the strongest intensity available for the

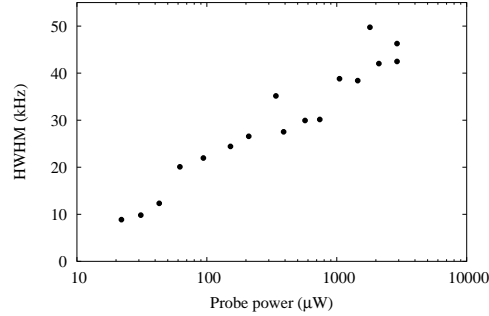


Figure 3.16: Linewidth of the coupling laser parametric dispersion as a function of the probe field power at a constant coupling power of $16 \mu\text{W}$. HWHM: half-width-at-half-maximum

coupling laser at the interaction zone.

For the absorption spectra, assuming that the change in amplitude was not covered by the detection noise (which could be suppressed down to about 1% of the signal), such an effect was not observed even for coupling laser power of about 8 mW and coupling to probe power ratios greater than about 100. Similarly, no transition from positive to negative dispersion was found, even in the power range where no detectable absorption signal was present but a dispersive signal was still to be detected (we concentrated our attention on this regime because the lack of a detectable absorption signal could have also been a hint for a change in sign of the absorption). Results of further simulations received while writing this work and targeted on the experimental conditions in which the measurements were performed seem, however, to confirm the experimental results [46].

3.5 Kerr coefficients

In this section, stimulated by the current research in the gravitational wave community, we want to transfer the information gained with the study of the dispersion in closed two-level systems to concepts which are closer to those used in the development of future gravitational wave detectors. It is expected that the coming generations of earth-based interferometers for the detection of gravitational waves will, at some point, be limited by quantum noise. The insertion in the interferometer cavities of a material exhibiting a non-negligible Kerr effect under the action of the applied electric field is one of the methods suggested to beat the standard quantum limit and to improve the performance of future detectors.

In recent times, it has been demonstrated that in the proximity of the two-photon resonance responsible for EIA in the caesium D_2 line, giant Kerr nonlinearities can be measured, which are orders of magnitude greater than those commonly available for usual Kerr media [3, 4]. Inspired by this research, we calculated—on the basis of the experimental data extracted from the dispersion measurements described in the previous sections—

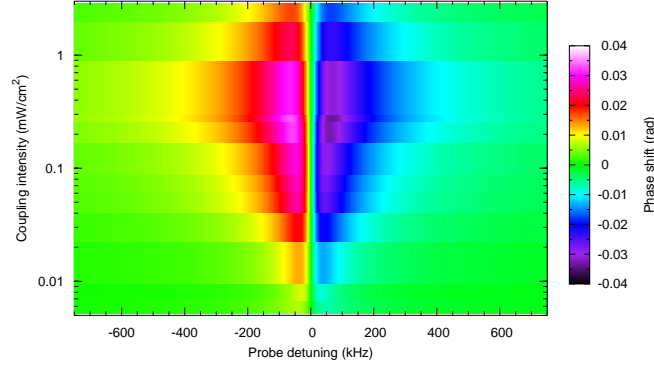


Figure 3.17: Probe laser phase shift for various probe laser detunings from the EIA two-photon resonance transition and various coupling laser intensities.

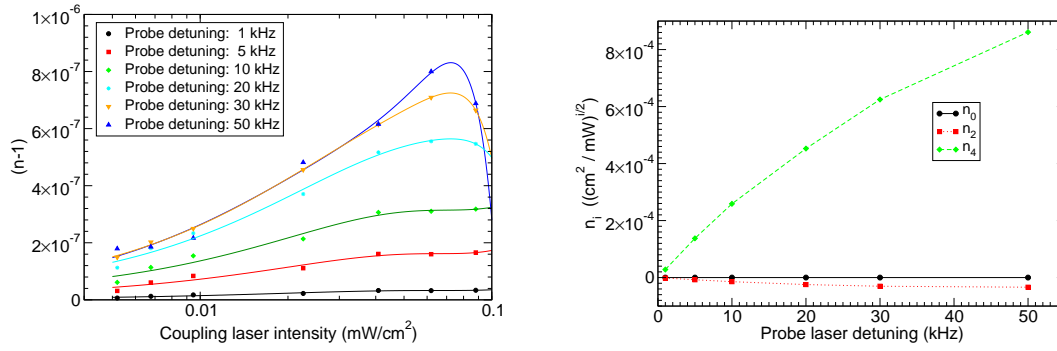


Figure 3.18: [Left] Probe refractive index difference from unity as a function of the coupling laser intensity. Each curve corresponds to a specific probe frequency offset. [Right] Kerr coefficients at various probe detunings from the EIA two-photon resonance

how the probe laser phase shift changed as a function of the probe laser detuning and of the intensity of the applied coupling field. The results are shown in Fig. 3.17. From the results for the phase shift it was possible to extract the refractive index of caesium as a function of the coupling laser intensity for various detunings of the probe laser from the EIA two-photon resonance (see Fig. 3.18).

It can be shown that the refractive index of a Kerr medium can be expressed as a function of the intensity I_{coupl} of the applied field (here the coupling field) in the form

$$n(I_{\text{coupl}}) - 1 = n_0 + n_2 I_{\text{coupl}} + n_4 I_{\text{coupl}}^2 + \dots$$

where n_0 is the linear part of the refractive index while n_2 and n_4 are the first two non-linear Kerr coefficients. Through a polynomial fit (based on the previous expansion) of the values of the refractive index obtained at various probe detunings from the two-photon

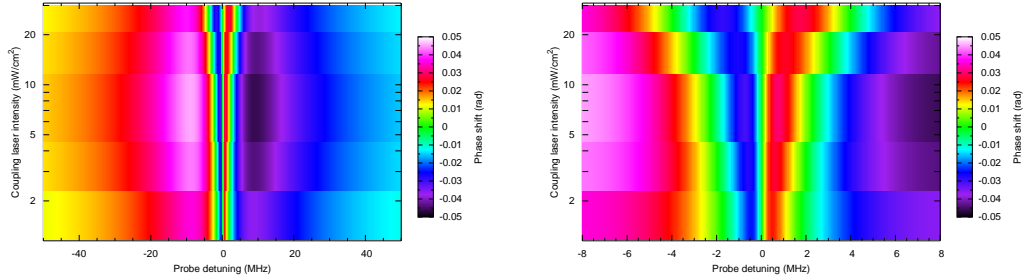


Figure 3.19: Probe phase shift as a function of the probe laser detuning from the EIT two-photon resonance for various coupling laser intensities. The figure on the right zooms the central feature of the figure on the left.

resonance, one could then obtain information on the linear and nonlinear components of the refractive index. These results are shown in Fig. 3.18.

The results for the Kerr coefficients can be properly understood only if one compares the values obtained for n_2 with the typical values for an ordinary material, such as glass. In glass one has $n_2 \simeq 10^{-20}$ cm²/mW whereas in the case of caesium the measured value was about 10^{-5} cm²/mW. The improvement is still remarkable even if compared with typical coefficients for Kerr media commonly used to generate Kerr nonlinearities, such as *GaAs*, which has a value of $|n_2| \simeq 2.7 \times 10^{-16}$ cm²/mW at a wavelength of 1064 nm [15], or polymers like polydiacetylene, the n_2 Kerr coefficient is $|n_2| \simeq 3 \times 10^{-11}$ cm²/mW [ibid.]. In conditions of extreme absorption at a wavelength of 852 nm the value $|n_2| \simeq 2 \times 10^{-7}$ cm²/mW was reported [26] for the Kerr coefficient of *GaAs*. However, at this wavelength, the absorption coefficient of *GaAs* has the value of $\alpha \simeq 10^4$ cm⁻¹ while the absorption coefficient for EIA measured in our experiment at the same frequency was of the order of 0.1 cm⁻¹.

Even if the absorption coefficient is small, the Kerr medium in the presence of electromagnetically induced absorption is characterised by an enhanced absorption with respect to a one-photon two-level transition. This might make it unattractive for implementation in a gravitational wave interferometer.

For this reason, since the electromagnetically induced transparency signals measured on the $F = 2 \rightarrow F' = 3$ closed transition had roughly the same width of the EIA signals on the closed $F = 4 \rightarrow F' = 5$ but were taken in the presence of transparency, we decided to calculate the Kerr coefficients also in this case. To do this we fitted once more the probe dispersion spectra to a theoretical dispersion profile obtaining the probe laser phase shift as a two-dimensional function of the probe laser detuning and of the applied coupling laser intensity. These results are shown in Fig. 3.19. Since the dispersion signals are characterised by a broader negative dispersion profile with a central positive dispersion profile at the two-photon resonance (see for example the typical dispersion signal for the $F = 2 \rightarrow F' = 3$ line shown in Fig. 3.7) we present two different plots which highlight

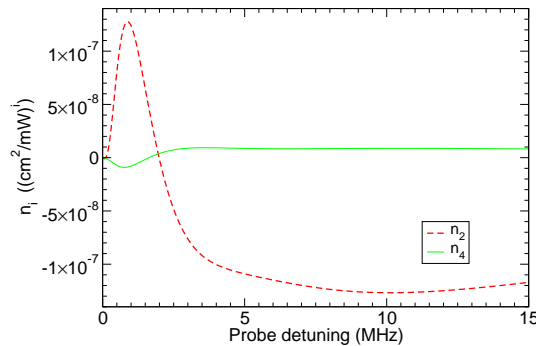


Figure 3.20: Nonlinear Kerr coefficients at various probe laser detunings from the EIT two-photon resonance frequency.

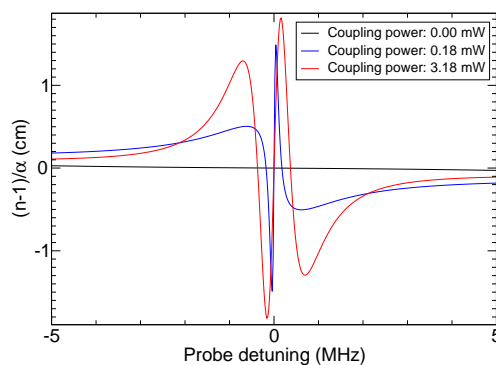


Figure 3.21: Figure of merit: ratio between the nonunitarian component of the refractive index and the absorption coefficient of the medium in the presence or absence of the coupling laser.

the two dispersive features.

With a procedure similar to that adopted for the probe laser acting on the $F = 4 \rightarrow F' = 5$ we extracted from the phase shift the probe refractive index at various probe detunings and, finally, the Kerr coefficients (Fig. 3.20). Even if the Kerr coefficients obtained in the presence of electromagnetically induced transparency were about two orders of magnitude smaller than those measured in the bright state, they were obtained for a medium which could be considered transparent for all practical purposes. Because of its almost lossless transmittivity an EIT-medium constitutes, therefore, an excellent candidate for the realisation of a Kerr interferometer.

Since in the EIT case the medium was transparent it was of particular interest to calculate a figure of merit which connected the dispersion at a fixed detuning with the induced transparency at the same detuning. In this way it was possible to locate the optimal working point for the medium, which was determined by a compromise between the transparency level and the induced phase shift. The optimal working point changed when the coupling laser intensity was varied. Two figures of merit obtained at two different coupling laser powers and the same probe laser power are shown in Fig. 3.21 together

with the figure of merit of a probe laser in the absence of coupling laser.

For a coupling power of 3.18 mW, which corresponded to the best working point for a probe laser power of 0.30 mW (with a beam radius of 2.2 mm), the maximum figure of merit was obtained for a probe detuning of 160 kHz from the two-photon resonance. At this maximum the figure of merit is 10^5 times greater than in the absence of the coupling laser (i.e. in the presence of a simple one-photon transition for the probe laser).

For coupling intensities higher than 3.18 mW the figure of merit decreased in its maximum value. The frequency corresponding to the maximum simultaneously shifted to higher frequency detunings. This behaviour could be ascribed to the lower steepness of the probe dispersion curve at high coupling powers which was accompanied by power broadening of the linewidth.

Outlook

In this work I analysed several atomic level configurations in caesium which can be considered as new optical media with a high refractive index or a giant Kerr effect. A particular focus of this research was dedicated to the degenerate two-level system, in which a transition from positive to negative dispersion was expected. Media in which a change of sign in the dispersion takes place are of particular interest for several applications such as the storage of light or opto-optical switches. However, the expected change of sign in the probe dispersion (or in its absorption) was not observed. More recent theoretical predictions which were stimulated by the results obtained in this research seem to confirm that no change of the dispersion should be expected, at least in the intensity range here investigated.

The aim of finding a medium showing a transition from positive to negative dispersion can be pursued through the experimental study of a four-level system for which such a transition is expected as a function of the intensity of one of the two applied coupling lasers. This system resembles the degenerate two-level system but the intensity ratio between the two coupling lasers is not limited by the atomic transition probabilities (as in the case of the degenerate two-level system). With a careful tuning of the ratio between the two coupling laser intensities it should then be possible to detect the desired transition between positive and negative dispersion. The hyperfine structure of the caesium D_2 line offers the possibility to investigate an N-system by simply adding a laser to one of the two already explored Λ configurations. This possibility could be explored with some technical improvements of the experimental apparatus.

Clearly, the study of a four-level system will require the implementation of a further laser in the heterodyne interferometer used so far. This new experimental configuration will also open the possibility to analyse a non-resonant bichromatic driven Λ -system, which is expected to be a transparent medium with negative dispersion, if the frequency difference between the two coupling lasers is greater than the reciprocal of the two-photon lifetime. In contradistinction to the two-level system, the non-resonant bichromatic driven Λ -system has the advantage that the frequency range in which the dispersion can be obtained is not affected by any lifetime but from the frequency difference between the two coupling lasers. Furthermore, negative dispersion can be reached at relatively low coupling frequencies. The non-resonant bichromatic driven Λ -system can be realised in caesium driving the outer ground level component of the D_2 line with two off-resonant coupling lasers.

The realisation of such a medium could improve the sensitivity of future gravitational wave detectors through the realisation of so-called white-light cavities, i.e. cavities—in

which the nonlinear medium is inserted—that maintain their finesse while their bandwidth is increased.

However, for the determination of the parameters needed for the construction of a white-light resonator, the ground level on which the non-resonant coupling fields act should be empty. We have seen in this work that both ground levels of the caesium D_2 line are almost equally populated (because of the thermal excitation and of collisions). For this reason a fifth laser would be needed to depopulate the desired ground level by exciting a transition to another hyperfine level. The use of so many coherent (apart from one) laser sources clarifies the reason why, in parallel to this project, the development of ECDL lasers into GEECDL lasers was stimulated and is followed with particular attention.

If the final realisation of the GEECDL laser will allow us its insertion into the experimental apparatus, it will be easy to proceed to a substantial upgrade of the setup, characterised by an enhanced stability of the whole measurement technique. In this case it will hopefully be possible to demonstrate the feasibility of white-light cavities, thus opening the way for an improvement in future generations of interferometric gravitational wave detectors and in other experiments based on advanced interferometric techniques.

Bibliography

- [1] Akulshin, A. M., S. Barreiro, and A. Lezama, 1998, *Phys. Rev. A* **57**, 2996.
- [2] Akulshin, A. M., S. Barreiro, and A. Lezama, 1999, *Phys. Rev. Lett.* **83**, 4277.
- [3] Akulshin, A. M., A. Ciminno, A. I. Sidorov, P. Hannaford, and G. I. Opat, 2003, *Phys. Rev. A* **67**, 011801(R).
- [4] Akulshin, A. M., A. I. Sidorov, R. J. McLean, and P. Hannaford, 2004, *J. Opt. B* **6**, 491.
- [5] Alzar, C. L. G., M. A. G. Martinez, and P. Nussenzveig, 2002, *Am. J. Phys.* **70**, 37.
- [6] Alzetta, G., A. Gozzini, L. Moi, and G. Orriols, 1976, *Nuovo Cimento Soc. Ital. Fis. B* **36B**, 5.
- [7] Arimondo, E., 1996, in *Progress in Optics*, edited by E. Wolf (Elsevier Science, Amsterdam), volume 35, pp. 257–354.
- [8] Bjorklund, G. C., M. D. Levenson, W. Lenth, and C. Ortiz, 1983, *Appl. Phys. B* **32**, 145.
- [9] Bloch, F., 1946, *Phys. Rev.* **70**, 460.
- [10] Boller, K.-J., A. Imamoglu, and S. E. Harris, 1991, *Phys. Rev. Lett.* **66**(20), 2593.
- [11] Cohen-Tannoudji, C., J. Dupont-Roc, and G. Grynberg, 1992, *Atom-Photon Interactions* (John Wiley & Sons, New York).
- [12] Cohen-Tannoudji, C., J. Dupont-Roc, and G. Grynberg, 1997, *Photons and Atoms* (John Wiley & Sons, New York).
- [13] Dahmani, B., L. Hollberg, and R. Drullinger, 1987, *Opt. Lett.* **12**, 876.
- [14] Drever, R. W. P., J. L. Hall, F. V. Kowalski, J. Hough, G. M. Ford, A. J. Munley, and H. Ward, 1983, *Appl. Phys. B* **31**, 97.
- [15] Flynn, M. B., L. O’Faolain, and T. F. Krauss, 2005, *J. Opt. Soc. Am. B* **22**(4), 792.
- [16] Goren, C., 2003, private communications.
- [17] Goren, C., A. D. Wilson-Gordon, M. Rosenbluh, and H. Friedmann, 2003, *Phys. Rev. A* **67**, 033807.
- [18] Goren, C., A. D. Wilson-Gordon, M. Rosenbluh, and H. Friedmann, 2004, *Phys. Rev. A* **69**, 053818.

- [19] Harris, S. E., 1997, *Phys. Today* **50**(7), 36.
- [20] Hau, L. V., S. E. Harris, Z. Dutton, and C. H. Behroozi, 1999, *Nature* **397**, 594.
- [21] Huke, P., 2004, *Stabilisierung eines Diodenlaser mit optischer Rückkopplung*, Diplomarbeit, Universität Hannover.
- [22] Kanorsky, S. I., A. Weis, J. Wurster, and T. W. Hänsch, 1993, *Phys. Rev. A* **47**, 1220.
- [23] Lezama, A., S. Barreiro, and A. M. Akulshin, 1999, *Phys. Rev. A* **59**, 4732.
- [24] Louisell, W. H., 1973, *Quantum properties of radiation* (John Wiley & Sons, New York).
- [25] Mair, A., J. Hager, D. F. Phillips, R. L. Walsworth, and M. D. Lukin, 2002, *Phys. Rev. A* **65**(3), 031802.
- [26] Miller, D. A. B., D. S. Chemia, D. J. Eilenberger, P. W. Smith, A. C. Gossard, and W. Wiegmann, 1983, *Appl. Phys. Lett.* **42**(11), 925.
- [27] Müller, G., 1997, *Kohärente Dunkelzustände in optischen Resonatoren*, Doktorarbeit, Universität Hannover.
- [28] Müller, G., A. Wicht, R.-H. Rinkleff, and K. Danzmann, 1996, *Optics Commun.* **127**, 37.
- [29] Müller, M., 2000, *Zerstörungsfreie Quantenmessungen*, Doktorarbeit, Universität Hannover.
- [30] Müller, M., F. Homann, R.-H. Rinkleff, A. Wicht, and K. Danzmann, 2000, *Phys. Rev. A* **62**, 060501(R).
- [31] Müller, M., F. Homann, R.-H. Rinkleff, A. Wicht, and K. Danzmann, 2001, *Phys. Rev. A* **64**, 013803.
- [32] Omont, A., 1977, *Progr. Quantum Electron.* **5**, 69.
- [33] Phillips, D. F., A. Fleischhauer, A. Mair, R. L. Walsworth, and M. D. Lukin, 2001, *Phys. Rev. Lett.* **86**(5), 783.
- [34] Pound, R. V., 1946, *Rev. Sci. Instrum.* **17**(11), 490.
- [35] Rinkleff, R.-H., and A. Wicht, 2005, *Physica Scripta* **T118**, 85.
- [36] Shore, B. W., and D. H. Menzel, 1968, *Principles of ATOMIC SPECTRA* (John Wiley & Sons, New York).
- [37] Spani Molella, L., R.-H. Rinkleff, and K. Danzmann, 2006, *Spectrochim. Acta, Part A* **63**, 987.
- [38] Swenumson, R. D., and U. Even, 1981, *Rev. Sci. Instrum.* **52**(4), 559.
- [39] Taichenachev, A. V., A. M. Tumaikin, and V. I. Yudin, 1999, *Phys. Rev. A* **61**, 011802(R).

- [40] Wang, L. J., A. Kuzmich, and A. Dogariu, 2000, *Nature* **406**, 277.
- [41] Wicht, A., K. Danzmann, M. Fleischhauer, M. Scully, G. Müller, and R.-H. Rinkleff, 1996, *Opt. Commun.* **134**, 431.
- [42] Wicht, A., P. Huke, R.-H. Rinkleff, and K. Danzmann, 2005, *Phys. Scripta* **T118**, 82.
- [43] Wicht, A., M. Müller, R.-H. Rinkleff, A. Rocco, and K. Danzmann, 2000, *Opt. Commun.* **179**, 107.
- [44] Wicht, A., R.-H. Rinkleff, L. Spani Molella, and K. Danzmann, 2002, *Phys. Rev. A* **66**(6), 063815.
- [45] Wicht, A., M. Rudolf, P. Huke, R.-H. Rinkleff, and K. Danzmann, 2004, *Appl. Phys. B* **78**, 137.
- [46] Wilson-Gordon, A., 2006, private communications.
- [47] Yoshikawa, Y., T. Umeki, T. Mukae, Y. Torii, and T. Kuga, 2003, *Appl. Optics* **42**, 6645.

Acknowledgements

I thank Professor Karsten Danzmann for giving me the possibility to perform my research at the Max Planck Institute for Gravitational Physics. Even if I remember with some nostalgia the times when I arrived here, when the institute was still like a small family, the incredible improvement of resources I have experienced in these years has had an impressive impact on my work, acting as a stimulus to always struggle for better results.

I am also very much indebted to my tutor, Dr. Rolf-Hermann Rinkleff, who was a constant source of inspiration for this work. He was the person with whom I could openly discuss all the details about the experiment and was always present when I had to measure one more spectrum. He also played a crucial role in criticising all unclear aspects of this work.

For the help in the laboratory I also wish to thank the students who have obtained their degrees in our group: Mathias Rudolf and Philip Huke.

For the reliable electronics used in the laboratory I wish to thank Heiko zur Mühlen (electronic workshop). Similarly I thank Jan Diedrich (mechanical workshop) who was always at disposal for any mechanical component I wished to design.

For the permission to use unpublished material I thank Dr. Chani Goren and Prof. Arlene Wilson-Gordon of the University Bar-Ilan in Israel. Even if our meetings did not coalesce into a formal collaboration I very much profited from the discussions which we had together.

For the great help in the study of the Kerr effect, especially concerning the processing of the measured data, I thank Dr. Gerrit Kühn.

For critically reading parts of this work I thank James di Guglielmo and Paul Cochrane. Without their help I wouldn't have managed many subtleties of the English language.

I acknowledge the Deutsche Forschungsgemeinschaft (German Research Foundation) which financed this work through the grant C2 of the Sonderforschungsbereich 407 (Collaborative Research Centre 407).

Finally, I thank all those whom I cannot list here: all the people who have made my environment enjoyable and, therefore, my work a pleasant burden.

Hannover, June 2006

Curriculum vitae

Luca Spani Molella
Dieckmannstraße 5,
30171 Hannover, Germany

Born on the 4th April 1974 in Piacenza, Italy.

Jul. 2005–present	Staff scientist, Max Planck Institute for Gravitational Physics, Hannover, Germany
Feb. 2004–Jun. 2005	Research grant, Max Planck Institute for Gravitational Physics, Hannover, Germany
Apr. 2001–Feb 2004	Doctoral grant, Max Planck Institute for Gravitational Physics, Hannover, Germany
Feb. 2001–Apr. 2001	Doctoral grant, Max Planck Institute for Quantum Optics, Hannover, Germany
Feb. 2001–present	Doctoral studies, University of Hannover, Germany
Nov. 1993–Mar. 2000	Degree studies, Università degli Studi di Pavia, Pavia, Italy
Sep. 1988–Jul. 1993	Upper secondary school, Liceo Scientifico L. Respighi, Piacenza, Italy
Sep. 1985–Jul. 1995	Conservatorium, Conservatorio di Musica G. Nicolini, Piacenza, Italy
Sep. 1985–Jun. 1988	Lower secondary school, Scuola Media G. Nicolini, Piacenza, Italy
Sep. 1980–Jun. 1985	Primary school, Scuola Elementare S. Giorgio, Codogno, Italy

Publications

- 2006 Luca Spani Molella, Rolf-Hermann Rinkleff and Karsten Danzmann: ‘Spectral measurement of the caesium D₂ line with a tunable heterodyne interferometer’, *Spectrochimica Acta Part A* **63**, 987–993.
- 2005 Luca Spani Molella, Rolf-Hermann Rinkleff and Karsten Danzmann: ‘Role of the coupling laser in electromagnetically induced absorption’, *Physical Review A* **72**, 041802(R), (1–4).
- 2003 Rolf-Hermann Rinkleff, Andreas Wicht, Luca Spani Molella, Karsten Danzmann: ‘Anomalous dispersion of transparent atomic two-, three-, and four-level ensembles’, *OSA Trends in Optics and Photonics (TOPS) 89*, Quantum Electronics and Laser Science (QELS), Technical Digest, Post-conference Edition, QTuG36.
- 2002 Andreas Wicht, Rolf-Hermann Rinkleff, Luca Spani Molella and Karsten Danzmann: ‘Comparative study of anomalous dispersive media’, *Physical Review A* **66**, 063815, (1–12).

